ACCELERATED TESTING OF AN ASPHALT PAVEMENT WITH THE THIRD-SCALE MODEL MOBILE LOAD SIMULATOR (MMLS3)

by
Lubinda F. Walubita

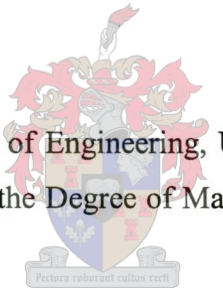

A Thesis submitted to the Faculty of Engineering, University of Stellenbosch, in partial fulfilment of the requirements for the Degree of Master of Science in Engineering in the Field of Pavement Technology.

Prof. Ir. MFC Van de Ven
Study Leader

Prof F Hugo, Pr. Eng, PhD, Ding
Internal Examiner

Dr P Straus
External Examiner

December 2000

Stellenbosch

DECLARATION

I, the undersigned, hereby declare that the work contained in this thesis is my own original work, and that I have not previously in its entirety or in part submitted it at any university for a degree.

ABSTRACT

Accelerated pavement testing (APT) is the application of a wheel loading, to a prototype or actual layered, structural pavement system to determine pavement response and performance under controlled, accelerated accumulation of damage in a compressed time period. It is a tool used for the evaluation of performance of new pavement materials, distress mechanisms, pavement distress, and selection of rehabilitation strategies. In this study, the research work that was done in Jacksboro, Texas (USA) with the third-scale Model Mobile Load Simulator (MMLS3) as part of the APT programme of the Texas Department of Transportation (TxDOT) is presented. The primary objective was to evaluate the performance of the different asphalt concrete (AC) materials (*Dustrol* and *Remixer)* used on highway US 281, in terms of rutting and distress due to wet trafficking. The other objective was to investigate the difference in rutting between the MMLS3 and the full-scale Texas Mobile Load Simulator (TxMLS). The scope of the study included fieldwork, laboratory work and theoretical analysis.

On average, the performance of the layer from the *Dustrol* process was found to be poorer than that of the *Remixer* process. The *Dustrol* process was more susceptible to moisture damage and less resistant to permanent deformation compared to the *Remixer* process. The MMLS3 and TxMLS permanent deformations in the upper 90 mm surface layers correlated well in terms of the respective vertical stresses imposed by the two APT devices, after allowing for the difference in environmental conditions during trafficking.

Overall, the study demonstrated that the MMLS3, used in conjunction with non-destructive field and laboratory testing, is a significant cost-effective APT device that can be used for evaluating the response and performance of the (surface) layers of full-scale, in-service pavements.

Samevatting

Versnelde Plaveisel Toetsing bestaan uit die gebruik van 'n wiellas op 'n prototipe of 'n bestaande gelaagde plaveiselstruktuur om die plaveiselgedrag onder beheerde en versnelde toename in skade in 'n verkorte periode te bepaal. Dit word gebruik om die gedrag van nuwe plaveiselmateriale, swigtingsmeganismes, plaveiselswigting en die keuse van rehabilitasie strategieë te evalueer. Die navorsingswerk met die derde skaal Model Mobile Load Simulator (MMLS3) wat onderneem is in Jacksboro, Texas (VSA), en deel uitmaak van die Versnelde Plaveisel Toetsingsprojek van die Texas Departement van Vervoer (TxDOT), word uiteengesit. Die hoofdoel van die studie was om die gedrag van twee verskillende asfaltmateriale, naamlik *Dustrol* en *Remixer*, wat gebruik is op die US 281-snelweg, in terme van sporing en swigting as gevolg van nat belastingstoestande te evalueer. 'n Verdere doelstelling was om die verskil in die gemete sporing tussen die MMLS3 en die volskaal Texas Mobile Load Simulator (TxMLS) te ondersoek. Die studie het veld- en laboratoriumtoetse en teoretiese analise behels.

Die gedrag van die *Dustrol* laag is oor die algemeen swakker as die *Remixer* lae. Die *Dustrol* laag, in vergelyking met die *Remixer* lae, is meer vatbaar vir vogskade en spoor makliker. Nadat die invloed van verskillende omgewingstoestande gedurende asbelasting inaggeneem is, korreleer die sporing vir die MMLS3 en die TxMLS in die lae van die boonste 90mm van die plaveisel goed in terme van die vertikale spannings soos opgewek deur die twee toetstoestelle.

In die geheel word bewys dat die MMLS3 tesame met nie-destruktiewe veld- en laboratoriumtoetse 'n belangrike koste-effektiewe versnelde plaveisel toetstoestel is, wat aangewend kan word in die evaluasieproses van die gedrag van (oppervlak) lae van volskaalse plaveisels in gebruik.

ACKNOWLEDGEMENTS

I hereby acknowledge my sincere appreciation and due gratitude to my study leader and mentor Professor MFC Van de Ven (SABITA Chair) for the academic guidance and advice rendered during the course of the research. Special thanks also go to Professor F. Hugo, particularly for facilitating the academic exchange program to the University of Texas at Austin in the USA and offering me an internship to complete my MSc.Eng. studies. Through the exchange program, I gained considerable academic knowledge and practical experience in accelerated pavement testing (APT).

The thesis is based on a study that was conducted for the Texas Department of Transportation (TxDOT) by the Center for Transportation Research (CTR) of The University of Texas at Austin, in collaboration with the Texas Transportation Institute (TTI) of the Texas A&M University System and with The University of Texas at El Paso. The support for the MMLS3 investigation as an integral part of the TxMLS research programme by Mr. Ken Fults P.E. (DES) and his successor as the project director, Dr. Mike Murphy P.E., is sincerely appreciated. This enabled the scope of the programme to be considerably expanded. I thank all the persons who rendered help and assistance during the investigations. In this regard I need to mention some of the team members and entities by name. Mebhuba Ehsan and Dae-Wook Park, from Texas A&M University. Michael Gray and Ray Donley from CTR. Andre Smit, Pieter Poolman and Johan Muller from the University of Stellenbosch. Special thanks are owed to Dr Deren Yuan (University of Texas at El Paso), for his assistance with the analysis of the seismic test data. The success of a research project of this nature is dependent on efforts and contributions by all of the persons that are involved. A special word of appreciation and gratitude is expressed to *The Institute for Transport Technology (ITT)* at the University of Stellenbosch which provided facilities and support for doing the extensive fatigue and related testing of specimens of the AC from the test site in Jacksboro.

Through Mrs LG van Kollenburg, I extend my sincere appreciation to NUFFIC (Eindhoven University of Technology, The Netherlands) for affording me the scholarship (for the period 1998-1999) through which I have been able to study and further my academic knowledge.

DEDICATIONS

I dedicate this "Thesis" to my mother Ms Grace Mwangala Muyunda. Thanks mum for all the hardships you have endured to bring me to where I am today. I will always cherish your love.

Table of Contents

Chapter 3

METHODOLOGY FOR APT TESTING WITH THE MMLS3

Chapter 4

FIELD MEASUREMENTS AND DATA COLLECTION

Chapter 5

LABORATORY TESTING AND MATERIAL CHARACTERISATION

Chapter 6

FIELD APT TEST RESULTS

Chapter 7

LABORATORY TEST RESULTS

Chapter 8

RELATING RUTTING PERFORMANCE OF THE MMLS3 WITH THE TxMLS

Chapter 9

DISCUSSIONS, CONCLUSIONS AND RECOMMENDATIONS

List of Tables

List of Figures

List of Symbols and Abbreviations

AASHTO	American Association of State Highway and Transportation Officials.
AC	Asphalt Concrete
APT	Accelerated Pavement Testing
BRD	Bulk Relative Density
E	Young's Modulus of Elasticity in MPa
FRR	Field Rut Ratio
ESAL	Equivalent Single Axle Load
h_{1-n}	Pavement layer thickness in mm
ITS	Indirect Tensile Strength in kPa.
HMA	Hot-Mix Asphalt
kPa	kilo Pascal ($1kPa = 1x10^{-3}N/mm^2$).
LDP	Layer Deformation Pin
LWAC	LightWeight Aggregate Asphalt Concrete
MDD	Multi-Depth Deflectometer
MMLS3	Model Mobile Load Simulator Mk3 (or MMLS Mk3)
MPa	Mega Pascal ($1MPa = 1N/mm^2$).
N_f	Fatigue Life
NDT	Non Destructive Testing
NST	Number of Specimens Tested
$PR_{rutting}$	Rutting Performance Ratio
PSPA	Portable Seismic Pavement Analyzer
RD	Rut Depth (mm)
RP	Rutting Potential (MPa*mm)
RPR	Rutting Potential Ratio
SASW	Spectral Analysis of Surface Waves
SCB	Semi-Circular Bending strength test
TRH	Technical Recommendations for Highways.
TRR	Theoretical Rut Ratio
TxMLS	Texas Mobile Load Simulator

Chapter 1

1 INTRODUCTION

Accelerated pavement testing (APT) is the application of a wheel loading, to a prototype or actual layered, structural pavement system to determine pavement response and performance under controlled, accelerated accumulation of damage in a compressed time period. APT is a tool that can be used for the evaluation of performance of new pavement materials (e.g. reinforced asphalt, cement treated bases, etc), distress mechanisms such as impact of water, pavement distress and selection of rehabilitation strategies (Hugo, 2000). Evaluation is often done to determine the present condition of a pavement in terms of remaining life and mechanisms of failure, and enable future performance to be predicted and/or for implementation of maintenance and rehabilitation strategies.

With APT, progressive distress of the pavement such as rutting, cracking, loss of stiffness, raveling, etc, under traffic loading and different environmental conditions (dry, hot, and/or wet) can easily be monitored and results obtained within a relatively short period of time. Parameters such as the axle loading, tyre pressure, trafficking speed, and temperature can be varied to simulate desired-critical conditions. Also water can be applied on the pavement surface to simulate wet conditions during trafficking. The one-third scale Mobile Model Load Simulator Mk3 (MMLS3) is one such APT device that can be used in this way. A detailed description of the MMLS3 is presented subsequently.

In this thesis, the research work that was done in Jacksboro, Texas (USA) with the MMLS3 as part of the accelerated pavement testing programme of the Texas Department of Transportation (TxDOT) is presented. The scope of the study included fieldwork, laboratory work and theoretical analysis. The study outline is shown in Figure 1.1.

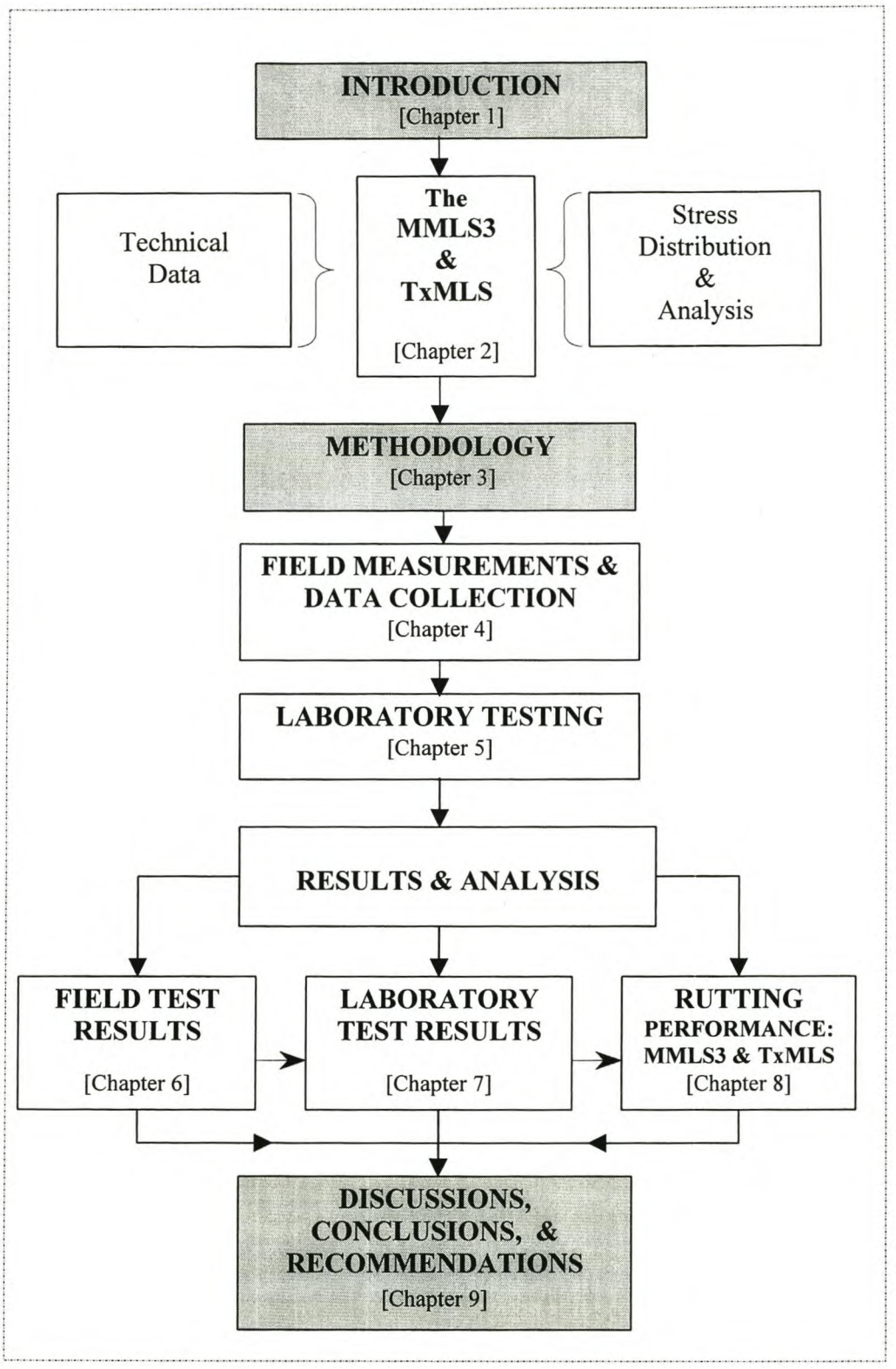

Figure 1.1: Study Outline

1.1 BACKGROUND TO THE MMLS3 TESTING IN JACKSBORO, TEXAS, USA

Stripping was found in the upper layers of the southbound outside lane of highway US 281, adjacent to the Texas Mobile Load Simulator (TxMLS) test site near Jacksboro, Texas (Smit et al, 1999). This led to a preliminary diagnostic study to determine the possible cause. It was found that water ingress into the pavement layers had substantially reduced the indirect tensile fatigue resistance of the lightweight aggregate concrete (LWAC) located in an underlying layer (Smit et al, 1999). Subsequently, testing with the one-third (1/3) scale MMLS3 was commissioned in 1998, to investigate the stripping phenomenon. This was achieved by trafficking the pavement in the field using the MMLS3 with a 1mm sheet of water flowing across the pavement surface (Smit et al, 1999). The other primary objective was to compare the MMLS3 rutting to that of the full scale TxMLS using the dry tests (Hugo et al, 1999 and Smit et al, 1999).

The rutting and SASW results of the first MMLS3 (1998) tests in Jacksboro led to the commissioning of a second set of tests in 1999 (Smit et al, 1999) (Hugo et al, 1999). SASW modulus results as well as surface micro-cracking under wet MMLS3 trafficking had indicated that the asphalt surfacing (overlay) on the northbound carriageway of US 281 was potentially susceptible to moisture damage (Smit et al, 1999). For this reason, additional wet MMLS3 testing was recommended on both the north and southbound carriageways of US 281 to ascertain whether the overlays and/or the underlying support layers were moisture susceptible, given that they had performed relatively well under dry trafficking conditions. This was to be achieved by milling off the overlay surfaces, and conducting both hot and wet tests on the original and milled surfaces. Milling off the top surfaces would also give an indication as to which layer was more susceptible to shear failure and rutting. By milling off the top surfaces, higher MMLS3 stresses would be induced deeper down within the pavement layers. This was expected to improve the comparison with the full scale TxMLS.

The 1999 MMLS3 tests also provided a comparative performance of the two rehabilitation processes, *Dustrol* and *Remixer* used on the northbound and southbound lanes, respectively. Hot tests were conducted to investigate the effects of high temperature on rutting.

During the period May 24 to July 9, 1999, six tests were conducted with a total application of 1.22 million axles.

1.2 TEST OBJECTIVES

As mentioned above, the 1999 MMLS3 tests in Jacksboro represented a continuation of the first MMLS3 tests conducted in 1998 under the TxMLS program. Figure 1.2 shows an overview of the MMLS3 and TxMLS tests under the TxMLS programme. The tests were conducted for the Texas Department of Transportation (TxDOT) by the Center for Transportation Research (CTR) of The University of Texas at Austin in collaboration with the Texas Transportation Institute (TTI) of the Texas A&M University System and with The University of Texas at El Paso.

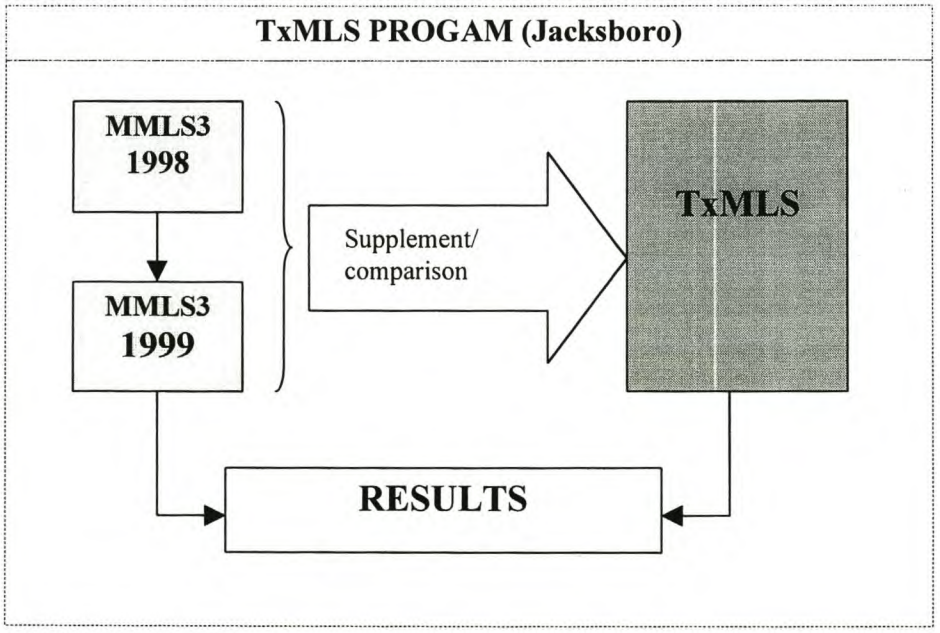

Figure 1.2: MMLS3 and TxMLS Tests under the TxMLS Program

The objectives of the 1999 MMLS3 tests in Jacksboro were:

(1) To investigate the relative performance of two overlays, namely, the *Dustrol* and *Remixer* processes used on the northbound and southbound lanes of US 281, respectively, in terms of rutting and distress due to wet trafficking. This finding would further validate the previous findings under the TxMLS testing.
(2) To investigate the difference in rutting between the TxMLS and MMLS3.

With the aforementioned objectives, a test programme as diagrammatically presented in Figure 1.3 was established. The results obtained from the tests were to be related and compared with those obtained from the previous MMLS3 and TxMLS tests.

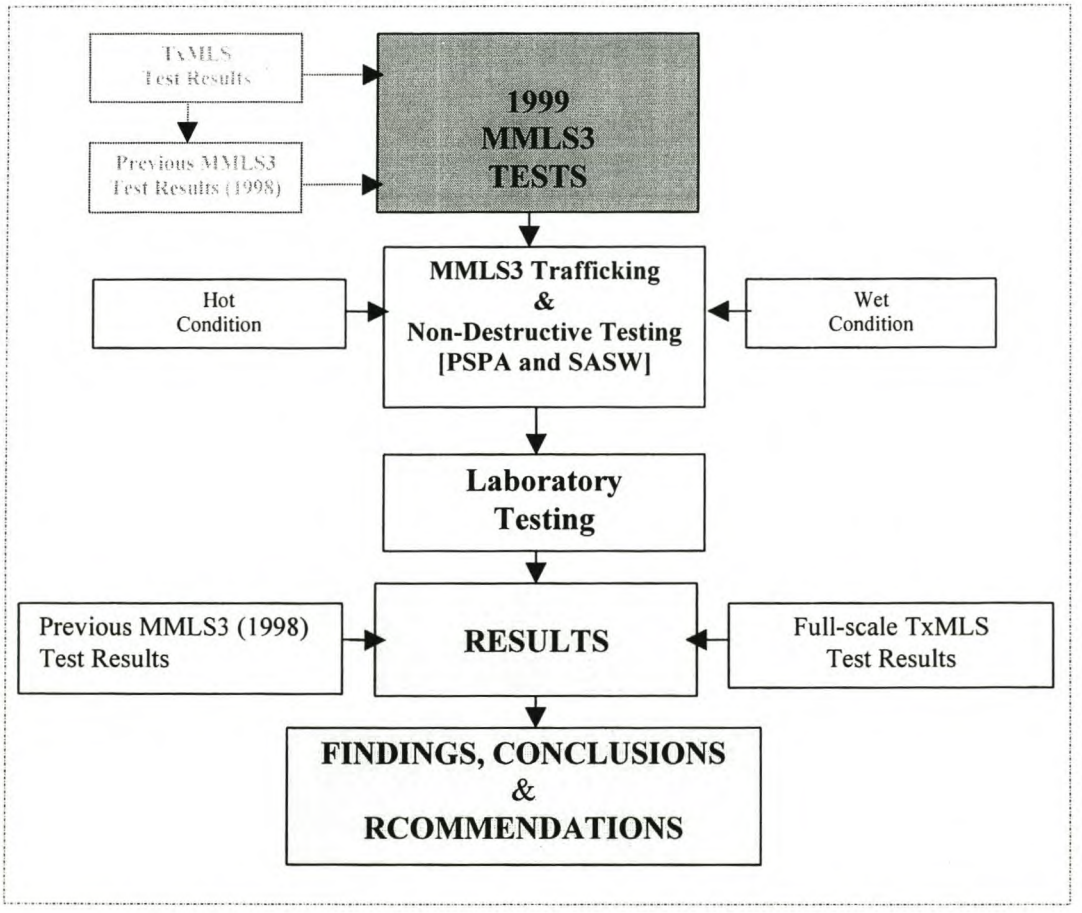

Figure 1.3: The 1999 MMLS3 Test Programme

1.3 SIGNIFICANCE OF THE STUDY

The effects of environmental factors (temperature and moisture) on an asphalt pavement under traffic loading are important and were investigated. The performance of different AC materials under different trafficking conditions was investigated and evaluated. A methodology for relating rutting performance of the MMLS3 to full-scale APT devices such as the TxMLS was developed.

The MMLS3 in conjunction with non-destructive field and laboratory testing as a cost-effective APT device for evaluating the response and performance of (surface) layers of full-scale in-service asphalt pavements were investigated and demonstrated.

1.4 METHODOLOGY

The methodology for the study consisted of computer stress analyses (theoretical), accelerated pavement testing (APT) in the field, non-destructive field testing and laboratory research.

1.4.1 Stress Analyses

Stress analyses were done to demonstrate the appropriateness of using the MMLS3 as an APT device. This illustrated how the loading influence with respect to pavement response and performance under MMLS3 can be related to full-scale APT devices such as the TxMLS and real traffic loading. A comparative analysis on rutting performance between the MMLS3 and TxMLS is also given. Computer program BISAR 3.0 was used for the stress computations.

An extensive BISAR 3.0 stress analysis on a two-layer pavement structure is presented in Appendix IV. The analysis gives an overview of the response and performance of an asphalt layer with regard to the axle load, the tyre pressure, the pavement layer thickness and the material constants (elastic modulus and Poisson's ratio).

1.4.2 Accelerated Pavement Testing (APT)

Accelerated pavement testing was done with the MMLS3. This involved application of numerous axle loads on an in-service pavement under different environmental conditions (hot and wet) to model response and performance of the pavement. Pavement temperatures, rutting and pavement layer deformations were measured during MMLS3 trafficking.

1.4.3 Non-Destructive Testing

Non-destructive in situ asphalt pavement stiffness measurements with the portable seismic pavement analyzer (PSPA) and spectral analysis of surface waves (SASW) devices were also done intermittently during MMLS3 testing. This was done to monitor the asphalt modulus change with trafficking under different environmental conditions.

1.4.4 Laboratory Research

Several laboratory tests were conducted to characterize the pavement materials and to supplement the field tests. These included volumetrics, moisture sensitivity, shear, indirect tensile strength (ITS), and fatigue life (in an indirect tensile mode), and semi-circular bending (SCB). Cores for laboratory testing were extracted from both the trafficked and untrafficked sections of the test pads in Jacksboro (Texas, USA). Most of the laboratory tests were done at the Institute of Transport Technology (University of Stellenbosch).

1.5 STUDY ORGANIZATION

As shown in Figure 1.1, this thesis consists of nine Chapters and four Appendices. At the end of each Chapter, a summary of the important points and findings is provided. This Chapter is the introduction, which gives a brief background and objective of this research study.

Chapter 2 discusses the MMLS3 and TxMLS APT devices. Technical data and schematic diagrams are given for clarity. Stress distribution under the two APT devices is also presented to illustrate how these relate to each other and subsequently pavement response and performance (i.e. permanent deformation).

The methodology for APT testing, field measurements and data collection are discussed in Chapters 3 and 4, respectively. Chapter 5 deals with the laboratory testing and material characterization. Field and laboratory test results are presented and discussed in Chapters 6 and 7, respectively. A comparative stress and rutting performance analysis of the MMLS3 relative to the TxMLS is presented in Chapter 8. Discussions, conclusions and recommendations are presented in Chapter 9.

Some calculations on the BISAR 3.0 stress analysis, field temperature measurements, and laboratory test results are included in Appendices I, II, and III, respectively. Appendix IV is analytical modeling of the load response of an asphalt-surfacing pavement. This is a comprehensive stress analysis involving a two-layer pavement system with emphasis on the top asphalt layer.

1.6 SUMMARY

The introduction outlined in a nutshell the significance of APT and it applications. This Chapter presented an overview of the use of the one-third scale MMLS3 machine as an APT device. The objectives, methodology and the study organization were presented.

Chapter 2

2 THE MMLS3 AND TxMLS

A detailed description together with the technical data of the third-scale Model Mobile Load Simulator (MMLS Mk3 or MMLS3) and the full-scale Texas Mobile Load Simulator (TxMLS or MLS) is given. A comparative stress analysis under the two APT devices is also presented. This was done to illustrate how the stress under MMLS3 loading compares to the full-scale APT devices such as the TxMLS3 (and real traffic loading), and how it can be related to permanent deformation. The theory of comparable stress and the 1/3-scale factor hypotheses are also analyzed and validated.

2.1 THE MMLS3 MACHINE

The one-third (1/3) scale Model Mobile Load Simulator Mk3 (MMLS3) is a low-cost APT device that applies a maximum of 7,200 single-wheel applications per hour. It is a uni-directional scaled down vehicle-load simulator used for accelerated trafficking of model or full-scale dry and wet pavements. With the MMLS3, different environmental conditions can be simulated and easily controlled during testing. It can be used in the field as well as testing laboratory constructed pavement structures, etc. For the laboratory constructed pavement structures, where the layer thicknesses are scaled, rutting performance as well as fatigue cracking of the AC layer can be modelled. It can also be used for modelling the response and performance of different layers and/or materials in a pavement structure. This is achieved through the process of milling off some layers/materials and trafficking directly on the layer of interest. All these processes are cost-effective relative to full-scale APT devices.

Maximum inflation pressure of the pneumatic tyres is 800kPa with a maximum single wheel load of 2.7kN. At these loading parameters, the circular tyre-pavement surface contact area is 3 375mm^2 and the contact radius is approximately 33mm, which is about 1/3 of the full-scale load. For the scale factor of 1/3, the load on a MMLS3 wheel is 1/9 of the full-scale load on a single tire of a dual set of tires on an equivalent single axle of a truck (1/4 ESAL). The nominal speed is about 9km/hr, which corresponds to a loading frequency of 4 Hz.

The machine dimensions are nominally 2400mm long by 1150mm high by 600mm wide (Muller Johan FP, 1999). Figure 2.1 shows the one-third (1/3) scale MMLS3 machine. The load configuration and technical characteristics are given in Table 2.1. Further MMLS3 details have been published elsewhere (Muller, 1999)

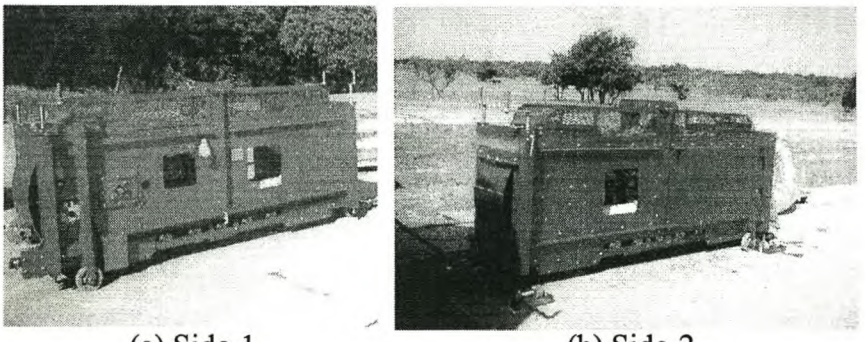

(a) Side-1 (b) Side-2

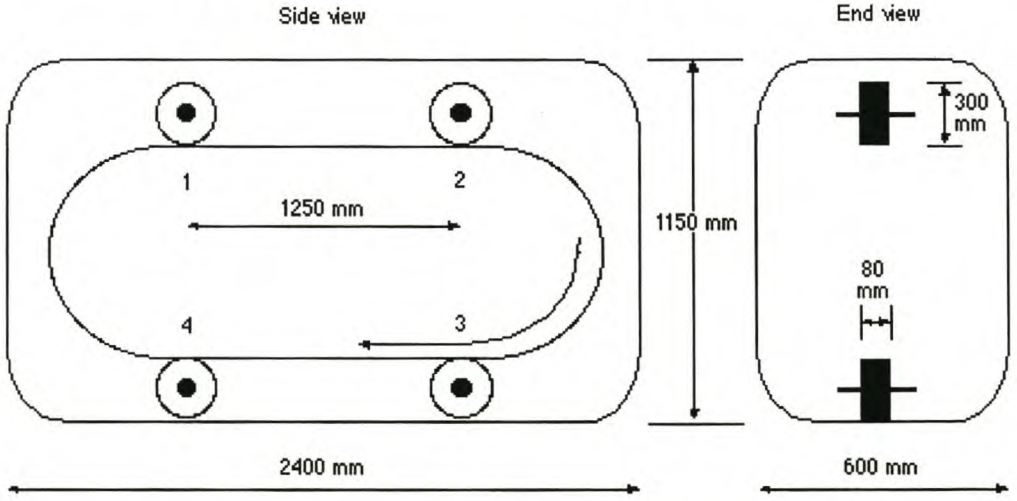

(c) Schematic view of the MMLS3

Figure 2.1: The Third-Scale Model Mobile Load Simulator (MMLS3)

Table 2.1: MMLS3 Load Configuration and Technical Data.

FEATURE	TECHNICAL DATA
No. of bogies	4
No. of axles per bogie	1
No. of tyres	4
No. of wheels	4 single
Tyre type	4.00-4, pneumatic rubber
Maximum tyre pressure (kPa)	800
Nominal tyre width (mm)	80
Nominal wheel diameter (mm)	300
Tyre footprint area (mm^2)	3 400
Nominal load per axle (kN)	2.7
Nominal load per wheel (kN)	2.7
Maximum wheel loads per hour	7 200
Load mechanism	Spring controlled
Load setting	Mechanical (suspension-spring system)
Suspension	Steel springs
Load control	Automatic (constant load)
Nominal Speed (uni-directional travel of wheels)	2.5m/s (~9km/hr, 4 Hz)
Duration of load pulse at operational speed (sec)	0.016
Nominal rest periods between load applications	0.5
Nominal time per cycle (sec)	2
Control Unit Housing – Dimensions (mm)	400 x 500 x 200
- Colour	Electric Orange
- Special Features	IP65 Weather Proof Metal Box
Supply Voltage	220 volts, 50/60Hz AC (single phase)
Power Consumption (kW)	1.5 (7Amp)
Lateral wander on each side of centerline (mm)	80 (right and left)
Total Maximum Track Width (mm)	240
Mobility	Trailer towed whilst supported on wooden base
Movement	On own wheels or by crane
Overall Operational Machine Dimensions (mm):	2400mm long x 600mm wide x 1150mm high
Total operational dead weight (kg)	672
Total Nominal Mass (kg)	800
Shipping weight (kg)	1 000
Test Section Size (mm)	1 200 x 500
Environmental control during tests (hot or wet)	Possible

2.2 THE TxMLS

The Texas Mobile Load Simulator (TxMLS) is operated at approximately 18km/h and achieves 6000 axle load repetitions per hour. The TxMLS or MLS is equipped with 6 full standard tandem axles travelling in one direction. The standard test procedure uses legal tandem axle loads of 150kN. The axle repetitions mentioned in this study represent half a tandem axle, or one 75kN axle. There are a total of 48 tyres; each is inflated to approximately 690 kPa. The dimensions of the TxMLS are nominally 31m long by 6m tall by 4.5m wide, as shown in Figure 2.2. The TxMLS operates at a maximum speed of 4.9m/sec (~18km/hr) which corresponds approximately to a 3 Hz frequency of loading for a tread length of 0.25m based on actual measurement of a similar tyre. A more detailed discussion of the TxMLS can be found elsewhere (Metcalf, 1996), (Chen et al., 1997), (Chen and Hugo, 1998). A succinct summary of the features of the TxMLS is contained in Table 2.2 (Hugo et al, 1999 [a], [b], [c]).

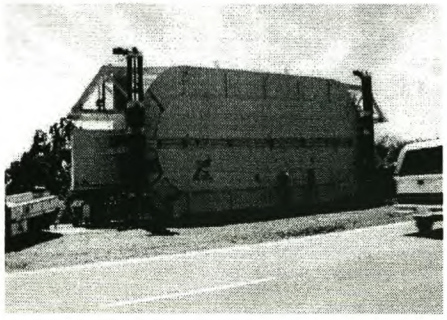

(a) Side View of the MLS

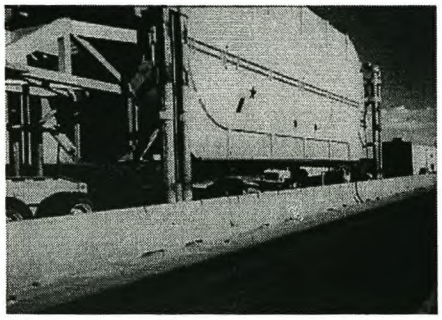

(b) Surveillance under the MLS

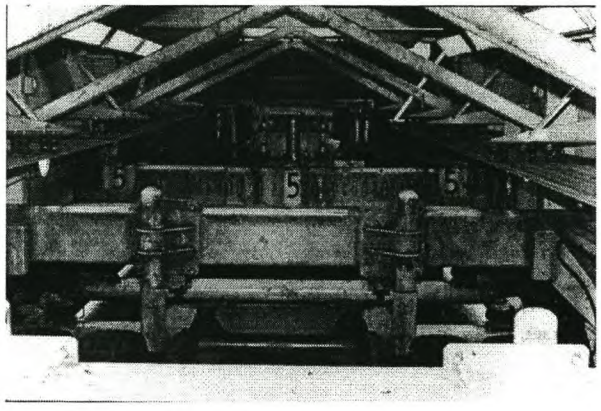

(c) Bogie #5 Inside the MLS

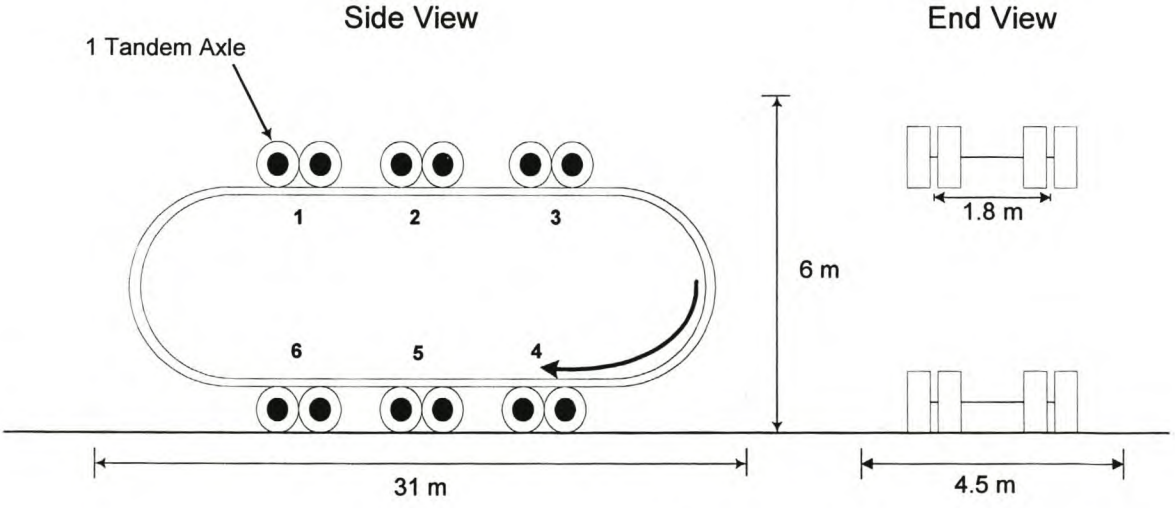

(d) Schematic view of MLS

Figure 2.2: The Texas Mobile Load Simulator (TxMLS)

Table 2.2: TxMLS Load Configuration and Technical Data

FEATURE	TECHNICAL DATA
No. of Bogies	6
No. of Axles/bogie	2 (dual tandems)
Total no. of full axles	12
• drive axles	2
• towed axles	10
No. of wheels	24 duals
Tyres/axle	4
Tyre type	295X75R22.5 Low profile radial
Tyre pressure (kPa)	690kPa
Nominal tyre tread width (mm)	230
Nominal distance between tyre centerlines (mm)	330
Nominal Wheel diameter (mm)	1000
Nominal load per axle (kN)	75.6
Nominal load per wheel (kN)	18.9
Load mechanism	Conventional highway truck springs
Load setting	Electro-mechanical
Suspension	Steel springs
Nominal Speed (uni-directional travel of axles) kph	18
Duration of load pulse at operational speed (sec)	0.05s
Nominal rest periods between load applications (sec)	Rest periods vary between 0.2s, 0.74s and 1.74s
Nominal time per cycle (sec)	8
Power	2x120 kVA DC motors
Maximum Production Rate/12 h shift (No. of Axles)	>50 000
Lateral wander (mm)	435 (left/right)
Mobility	Tractor towed supported on special bogies
Overall Operational Machine Dimensions (m):	
length	26.2
width	3.9
height	6.4
Total nominal mass (metric ton)	120
Test section size (m)	12 x 3
Temp control during tests	None-except for cover by structural shell

2.3 COMPARISON OF LOADING (STRESSES) UNDER MMLS3 AND TxMLS

Stress analysis was done to show the relative loading influence on the pavement of the two APT devices, and to also show how the MMLS3 stress influence could be related to the full -scale TxMLS, and subsequently permanent deformation. The following are presented;

- The theory of comparable vertical stresses and the 1/3 scale factor hypothesis of the MMLS3 relative to full-scale devices are discussed, based on a simplified two-layer pavement system.
- Vertical stress analysis on a model pavement structure where the corresponding layer thicknesses under the MMLS3 are scaled by a factor of 1/3, but using the same material properties and assuming similar environmental conditions.
- A vertical stress distribution comparison based on the surface layers of a pavement structure and the effect of milling (i.e. removing some of the top layers/materials) on the stresses under the MMLS3 in comparison to the full-scale loading (TxMLS) is also analysed.
- The shear stress distribution in a hypothetical 200 mm asphalt layer under the MMLS3 and TxMLS.

Computer program BISAR 3.0 (Shell Bitumen, 1978) was used for the stress calculations, based on linear-elastic theory. The calculations represent a single load application, and were done directly under the center of the wheel load, where the load is most concentrated.

2.3.1 Comparable Vertical Stresses and the 1/3 Scale Factor Hypotheses

The application of the MMLS3 is based on the hypothesis that for a simple pavement structure with only a single AC layer and similar tyre pressures, the distribution of maximum vertical compressive stress beneath the MMLS3 will be comparable to that beneath a single truck tyre with a standard load of 1/4 ESAL. This holds, if the scaling factor of one-third and dimensionless depth are considered (Allen et al, 1998, and Kim et al, 1995). In terms of the foregoing hypotheses, the vertical stress at mid-depth of a 300mm AC layer on a stiff subgrade under full-scale loading is expected to be equivalent to the stress at mid-depth of a 100mm (1/3 * 300mm) layer under the MMLS3 (Epps et al, 2000). This to imply that, the vertical stresses at a depth point under the MMLS3 (within the same layer), which is one-third of the depth point under a single wheel of a full-scale APT device (i.e. the TxMLS) must be equal. On the same principle, if the whole pavement structure is considered, the total area enclosed within the vertical stress curve under the MMLS3 should be approximately one-third of the stress area under the wheel of a full-scale APT device.

In the same vein, the pavement performance in terms of permanent deformation in the entire AC layer, under the full-scale loading, will be scaled by a factor of three times compared to the rutting performance under the MMLS3. That is if only a single wheel is considered under full-scale loading. On the basis of the same principle, it is hypothesised that the rutting in a selected portion of a single layered pavement structure (e.g. the top layer) is directly proportional to the area under the maximum vertical compressive stress curve, relating to the depths pertaining to the same selected portion (Epps et al, 2000).

2.3.1.1 Loading Parameters and Pavement Structure

The loading parameters and the pavement structure for the analysis is shown in Figure 2.3. In the case of the full-scale TxMLS with dual wheels, only a single wheel was considered (for comparative purposes) as shown in the Figure.

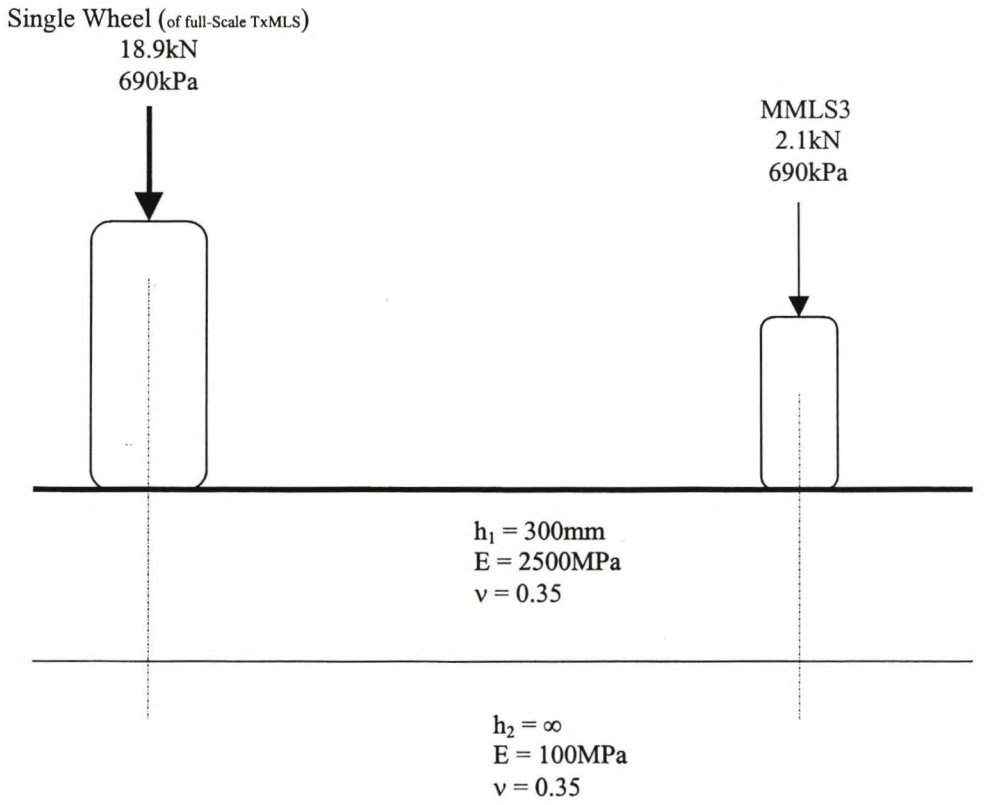

Figure 2.3: Loading Parameters on a Simplified Two-Layer Pavement System

Figure 2.3 shows a simplified hypothetical two-layer pavement system with a top 300 mm AC layer of about 2500 MPa modulus (E) resting on a subgrade of 100MPa modulus. For simplicity reasons, a constant E-value was assumed over the asphalt thickness. Environmental conditions were assumed constant and the same under both devices.

2.3.1.2 Vertical Compressive Stresses

The computed stresses are plotted in Figure 2.4 below. Some examples of the stress calculations from BISAR 3.0 are included in Appendix I.

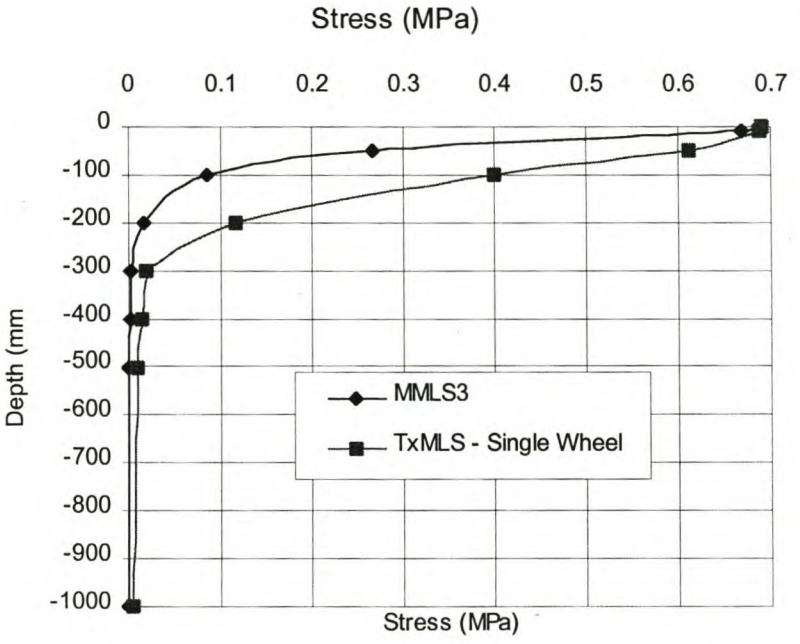

Figure 2.4: Vertical Stress Profiles for a Simple Two-Layer Pavement System
[h_1 = 300mm (asphalt), E_1 = 2 500MPa, $h_2 = \infty$ (subgrade), E_2 = 100MPa]

For the given pavement structure and loading parameters, the theory of comparable stress and the third-scale factor hypothesis were validated. At a depth under the MMLS3, which is one-third that under the TxMLS-single wheel, the stress magnitude was approximately equal. Some examples from Figure 2.4 are shown in Table 2.3.

Table 2.3: Comparable Vertical Stresses under MMLS3 and TxMLS (single wheel)

Depth (mm)		Stress (MPa)	
MMLS3	**TxMLS**	**MMLS3**	**TxMLS (single wheel)**
25	75	0.52	0.54
33	99	0.4	0.43
45	135	0.31	0.32
50	150	0.27	0.24
75	225	0.14	0.09

The total area encompassed within the MMLS3 vertical stress curve was calculated to be 38.2 MPa*mm. This is about 0.34 to that calculated under the TxMLS (114 MPa*mm). If the areas encompassed by the maximum vertical compressive stress distribution with depth for each loading condition (MMLS3, full-scale) are defined as the corresponding rutting potentials (RPs) of a specific pavement section or layer (Epps et al, 2000), the expected rutting under the MMLS3 on the same pavement structure must be approximately 0.33 of the TxMLS (if a single wheel is considered). Of course, this is assuming that environmental trafficking conditions are the same under both devices. When the TxMLS dual wheels were used and analysis done under the center of one wheel, there was no significant difference in the vertical stress magnitude compared to using only one wheel.

With this result, accumulated permanent deformation under full-scale loading of a simple pavement structure consisting of either a single material type or a layered structure on a stiff base can be predicted using a factor of three applied to the rut depth (RD) measured in the top third of the AC layer under MMLS3 loading (Epps et al, 2000).

2.3.2 Scaled Model Pavement under MMLS3

If a pavement structure under the MMLS3 is scaled by a factor of one-third in terms of depth (layer thickness) relative to a full-scale pavement, stresses and strains within the respective layers must be of the same magnitude. Material properties and environmental conditions must be constant and the same under both APT devices. On this basis, deformation of a scaled pavement under MMLS3 loading can be considered to be equivalent to deformation of a full-scale pavement under TxMLS (or real traffic loading).

2.3.2.1 Loading Parameters and Pavement Structures

A four-layered pavement structure (Figure 2.5) was used for the analysis. In the case of the MMLS3, the first three layers were scaled by a factor of 1/3 relative to the structure under the TxMLS-single wheel. The loading parameters are indicated in the Figure. The moduli for the respective layers under both devices were the same as indicated in Table 2.4.

Table 2.4: Material Properties

Layer Number	Modulus (MPa)
1	2500
2	1000
3	400
4	100
Poisson's ratio (ν) = 0.35	

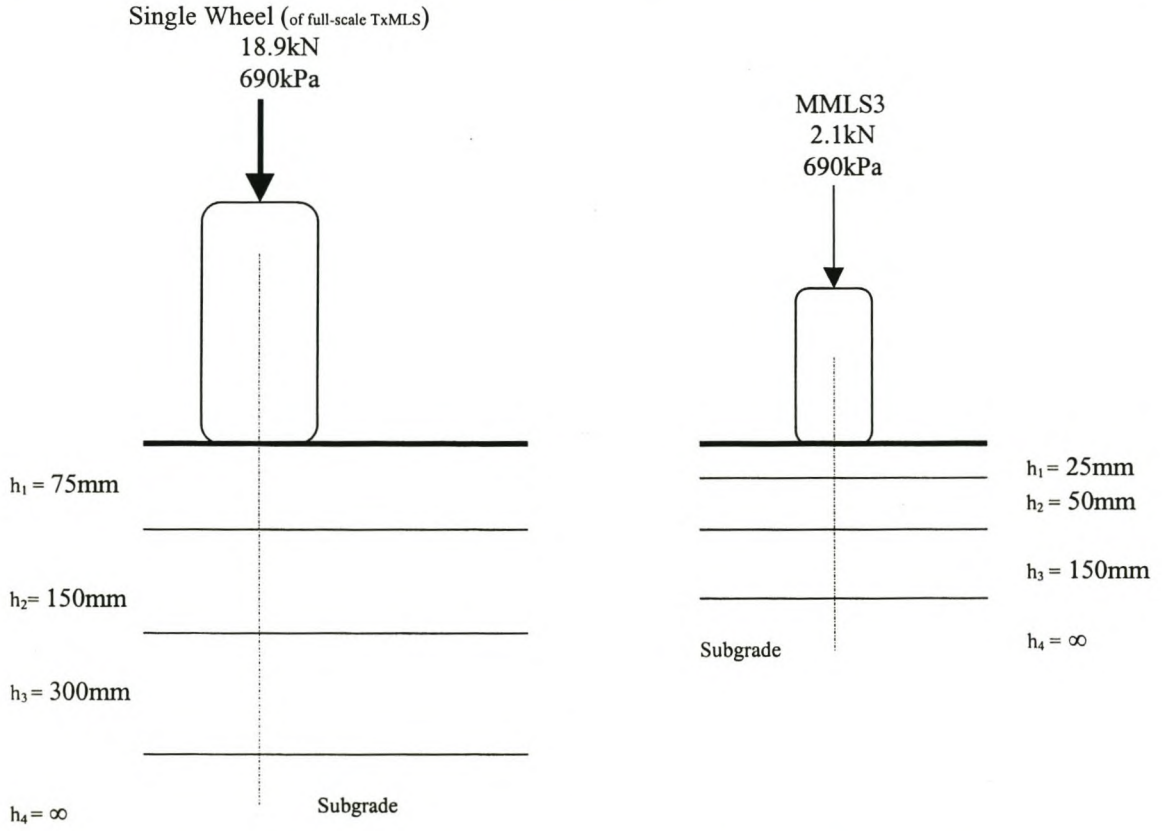

(a) Full-Scale Pavement (b) Scaled Model Pavement

Figure 2.5: Loading Parameters and Layer Thicknesses

2.2.3.2 Vertical Compressive Stresses

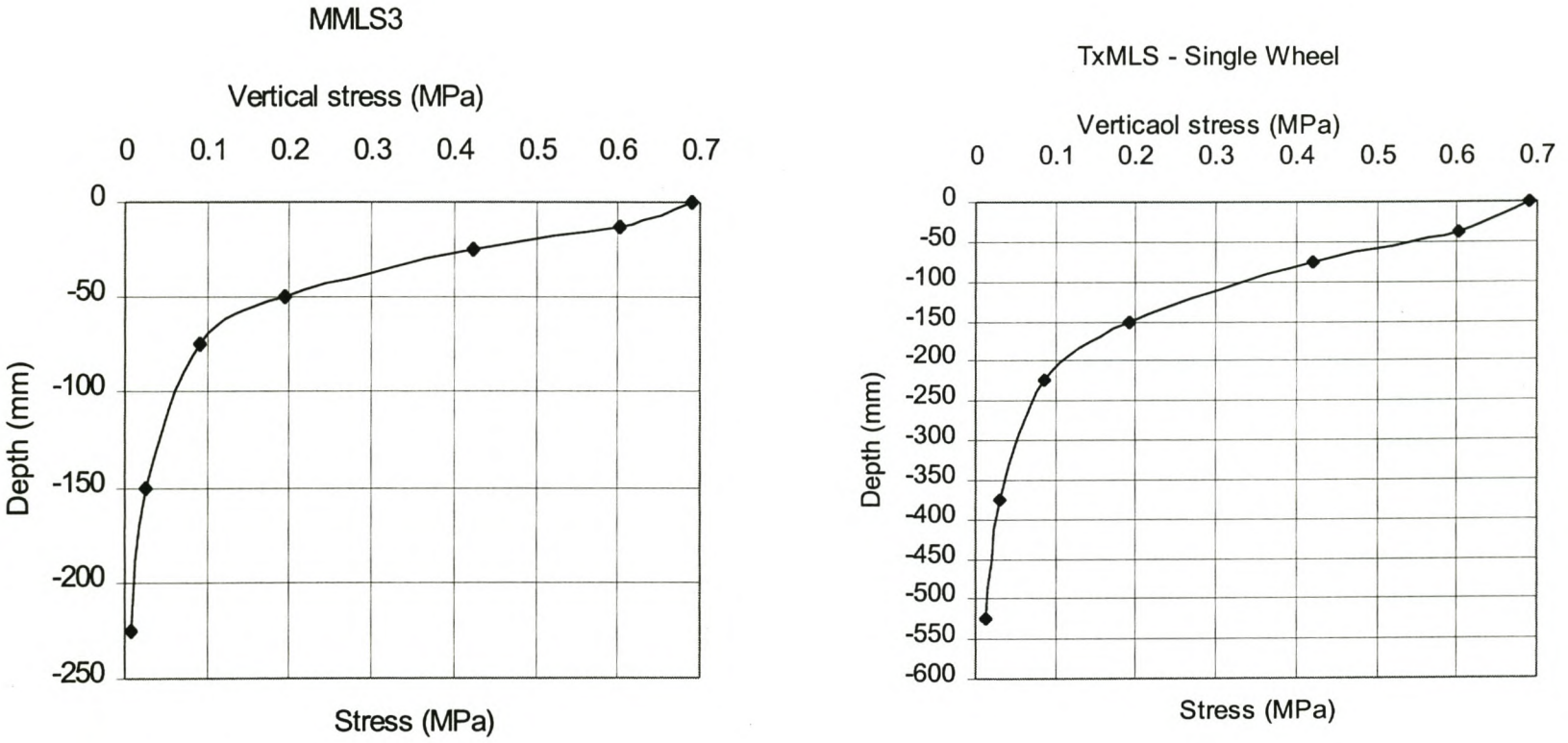

Figure 2.6: Vertical Stress Profile in a Scaled (MMLS3) and Full-Scale (TxMLS-Single Wheel) Pavement

The results of the calculations are included in Appendix I. Figure 2.6 shows that for the scaled model pavement under the MMLS3, the vertical stress magnitude within the layer depth are equal to those under the TxMLS. For example, the stress at the mid-point (12.5mm) of the top 25 mm layer under the MMLS3 is equal to stress at the mid-point (37.5mm) of the top 75 mm layer under the TxMLS. The stress magnitude at these depth points (12.5 and 37.5 mm) is 0.6MPa. Some examples from Figure 2.6 are shown in Table 2.5.

Table 2.5: Vertical Stresses for Scaled and full-scale Pavement

MMLS3 (Scaled Pavement)		**TxMLS – Single Wheel**	
Depth (mm)	Vertical Stress (MPa)	Depth (mm)	Vertical Stress (MPa)
0	0.69	0	0.69
-12.5	0.60	-37.5	0.60
-25	0.42	-75	0.42
-50	0.19	-150	0.19
-75	0.09	-225	0.09
-150	0.02	-375	0.03
-225	0.01	-525	0.01

The area (Figure 2.6) enclosed within the MMLS3 stress curve in the top three layers up to 225 mm depth was found to be about 0.35 that of the TxMLS (up to 525 mm depth). This is reasonably close to the expected ratio of 0.33. If the vertical stresses are assumed proportional to deformation, then the deformation (rutting) in a one-third factor scaled pavement under MMLS3 loading must be equivalent to the deformation on a full-scale pavement under TxMLS loading. Therefore, rutting performance prediction of a full-scale pavement under TxMLS (or real traffic) can be predicted based on MMLS3 testing of scaled model pavements. The application of this principle is useful for laboratory constructed or model pavement structures which can be scaled to simulate full-scale APT testing (and/or real traffic loading).

Fatigue (cracking) due to tensile stresses can also be modeled on the same principle of using a scaled pavement structure under the MMLS3. The results can then be related to an equivalent pavement structure under the TxMLS (or real traffic loading), provided similar materials and environmental conditions are used.

2.3.3 Surface Layers and the Effect of Milling

If only the surface layers are analyzed in a complex multi-layered pavement structure, the vertical stresses under the MMLS3 and TxMLS are comparable to each other.

If milling of some top layers is done, the vertical stress on the deeper layers under the MMLS3 is increased, thus to some extent making a closer simulation of full-scale loading, and providing a basis for exploring the hypothesis pertaining to vertical stress bowls and permanent deformation (rutting). For theoretical analysis, some of the top layers can be discarded so that analysis is done directly on the second layer or layer of interest. Figure 2.7 shows the results of this analysis. The TxMLS dual wheel configuration was used and analysis was done under one wheel.

Figure 2.7 shows that the vertical stresses are comparable after discarding off the top 100 mm AC layer under the MMLS3. The stress magnitude is infact higher under the MMLS3 at the top layer from about 100 to 200 mm depth. This is because, under the MMLS3 the new surface is the 100 mm depth under the TxMLS. In the field, milling of some of the top layers can also give an indication of the different pavement layers'/materials susceptibility to deformation.

Therefore, by analyzing only the top AC layers and/or by milling off some layers in a complex multi-layered pavement structure, vertical stress (and subsequently deformation) under the MMLS3 can be related to the TxMLS. This was the basis for deformation/rutting comparison in the Jacksboro project. This is discussed subsequently.

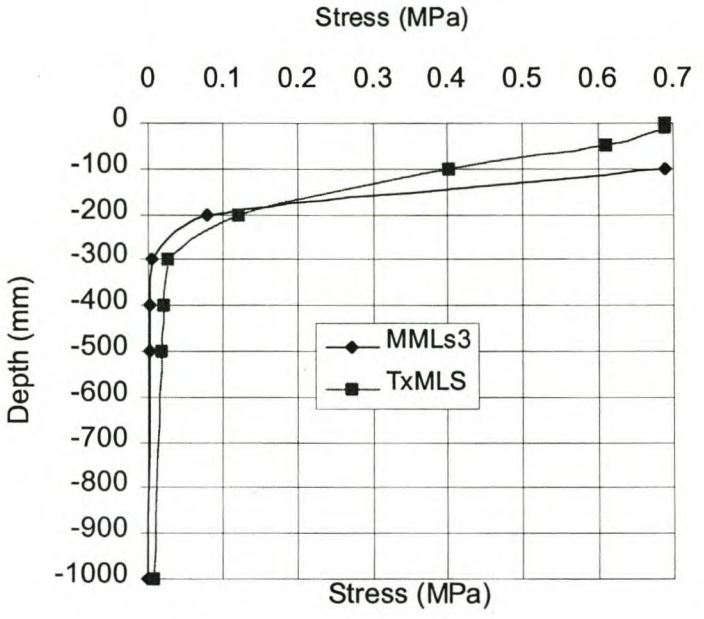

Figure 2.7: Vertical Stresses after Discarding Top 100 mm under the MMLS3
[h_1 = 300mm (asphalt), E_1 = 2 500MPa, $h_2 = \infty$ (subgrade), E_2 = 100MPa]

2.3.4 Shear Stresses

Figure 2.7 shows an example of the stress distribution under the center of the wheel in the top 200mm-asphalt layer for a simple two-layer pavement system with a stiff subgrade. Dual wheels were used for the TxMLS and analysis was done under one wheel. The Figure shows that with respect to the maximum shear stress in this particular asphalt layer, the critical zone in the case of the full scale TxMLS is the bottom of the layer. In the case of the MMLS3, the critical point is in the top zone around the 50mm depth. At this depth, the TxMLS also exhibits maximum shear stresses, which are comparable to the MMLS3, and therefore even shear deformation could be comparable at this depth level.

Overall, if deformation due to shear under the MMLS3 is considered, the top zone will be most affected, and the bottom most zone, in the case of the TxMLS. This analysis demonstrates the differences in the loading effect, which need to be taken into account when analyzing pavement response under these devices, especially in comparative studies.

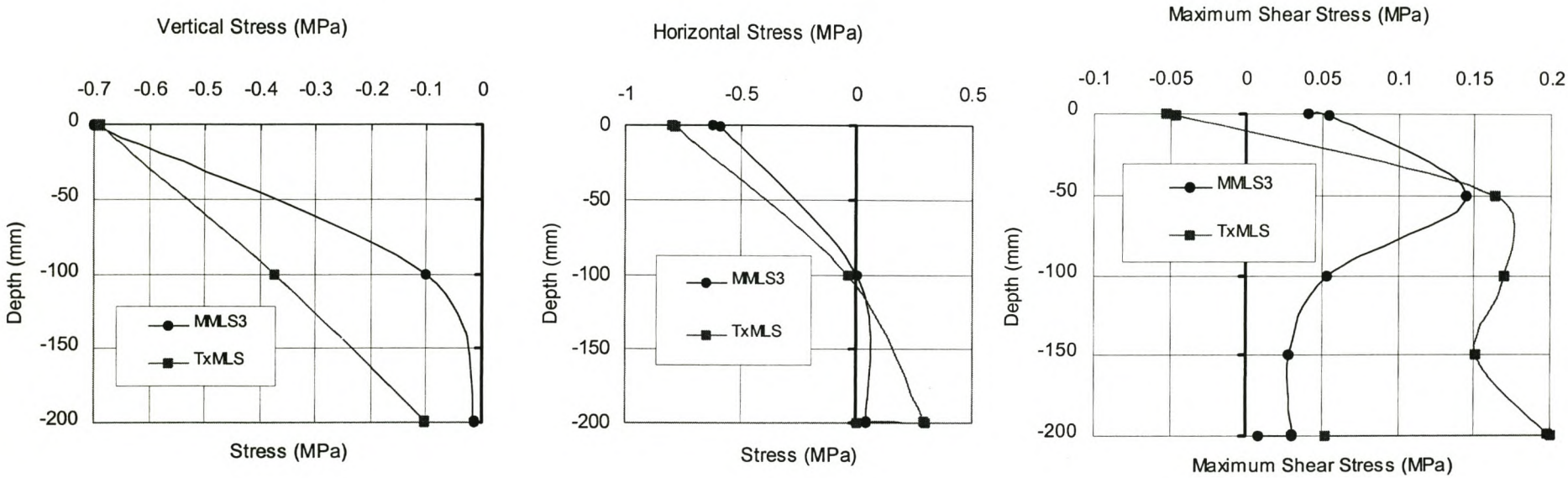

(a) Vertical stress ($\sigma_V \approx \sigma_1$) (b) Horizontal stress ($\sigma_H \approx \sigma_3$) (c) Shear stress ($\tau = 0.5(\sigma_1-\sigma_2)$)

Figure 2.8: Example of Stress Distribution in the Top 200mm Asphalt Layer

[h_1 = 200mm (asphalt), E_1 = 2500MPa, $h_2 = \infty$ (subgrade), E_2 = 400MPa, ν = 0.35]

2.4 SUMMARY

The technical details and modes of operation of the third-scale MMLS3 and full-scale TxMLS together with some schematic diagrams were given for clarity. Where as the TxMLS simulate real traffic loading, the 1/3 MMLS3 is relatively cost effective and can be used for testing on both full-scale in-service and modeling laboratory constructed pavement structures under different environmental conditions.

Stress distribution in the pavement under the MMLS3 and TxMLS- single wheel loading was analyzed. The theory of comparable stress distribution and one-third-scale factor hypothesis were investigated and validated. For the same material, pavement structure, and under similar environmental conditions, deformation or rutting under the MMLS3 is expected to be one-third of the TxMLS (or real traffic loading). If an equivalent scaled model pavement is used with similar material properties and environmental conditions, stresses are equal in magnitude to those under the TxMLS for a full-scale pavement structure. On this basis, response and performance can be predicted from the MMLS3 testing results of laboratory constructed or model pavement structures.

When only the surface top layers are considered, vertical and shear stress distribution under the MMLS3 are quite significant and can be comparable to the TxMLS. Discarding (or milling in the field) of some of the top layers/material induces stresses deeper down the pavement under MMLS3 loading, thus providing for a better vertical stress and deformation analysis in comparison to the TxMLS. As presented subsequently, this was the basis for the MMLS3-TxMLS deformation comparison analysis in the top AC layers of the Jacksboro pavement structures.

Since a stiff subgrade was used and only a single shear stress analysis was done, further research is recommended to supplement/validate the analytical findings reported for the shear stress distribution under the two APT devices.

Chapter 3

3 METHODOLOGY FOR APT TESTING WITH THE MMLS3 IN JACKSBORO

This Chapter presents in detail, the description of the test site, the pavement structures and the AC rehabilitation processes. The MMLS3 test pad details including dimensions, marking, instrumentation and set-up are also discussed. The type of tests, loading and number of axles applied on each test pad including the test methodologies is presented. An overview of the MMLS3 test operations and time-productivity is also given.

3.1 TEST SITE

The MMLS3 testing was done on highway US 281 near Jacksboro district in the state of Texas, USA. US 281 is an in-service four-lane highway, with two lanes in either directions (north and south respectively). The Fort Worth district engineer had indicated that there was an average of 3,100 vehicles traveling the highway per day (~1,550 per direction) in 1994, and that approximately 17.4% of the traffic was composed of trucks (Hugo et al, 1999 [c]). Approximately 10% of all the traffic travels on the inner lane. According to the "vehicle per day per lane" description criterion given in TRH4, and considering traffic growth since 1994, the US 281 traffic volume can be considered high and the pavement classified as ES8 (Department of Transport, 1997).

The north and southbound lanes are separated by a median of approximate 15m wide and are of different top surfacing material as will be discussed later. Testing was done on the inner-faster lanes, whilst the out side lanes remained open to traffic. The inner lanes were trafficked so as to test and model the less stressed pavement sections in terms of conventional (real) traffic loading. The outer slow lanes are mostly trafficked by heavy-duty trucks and would therefore be expected to be more stressed and/or damaged, which is undesirable for selection as APT test sections.

3.2 PAVEMENT STRUCTURES

The US 281 southbound (S) and northbound (N) lane pavement structures are shown below:

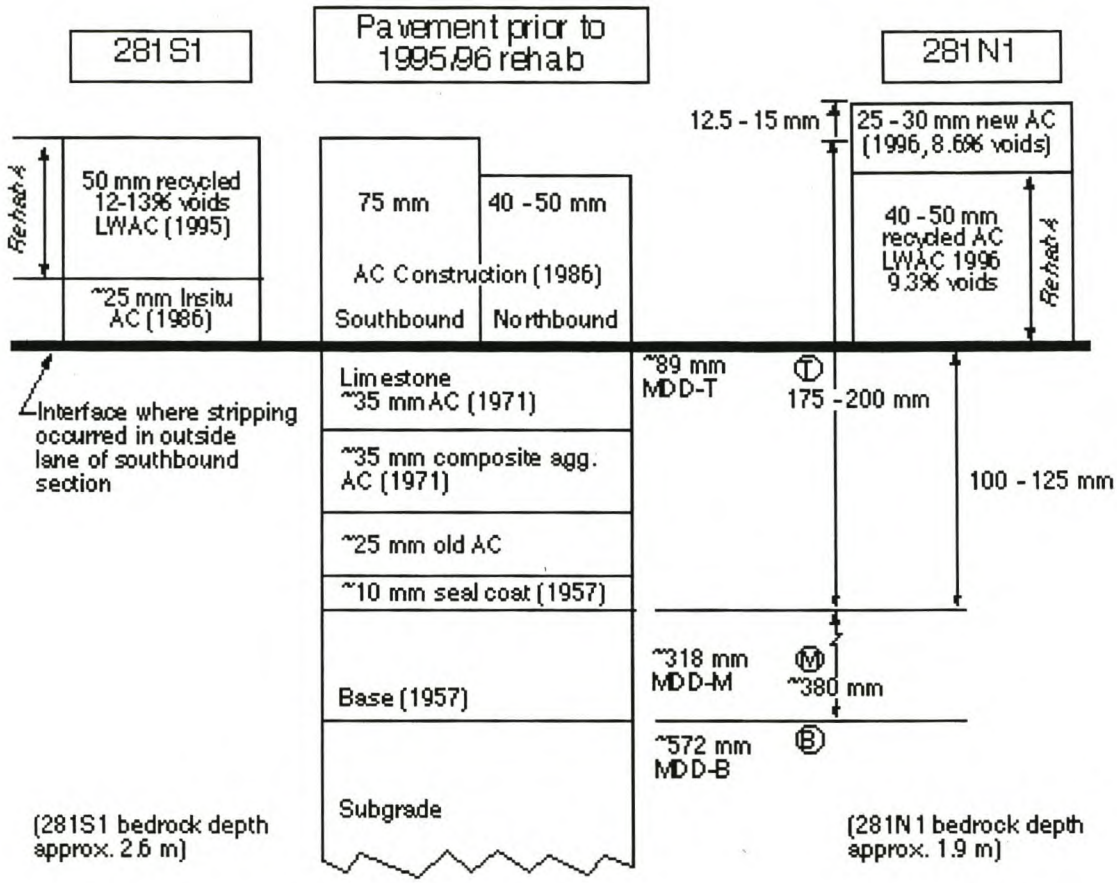

Figure 3.1: US 281 Pavement Structures

Prior to the application of the latest rehabilitation processes, the US 281 highway lanes (both north and south) were of similar material composition (Figure3.1). Both surfaces consisted of 50 to 75 mm of lightweight asphalt concrete (LWAC, overlaid in 1986), 85 mm of old asphalt surfacings (constructed in 1971 and 1976), and the original 15 mm seal coat, 380 mm flex base, and subgrade (constructed in 1957). The only difference was the depth to the bedrock, which is approximately 2.6 m on the southbound lanes and 1.9 m on the northbound lanes.

In 1971, 1976, and 1986, all the US 281 lanes were given a similar rehabilitation treatment of ordinary asphalt concrete (AC), composite aggregate AC, limestone AC, and lightweight aggregate asphalt concrete pavement (ACP), respectively. In the latest rehabilitation operation, the northbound and southbound lanes were overlaid differently using the *Dustrol* and *Remixer* processes, respectively.

3.3 THE REHABILITATION PROCESSES

The rehabilitation processes and materials used for the surface layers of the north and southbound lanes, respectively, are discussed below.

3.3.1 US 281 Northbound Lanes (*Dustrol*)

The Northbound lanes were re-constructed in 1996, using a *Dustrol* process. This entailed scarifying the LWAC insitu and treating it with *Reclamite* before compaction. *Reclamite* is rejuvenating oil. Thereafter it was overlaid with conventional limestone asphalt (about 25 mm thick). The conventional asphalt had an air void content of approximately 8.6% and the *Dustrol* 9.3% (Figure 3.1). Below the 25mm thick conventional asphalt is approximately a 45mm thick LWAC of which the upper 25mm was processed.

During the diagnostic studies it was found that there was a difference in the layer structure between the left and right wheelpaths of the trafficked inner lane. The left wheel-path cores had a distinct 25 mm top limestone asphalt surfacing layer, whilst some cores from the right wheel-path had an average of 15 mm thickness. This is discussed in more detail in Chapter 5.

3.3.2 US 281 Southbound Lanes (*Remixer*)

The two southbound lanes were rehabilitated in 1995 using the *Remixer* process, which is a 50mm (nominal) overlay of recycled and repaved lightweight aggregate with some fresh limestone asphalt added along with a dosage of *Reclamite*. The average air void content was about 12.5%. Immediately below the Remixer is an approximately 20mm thick insitu LWAC layer.

3.4 TEST PAD SELECTION AND MARKING

Once on site, the first step was to select a suitable test section and mark it. In this case, sections close to the TxMLS test section and the previous MMLS3 (1999) test pads were selected. It was assumed that test sections close to previously tested sections would provide a better comparison basis with regards to the response and performance of the pavement.

The MMLS3 test pad is shown in Figure 3.2 and consisted of a rectangular section of dimensions 500mm wide by 1200mm long with transverse gridlines at 200mm interval. The grids were marked by painting for easy positioning and centering of the MMLS3 machine as well as installation of the layer deformation pins (LDPs) and thermocouples, and taking of measurements with the Profilometer, portable seismic pavement analyzer (PSPA) and spectral analysis of surface waves (SASW) devices. Transverse profile measurements were taken along the seven (7) transverse gridlines whilst the grid intersection points were used for the PSPA and SASW measurements.

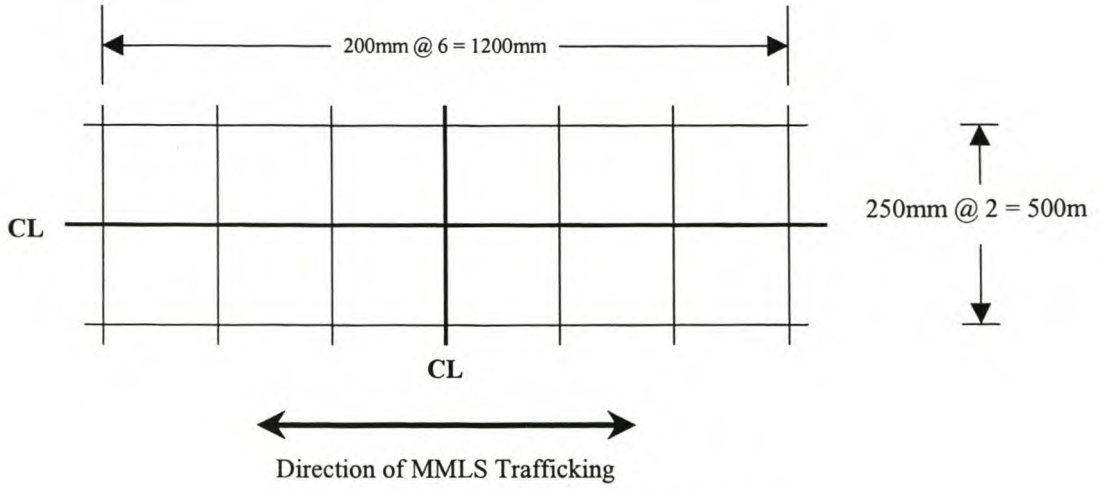

(a) Typical Test Pad Dimensions

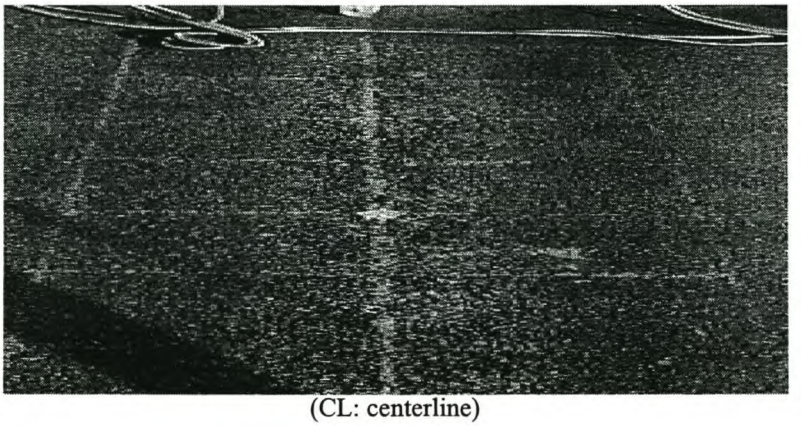

(CL: centerline)

(b) A Marked Test Pad on the Pavement Surface

Figure 3.2: MMLS3 Test Pad

An important requirement is to select a flat area with even surface (and if possible uniform material properties) as the MMLS3 test site, so as to ensure a uniform surface-contact load and comprehensive results. Such a site also facilitates easy MMLS3 setup and trafficking. A flat, even surface reduces mechanical problems during trafficking and facilitates easier measurements. Uncontrolled dynamic load effects are also minimized. In addition to these requirements, the surface also had to be crack free with no visible ruts. The presence of non-MMLS3 associated distresses (e.g. cracks and/or ruts) could adversely affect the final results (i.e., the defects could exaggerate the MMLS3 trafficking effect on the pavement and thus distort the results).

It is also important to do radar scanning and coring for material characterization tests to determine the homogeneity of the pavement materials and provide insight into the expected performance prior to selecting the pads. This is particularly important if the test pad performances are to be compared. Prior knowledge of the pavement layer structure such as thickness details is also necessary.

3.4.1 Test Pads

Six tests were conducted during the months of May, June and July 1999 on six test pads namely, *n1, n2, n3, s1, s2,* and *s3.* The test pad details and test types that were conducted are shown in Table 3.1. The tyre pressure was 420 and 690 kPa for the hot and wet tests, respectively. The MMLS3 axle load was 2.1kN for all the tests.

Table 3.1: Test Pad Details and Type of Tests

Test No:	Test Pad	Surface Type	Test Type	Tyre Inflation Pressure (kPa)	Trafficking Temperature @ 25mm depth (°C)	Axle Loads Applied
1	*n1*	Smooth (Top Surface)	Hot	420	50	320,000
2	*n2*	Rough (~25mm milled off)	Hot	420	50	160,000
3	*n3*	Rough (~25mm milled off)	Wet (1mm water)	690	30	320,000
4	*s1*	Smooth (Top Surface)	Hot	420	50	180,000
5	*s2*	Rough (~40mm milled off)	Hot	420	50	80,000
6	*s3*	Rough (~40mm milled off)	Wet (1mm water)	690	30	160,000
Total axles applied						**1,220,000**
Axle load in kN:						2.1
Temperature tolerance during MMLS3 trafficking						±2°C

The *n*-tests (*n1, n2, n3*) were conducted on the inner-fast northbound lane of US 281, whilst the s-tests (*s1, s2, s3*) were conducted on the inner-fast southbound lane of US 281. The milled sections were of nominal dimensions 5.0m long and 2.5m wide.

3.4.2 Instrumentation and Machine Set-Up

Once a test pad was selected and marked by painting, four-layer deformation pins (LDP) were installed on the center-longitudinal grid line to measure the relative deformation of the pavement layers with MMLS3 trafficking. Figure 4.5 (Chapter 4) shows the LDP measuring gauge and LDP pin installation details. Thermocouples were then installed at various depth points within the pavement structure to monitor the pavement temperature. Two temperature probes as shown in Figure 4.2 (Chapter 4) were used for measuring the temperature.

Figure 3.3: Drilling to install LPDs on Test Pad *S3*.

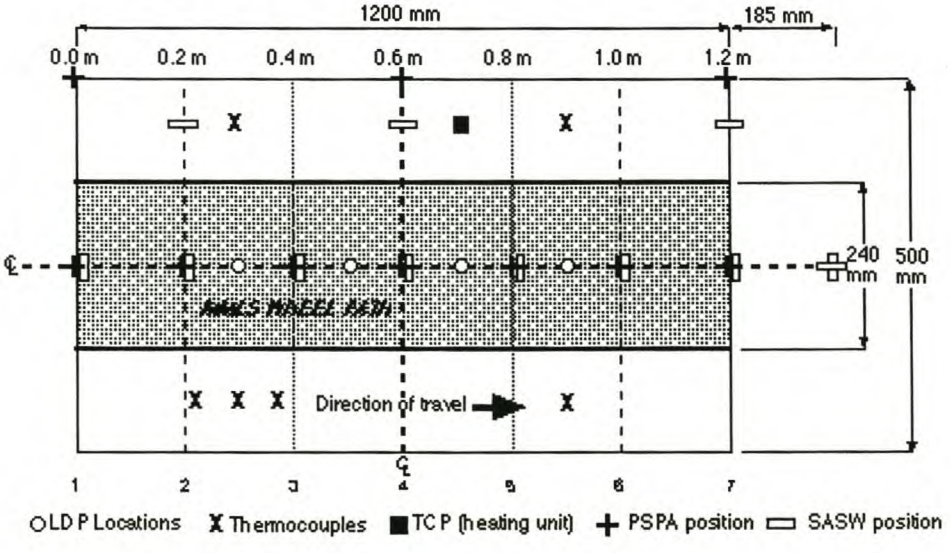

Figure 3.4: LDPs and Thermocouple Locations.

Finally, the profilometer guide rails used in taking profile measurements were fixed into the pavement (with nails) longitudinally along the test pad. The test pad was then thoroughly swept in preparation for taking the initial zero (0k) measurements. These included the transverse profiles (with the profilometer), LDPs, PSPA, and temperature measurements. An air compressor was also used for blowing away loose particles from the test pads prior to MMLS3 trafficking and measurements, (loose particles on the test pad surface distort profilometer readings).

The MMLS3 machine would then be positioned on to the test pad by longitudinally and transversely centering it along the two centerlines (transverse and longitudinal) of the test pad. Its mobility wheels would be detached and the machine would be set on to the test pad as described in the MMLS3 operations manual (Muller, 1999).

3.4.2.1 Hot Tests

For the hot tests (*n1, n2, s1,* and *s2*), the MMLS3 machine and test pad would be covered in the heating chamber prior to commencement of trafficking and heated until the 50° C desired trafficking temperature at 25 mm depth was reached. The heating process entailed blowing heated air across the test area intermittently from both sides. During trafficking, the temperature tolerance was 50±2° C. The average heating time prior to start of trafficking was 5 hours. To maintain the 50° C trafficking temperature, heating was continued through out the MMLS3 runs. The heating unit had an automatic control thermostat to regulate the heating process. The heating unit was set to a control temperature of 55° C with a differential temperature range of 2° C. The thermostat probe (TCP) was embedded at a depth of 10mm within the test pavement.

The pavement was heated so as to traffic the surface at a temperature (50° C) more realistically related to the critical temperature of the asphalt mix for the region. This gave an indication of the effects of high temperature on the rutting of asphalt. The heating unit together with the temperature chamber is shown in Figure 3.5.

(a) Heating unit

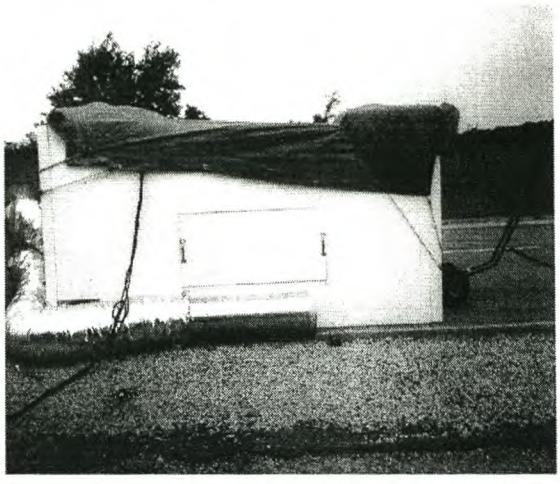

(b) Temperature chamber

Figure 3.5: The MMLS3 Heating System

The dimensions of the temperature chamber are nominally 3 100mm long x 1 250mm wide x 1 310mm high.

3.4.2.2 Wet Tests

MMLS3 trafficking commenced immediately after set up on the wet tests on test pads *n3* and *s3*. Heating was in most instances unnecessary as the temperature at 25mm depth was always at the desired 30±2° C trafficking temperature. During trafficking, approximately 1mm thick sheet of hot water (at about 45° C) flowed across the milled test pads. One-mm thick sheet of water is equivalent to about 5mm rain per hour (Smit et al, 1999). The application of hot water also aided in maintaining the 30±2° C trafficking temperature.

2.4.2.3 Milled Test Pads

On the northbound sections, the top 25mm fresh overlay limestone asphalt was milled off to allow trafficking to be done on the surface of the *Dustrol* layer on test pads *n2* (hot) and *n3* (wet) respectively. In the southbound structure, *s2* (hot) and *s3* (wet) had a nominal 40mm top surfacing *Remixer* layer milled off. The intention was to traffic the second LWAC underlying layers, and compare their response to that of the new rehabilitation surfaces.

Prior to marking and painting of the milled test pads, the rough milled surfaces were smoothened using an electric grinder. This was necessary to have a uniform contact load with the surface along the entire section of the test pad.

Figure 3.6: Grinding to smoothen Pad *s3* (southbound lane)

3.5 MMLS3 TEST-OPERATIONS

During MMLS3 trafficking, the machine was stopped hourly to check the tyre pressure, tyres, and rims. Rim bolts and nuts frequently sheared off during trafficking on the milled surfaces (*n2, n3, s2,* and *s3*), resulting in skew of the rims and tyre punctures. This problem necessitated a regular check of the MMLS3.

For operations on the s-test pads (southbound lane), traffic cones had to be put on the road at around 6 a.m. or 7 a.m. and removed at 5 p.m. or 6 p.m. for traffic control. Sand and 25 mm thick steel plates (Figure 3.7) were used for covering the milled test pads (*s2* and *s3*) to allow traffic flow after working hours, at night, and during weekends and holidays.

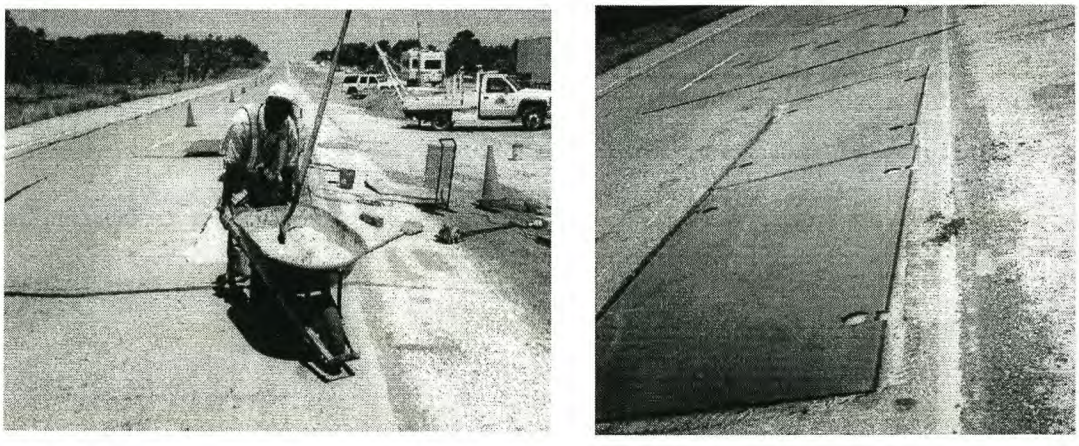

(a) Removing sand (b) 2 440 x 1 250 x 25 mm steel plates

Figure 3.7: Operations on Test Pads *s2* and *s3* (southbound lane)

The sand was intended to prevent the steel plates from resting directly on the pads. It also cushioned the test pads against any form of non-MMLS3 induced distress or damage that could result from uneven contact with the steel plates. The holes and grooves in the steel plates were used for chain hooking the steel plates for easy handling. A TxDOT crane was used for lifting the steel plates.

After work hours and during weekends, the MMLS3 machine was moved to the northbound lane and onto the *n*-test pads for continued trafficking. The inner northbound lane was permanently closed to traffic at the test site.

3.6 MMLS3 TIME-PRODUCTIVITY AND PROBLEMS FACED

After a specific number of axles had been applied, the MMLS3 machine and the heating unit (in case of the hot tests) were stopped and the whole set-up (MMLS3 machine, heating unit and temperature chamber) removed from the test pad. Data were collected, and the machine (together with its heating accessories, for the hot tests) re-set on to the test pad for continued trafficking. This procedure was repeated for each test pad until a target axle count to yield reasonable rutting as theoretically anticipated was reached, or the testing terminated.

A total of 800,000 axle loads were applied on the northbound lane (*n*-tests) and 420 000 on the south (*s*-tests). Time factor and logistical constraints did not allow for the continuation of the *s*-tests to 800 000 axle loads like their counterparts on the northbound lane (*n*-tests). Therefore, some of the *s*-test results were extrapolated/interpolated as presented subsequently in Chapter 6.

During trafficking, the MMLS3 was interrupted only for the hourly inspections, measurements at the end of target axle counts, and mechanical breakdowns. Mechanical problems were encountered especially on the milled test pads due to the uneven surface.

Figure 3.8 shows the breakdown of the test period into test set-up, heating, MMLS3 trafficking, data collection (measurements and taking of readings), maintenance, and non-operational time.

3.6.1 Test Set-Up

Test set-up time included test site selection, test pad marking, LDP and thermocouple installation, power supply set-up, MMLS3 and heating system set-up, removing and putting back of traffic cones, sand and steel plates on the road and milled test pads respectively, as well as fetching of hot water.

3.6.2 Maintenance and Mechanical Problems

Maintenance included MMLS3 inspection, repair to the machine and time spent looking for spare parts as well as fitting the new parts. The major mechanical problems experienced were:

- The internal drive belt had snapped off and a new fan belt had to be bought for replacement.
- One rim was ripped off and completely skewed beyond repair.
- Two tubes were extensively punctured beyond mending due to sheared off bolts and skew rims, and two new tubes had to be bought.
- Rim bolts and nuts on the old rims had continuously sheared off, apparently due to non-uniform tyre/load contact with the surface, and had to be replaced continuously. This problem was encountered especially on the rough milled surfaces.

However, some of these problems were subsequently addressed with the switch to more robust wheel rims, and grinding of the surfaces to make it even, in the case of the milled pads.

3.6.3 Electrical and Water

One minor electrical problem experienced was fusing, probably due to overload caused by failure of the drive wheels to rotate resulting in more electrical power being drawn from the power source. No water related problems were encountered.

3.6.4 Non-Operational Time

Non-operational time is defined as that time during the test period when the machine was intentionally not run (or due to uncontrollable circumstances). This included the times when a target axle count was reached say at mid-night, and measurements could only be conducted in the morning, the following day. It also included the times when there was no power supply, thunderstorms and rainfall.

3.6.5 The Time Chart

As seen from the time-pie chart (Figure 3.8), the test set-up (15%), data collection (12%) and maintenance (10%) times were unreasonably high. The high set-up time arose from the MMLS3 set-up on the milled test pads including traffic control and handling of the sand and steel plates on the southbound lane. Measurements on the milled surfaces equally required extra care and precision. PSPA measurements had to be repeated several times to get good readings. The high maintenance time was basically due to the mechanical problems outlined in subsection 2.6.2.

On overall, about 60% of the total test period was active heating and MMLS3 trafficking, and 40% was spent on test set-up (15%), data collection (12%), maintenance (10%) and non-operational (3%) time.

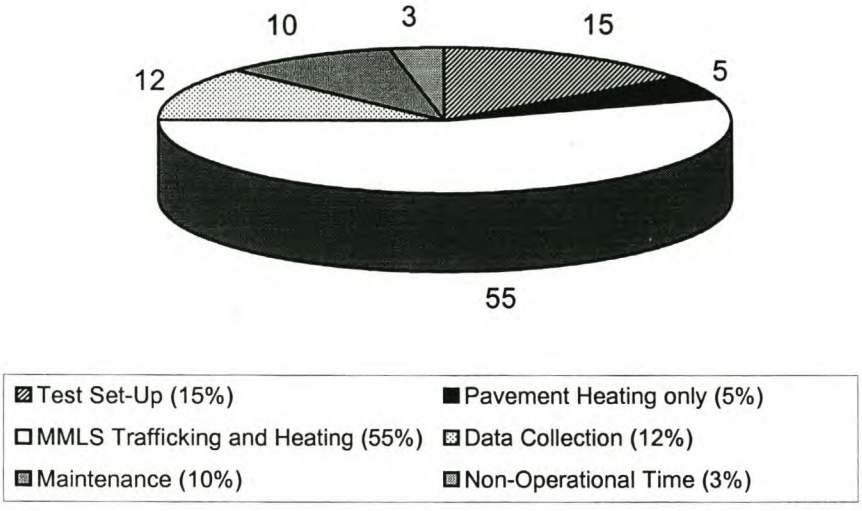

Figure 3.8: MMLS3 Time-Pie Chart

3.7 SUMMARY

An overview of the test site location and an indication of traffic in terms of volume on highway US 281 were given. The traffic volume reported indicates that highway US 281 is quite a busy road. The pavement structures together with the rehabilitation processes were described. The test pad details, tests conducted and some of the problems encountered during testing were highlighted.

The development of the MMLS3 test set-up was described. During MMLS3 trafficking, it is important that there is a uniform contact load with the pavement surface along the entire trafficking sections; otherwise uneven load contact can distort the results. Surface evenness and non-existence of physical distress are some of the key factors influencing the choice of an MMLS3 test section. Knowledge of the pavement material characteristics and the pavement layer structure is also very significant. Prevailing site conditions are another contributing factor, which cannot be ignored.

A solution had to be found for the conventional traffic flow on the test pads during the rest periods on the southbound lane. In this case, sand and 25mm thick steel plates were used to cover the milled test pads.

Chapter 4

4 FIELD MEASUREMENTS AND DATA COLLECTION

The following were monitored during MMLS3 trafficking;

- Axle Counts
- Temperature
- Surface Rutting
- Surface Cracking
- Pavement Layer Deformation
- Pavement in situ Asphalt Moduli (PSPA and SASW)

4.1 MMLS3 TRAFFIC AXLE COUNTS

Axle counts were monitored hourly from the electronic counter installed in the MMLS3 control unit (Figure 4.1) till a target axle count was reached. Target axle counts were done in the following sequence; 0k→20k→40k→80k→160k→320k. The notation "k" stands for 1 000.

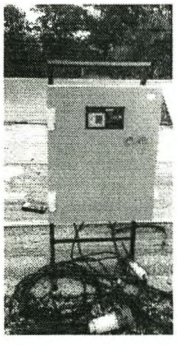

Figure 4.1: The MMLS3 Control Unit

The MMLS3 control unit also houses the main start (Green) and stop (Red) switches as well as the frequency monitor for the MMLS3 machine. In the 1999 tests, the control frequency was preset to 46mHz with a total load application of 6, 900 axles per hour.

4.2 TEMPERATURE MEASUREMENTS

Temperature measurements were taken hourly to effectively monitor the temperature variations during MMLS3 trafficking. Readings were taken of the air temperature, the pavement surface, the control unit of the pavement heating system, and from the thermocouples installed within the test pads at various depths within the pavement layers. The six temperature readings were denoted as follows:

Table 4.1: Thermocouple Depths

No:	Thermocouple Designation	Depth (mm)	Purpose
1	Air	Air	Air temperature
2	TS	00	Pavement surface temperature
3	T1	25	Pavement temperature
4	T2	75	Pavement temperature
5	T3	95	Pavement temperature
6	TCP	10	Control of Heating Unit

Thermocouples and temperature probes (shown in Figure 4.2) were used for measuring the temperature. Three thermocouple wires marked T1, T2, and T3 were imbedded in the pavement at various depths as indicated in Table 4.1 above. The temperature control pin (TCP) of the thermostat was used to control the heating process. The measured mean MMLS3 trafficking temperatures are shown in Table 2.4.1, in Appendix II.

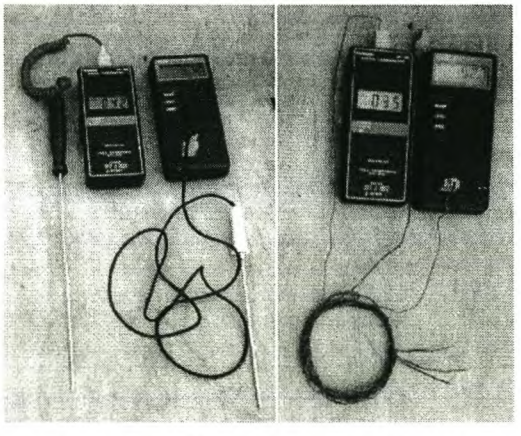

Figure 4.2: Temperature Probes and Thermocouple Wires

4.3 SURFACE RUT MEASUREMENTS

A profilometer was used to measure transverse profiles across the test pad after each target axle count at an interval of 10mm, to monitor the surface rut growth. For every target axle count, seven transverse profiles were measured along the 0.0m, 0.2m, 0.4m, 0.6m, 0.8m, 1.0m, and 1.2m lines respectively, from left (L), designated as the zero reference point, through the centerline (C) to the right (R) end of the test pad as shown in Figures 4.3 and 4.4. No longitudinal profile measurements were done. The profilometer measures change in height relative to a position that is assigned fixed co-ordinates.

(a) Computer data set-up

(b) Data capturing system [Taking readings on test pad *n1*]

Figure 4.3: The Profilometer Device

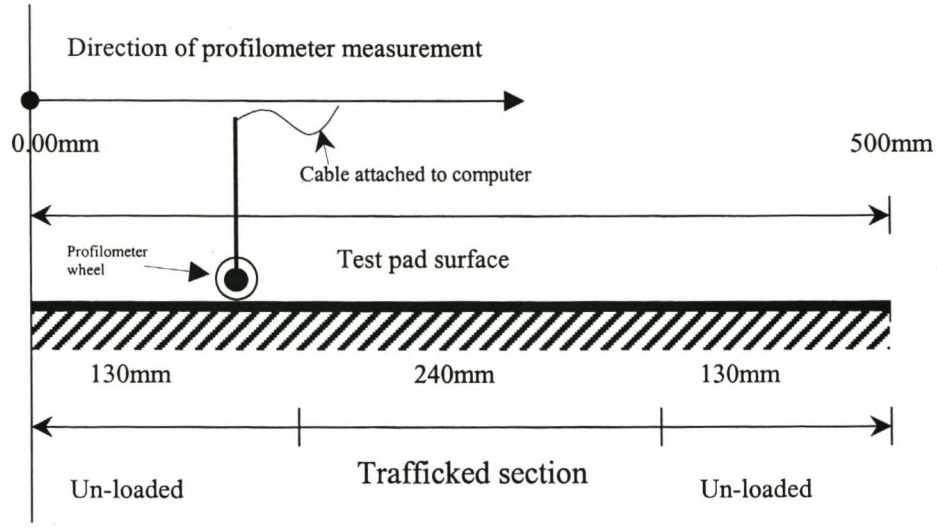

Figure 4.4: Transverse Surface X-Section of the Test Pad
[Also see Figure 6.3]

As can be seen from Figure 4.4, transverse profile measurements ran across the test pad from the zero point (left) to the 500 mm point at the right end of the test pad (covering both the untrafficked and trafficked sections). The profilometer measured to a positional accuracy of ±0.125 mm

4.4 SURFACE CRACKING AND STRIPPING

Surface crack development and stripping were visually monitored prior to testing and after each target axle count. Micro cracks and stripping were only evident on the wet test pads *n3* and *s3*, at the end of MMLS3 trafficking.

4.5 PAVEMENT LAYER DEFORMATION

Four small Layer Deformation Pins (LDP) were installed within the pavement layers at various depths to measure the relative deformation in the top asphalt surface layers. The LDPs were denoted as follows:

Table 4.2: LDP Depth Details

No:	LDP Designation	Depth in mm	
		s-Test Pads (Southbound lane)	*n*-Test Pads (Northbound lane)
1	D1	25	25
2	D2	50	50
3	D3	70	70
4	D4	85	95

The depths were selected to obtain information at layer interfaces, and to enable a well-distributed profile of deflection with depth to be established. LDPs readings were taken every after each target axle count beginning from the 0k. All LDPs were installed directly under the centerline (C) of the test pad as shown in Figure 4.5. Figure 4.6 shows the LDP gauge and installation details.

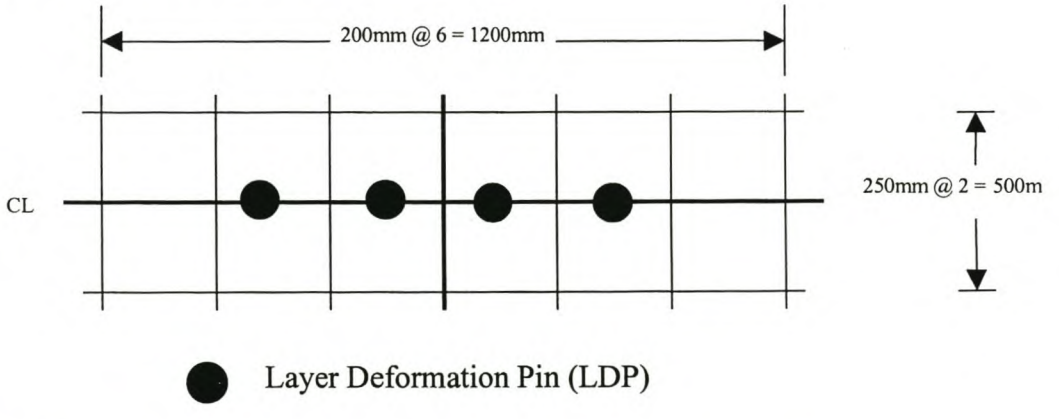

Figure 4.5: LDP Location Points on the MMLS3 Test Pad

After the 10mm diameter hole was drilled to the required depth level of measurement, the LDP was inserted into the hole and its base firmly anchored using epoxy to the sides and base of the hole as shown in Figure 4.6. A hard plastic or steel tube big enough to fit tightly was then inserted into the hole up to the point where it touches the LDP base. This was to prevent the sides of the hole from collapsing under MMLS3 traffic loading. It is important that the LDP is well assembled and securely anchored to the base of the hole. Any movement within the LDP mechanism or of the anchor position can distort the readings.

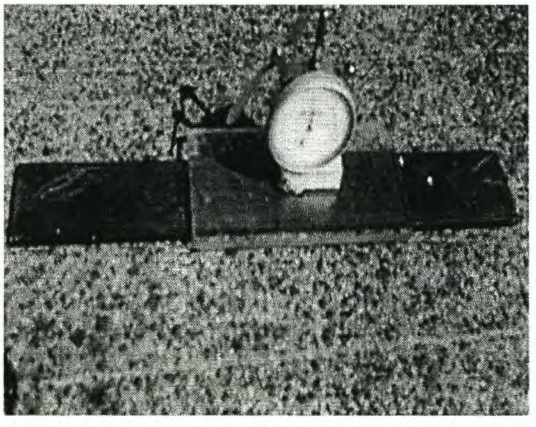

(a) LDP Measuring Gauge

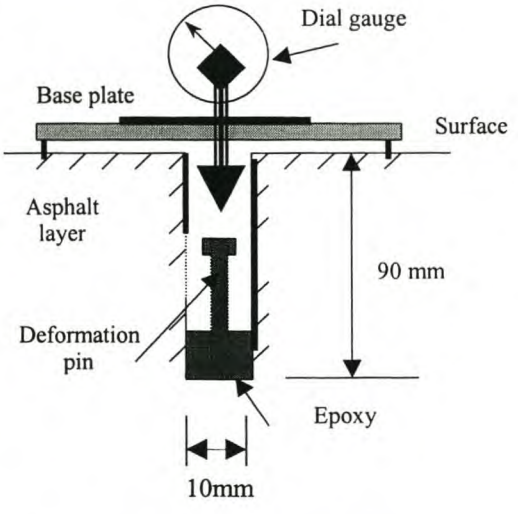

(b) LDP installation details

Figure 4.6: The Layer Deformation Pins (LDP)
[The 5mm thick steel bar acted as the reference base (benchmark) during measurements]

The vertical distance from a reference fixed point (in this case the steel base plate) on the pavement surface to the head of the pin is the measurable parameter. This was measured with the dial gauge as shown in Figure 4.6 above. The gauge measures to an accuracy of ±0.002 mm. The steel base plate was not permanently fixed on the pavement, but rested on steel nails, whenever measurements were taken. The steel nails were permanently nailed/fixed into the pavement using epoxy on either side of the MMLS3 wheel track.

The deformation pin is assumed to move along with the pavement as it deforms vertically. By comparing the readings measured after applying some axles to the readings taken at 0k (without any axle loads), the vertical movement at that depth level was obtained. The difference between the vertical movement measured at a given depth level and the total surface rut measured on the pavement surface is the deformation of the layer/material between the surface and that depth level. Similarly, the difference in vertical movements between two LDPs inserted at different depth points can give information on the deformation of the layer/material between those two depth points.

4.6 THE INSITU PAVEMENT AC MODULI

The Portable Seismic Pavement Analyzer (PSPA) and the Spectral Analysis of Surface Waves (SASW) devices were used to measure the in situ pavement AC Moduli. The intention was to monitor the in situ AC (asphalt) moduli change with MMLS3 trafficking. The moduli measurements are based on the velocity of wave travel through the pavement (Hugo et al, 1999 [c]).

4.6.1 The Portable Seismic Pavement Analyzer (PSPA)

PSPA measurements were done after each target axle count beginning from 0k up to the termination of the tests. The measurements were conducted at seven longitudinal and seven transverse positions along the test grid on the centerline as indicated in Figure 4.7 The grid positions 250 mm left from the trafficking line (centerline) were used as the control points. Three longitudinal and three transverse PSPA measurements were taken from the control gridline at control points 0.0m, 0.6m, and 1.2m, respectively. Thus for each set of PSPA measurements, 20 readings were taken, 10 transverse and 10 longitudinal. The PSPA measured to a depth of approximately 80mm. Air and pavement surface temperature measurements were also taken during PSPA measurements, precisely at the start and stop of the PSPA measurements, as shown in Table 2.4.3, in Appendix II.

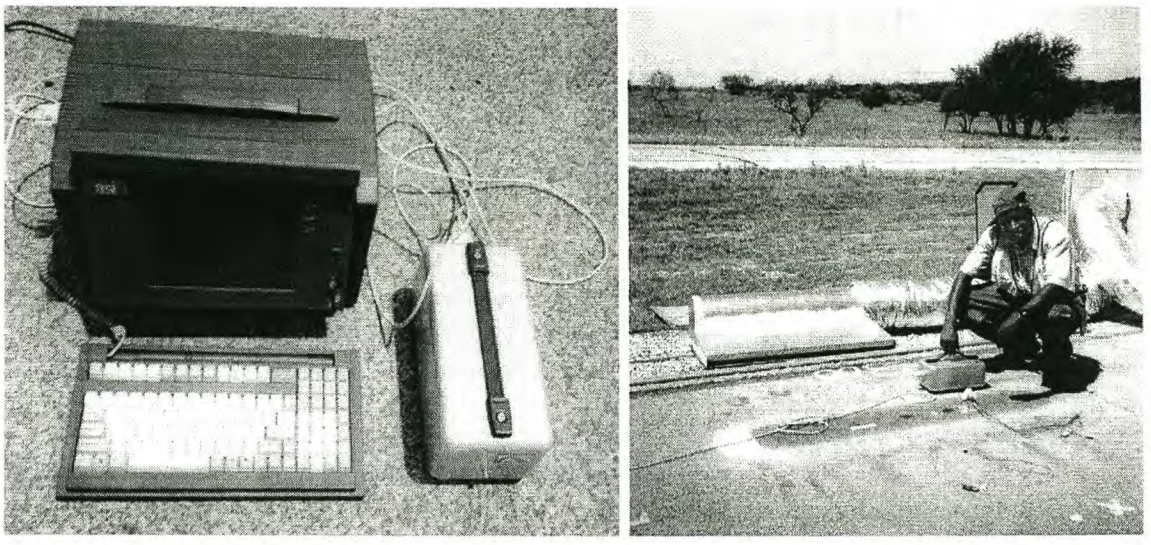

Figure 4.7: PSPA Instrument and Taking of PSPA Measurements on Test Pad *n1*

4.6.2 The Spectral Analysis of Surface Waves (SASW)

Sets of SASW measurements and corresponding pavement surface temperatures (Table 2.4.2, Appendix II) were taken for each test pad at selected points. Like the PSPA, the SASW measures wave velocity through the pavement, which is related to the material stiffness (Auad et al, 2000, 1993, and Nazarian et al, 1986 and 1986). Wave velocity measurements with the SASW device (Figure 4.8) were conducted at the points shown in Figure 4.9. These measurements were conducted to calculate the approximate asphalt moduli during trafficking compared with those from the untrafficked sections (i.e. SASW measurements T8 to T13).

Control measurements on the untrafficked sections were measured from positions T8 to T12. Measurements T11 and T12 were either taken at position A or B as shown in Figure 4.8 The SASW device was set to a maximum measuring frequency of 50kHz, and the spacing between the sensors was 150 mm. This meant it could measure up to a maximum depth of 150 mm within the pavement structure. However, interest was only in the top surface layers.

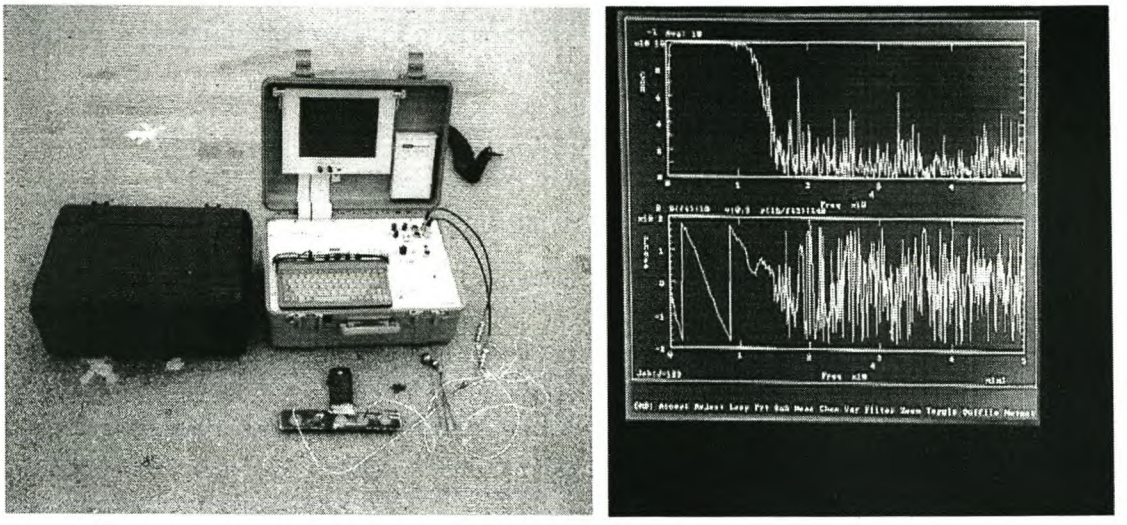

(a) SASW device

(b) SASW wave display

Figure 4.8: The SASW Device

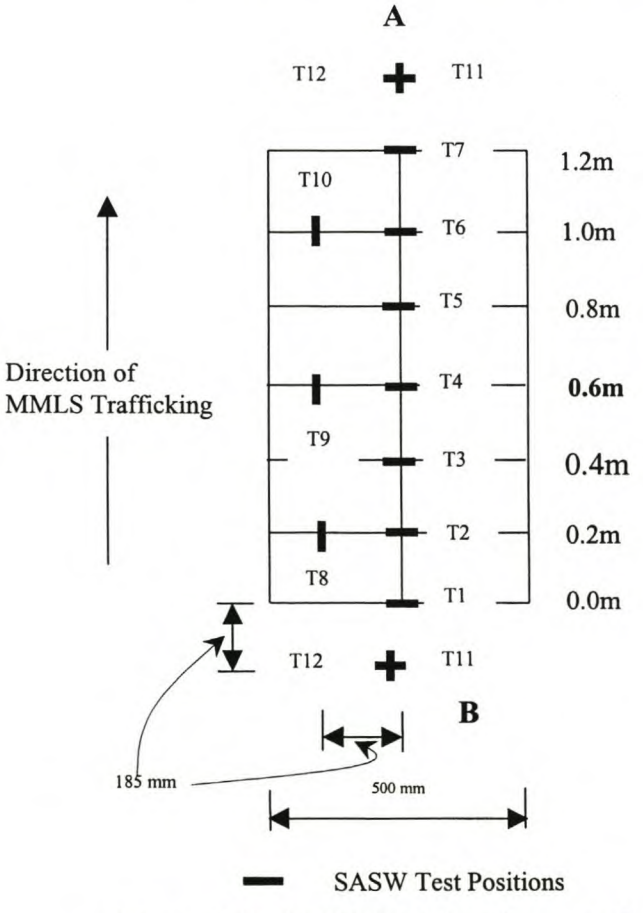

Figure 4.9: SASW Test Positions on the Test Pad

4.7 SUMMARY

Among the parameters monitored during MMLS3 trafficking were; the axle load repetitions, temperature, surface rutting, surface cracking, pavement layer deformations and the in situ asphalt stiffness. These are some of the basic data measurements required for evaluating pavement response and performance under APT testing.

When installing the LDPs (for measuring layer deformations), care should be taken to ensure that they are firmly anchored in the pavement at the depth level of measurement. The LDPs should also be well assembled and fixed properly so as not to allow any movement within the LDP mechanism. Movement of the LDP anchor position or of the LDP mechanism can influence the measurements and thus distort the results. Due to the sensitive nature of the LDP measurements, the rest points (in this particular case, steel nails) for the steel base plate (reference point for the LDPs measurements) must be well secured outside the MMLS3 wheel path. Movement of the steel nails or disturbance to them can distort the readings.

The asphalt stiffness exhibits great sensitivity to temperature. It is strongly recommended to always make a record of the pavement temperature whenever in situ asphalt stiffness measurements are being done. Furthermore, the measured temperatures may be required to normalize the asphalt moduli to one standard temperature value, say 25° C.

Chapter 5

5 LABORATORY TESTING AND MATERIAL CHARACTERISATION

Several laboratory tests were conducted to supplement the MMLS3 field tests and to characterize the pavement materials. This provided information on;

- Volumetric properties of the materials;
- The shear and elastic stiffness, as well as the phase angle, of AC at different temperatures and loading frequencies;
- Material strength before and after MMLS3 trafficking under different conditions (hot, dry, and wet);
- The remaining fatigue life after MMLS3 trafficking, as well as relative fatigue damage caused by MMLS3 trafficking; and
- Susceptibility of the asphalt material to water damage.

The laboratory test results served as an assessment of the material resistance to permanent deformation, loss in strength, degradation, stripping, and MMLS3 traffic damage under different conditions (hot, dry, and wet). This greatly enhanced insight into the field performance of the three upper layers of asphalt concrete under MMLS3 trafficking. The findings were then correlated to the field results to enable conclusions to be drawn and recommendations made.

Table 5.1 shows the test programme.

Table 5.1: Laboratory Test Programme

No:	Test	Purpose	Test Specifications & References
1	Volumetrics	Material density, BRD	Standard Test Method C3 – TMH1
2	Frequency-Shear	Shear and elastic modulus, and phase angle	At 25°C and 40°C (Epps, 1999)
3	Moisture Sensitivity	Retained ITS after wet processing for 2hrs	AASHTO test method T283 (1998)
4	Indirect Tensile Strength Test (ITS)	Material indirect tensile strength	Indirect strength determination in axial (diametral or ITS) mode. Displacement-loading rate: 50mm/min at 20°C
5	Indirect Tensile Fatigue Tests	Measure of fatigue life (count of number of load repetitions to fatigue failure) at fixed temperature	Repeated haversine load at 10Hz frequency (10 pulses per second), in diametral (axial or ITT) mode and at a stress level of 20% ITS core strength. 90° in the direction of MMLS3 trafficking. 100N pre-load and 2-24hrs temperature conditioning to 20°C.
6	Semi-Circular Bending (SCB) Test	SCB strength and tensile stresses	Strength determination in the Semi-Circular Bending (SCB) mode. Displacement rate, 5mm/min at 20°C.

5.1 CORING AND SPECIMEN PREPARATION

Cores 100 mm and 150 mm in diameter, with an average length of 100 mm, were taken from within the eight test pads (*n1, n2, n3, s1, s2, s3, n-dry,* and *n-wet*) and from outside the test pads from untrafficked sections. At least four cores were extracted from each test pad and four from the untrafficked sections of each of the two lanes (northbound and southbound). Test pads *n-dry* and *n-wet* refer to MMLS3 tests that were performed in 1998 by Smit et al (1999) under dry and wet conditions, respectively. Figure 5.1 shows the core extraction points for the 1999 test pads.

During specimen preparation, cores were cut to the required thickness as per pavement structure layer thickness and those needing conditioning i.e. temperature and wetting, etc, were conditioned for a specified number of hours prior to doing the actual tests. The minimum conditioning period was 2 hours.

The core-layer designations and average thicknesses are shown in Figure 5.2. Only the three top most layers to a total depth of about 70mm were tested. For each layer and test type, at least two core-specimens were tested. In some instances up to twelve specimens were tested.

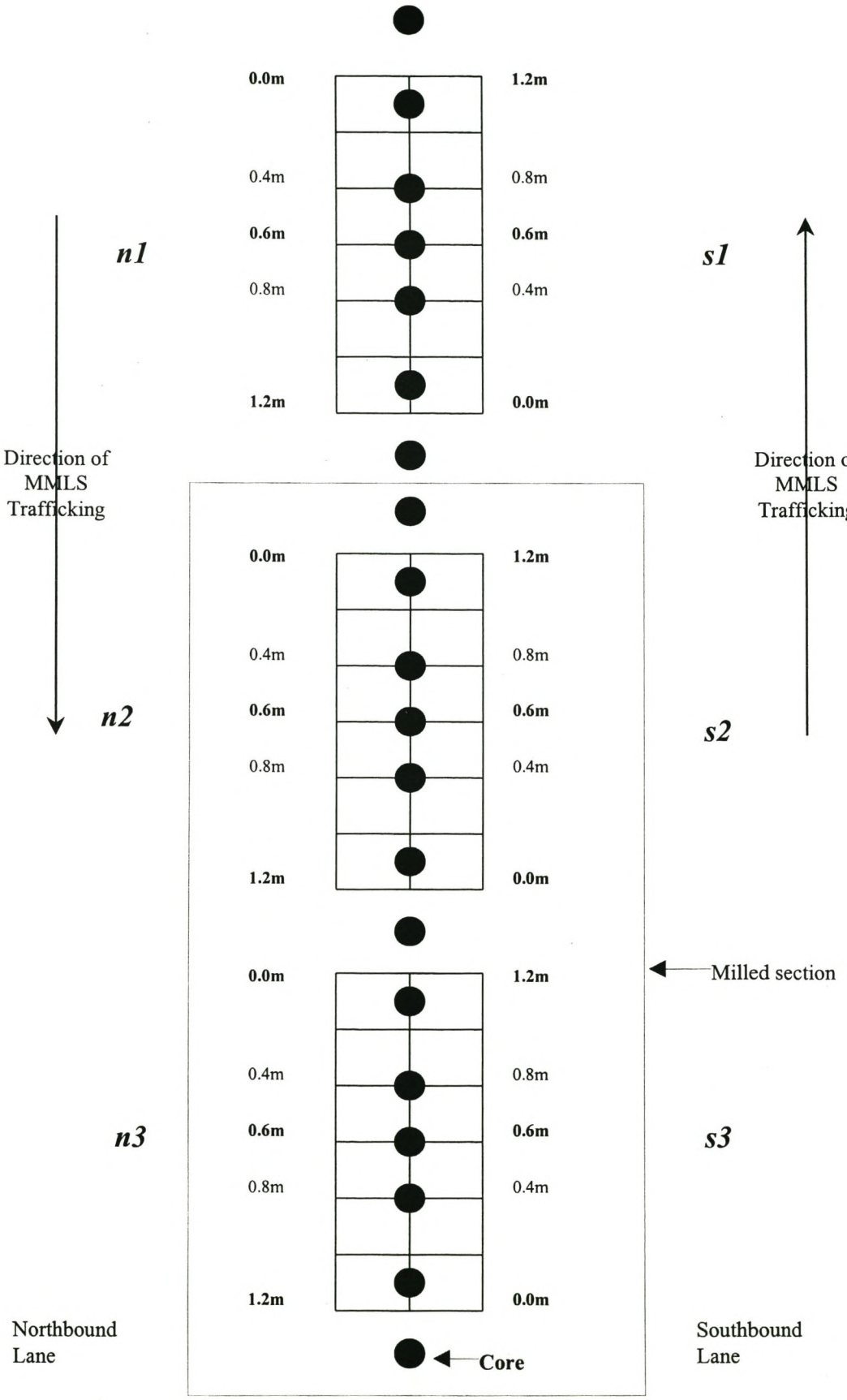

Figure 5.1: Core Extraction Points

5.1.1 Core Designations

The core-specimens from the top surface layers were denoted 'S' or 'L1' for surface or layer 1 respectively. Specimens from layers 2 and 3 were labelled 'L2' and 'L3' accordingly. 'C' was used to denote specimens of composite material such as a combination of layers 1 and 2. 'L*' designates a composite layer comprising L2 and L3. The actual average specimen thickness was 20mm except where otherwise designated.

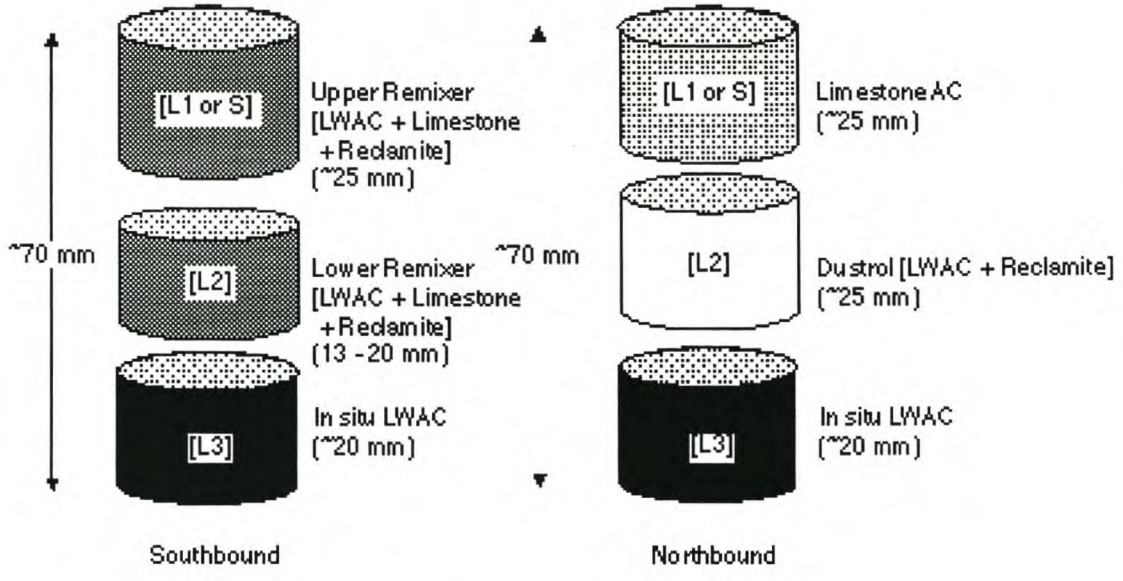

Figure 5.2: Core-Pavement Structures

5.1.2 Labelling of Core-Specimens

Cores were labelled using the following notations: small "*s*" for southbound; small "n" for northbound; "*u*" for untrafficked; "*d* or *dry*" and "*w* or *wet*" for dry and wet pads, respectively (Smit et al. 1999). So "*su*" and "*nu*" define untrafficked cores from the southbound and northbound structures, respectively, and "*nd*" specifies a core from the dry test from the northbound structure. "*su2-L1*" defines untrafficked southbound core number 2 from layer 1 (or the surface layer if "S" is denoted). These "core" notations should not be mixed with the 1999 "test pad" labels (*n1*, *s1*; *n2*, *s2*; and *n3*, *s3*), which denote surface hot; milled hot; and milled wet tests for the north- and southbound sections, respectively. In both the core and test pad labelling, "*n*" and "*s*" define north- and southbound, respectively.

For the northbound structure (trafficked inner lane), the top surfacing layer thickness from the right wheel path cores was 25 mm or more. For the left wheel-path cores, it varied and was not well defined on some sections. For cores from the 1998 dry section, the average thickness was 15 mm and the top limestone AC surfacing layer was highly inter-mixed with the underlying LWAC. This difference in layer structure probably influenced both the MMLS3 trafficking and laboratory test results as will be shown later, in Chapters 6 and 7.

5.2 THE MATERIAL TESTING SYSTEM (MTS)

Indirect tensile strength (ITS), semi-circular bending (SCB) strength and indirect tensile fatigue tests were conducted in the MTS machine (University of Stellenbosch). The Material Testing System (MTS) consists of the specimen loading plate enclosed in a temperature chamber with a hydraulic loading mechanism, the control panel, a computer data acquisition system, a temperature control device, and a hydraulic pump.

The loading and all other electronic manipulations are done from the control panel. Graphical wave displays and numbering counts are also monitored from the control panel. A computer is attached to both the control panel and the loading plates in the temperature chamber to capture and store raw data. Data capturing is done via four Linear Variable Displacement Transducers (LVDTs); two connected to the control panel and the other two, directly to the specimen loading plate. The temperature control device, through a mechanism of heating and cooling, controls the temperature of the test specimen within the temperature chamber. An automatic control thermostat is provided to regulate to any desired pre-set temperature within a specified differential temperature range. All the tests were conducted at 20±0.5°C. This temperature was selected because it is realistically closer to the average asphalt temperature.

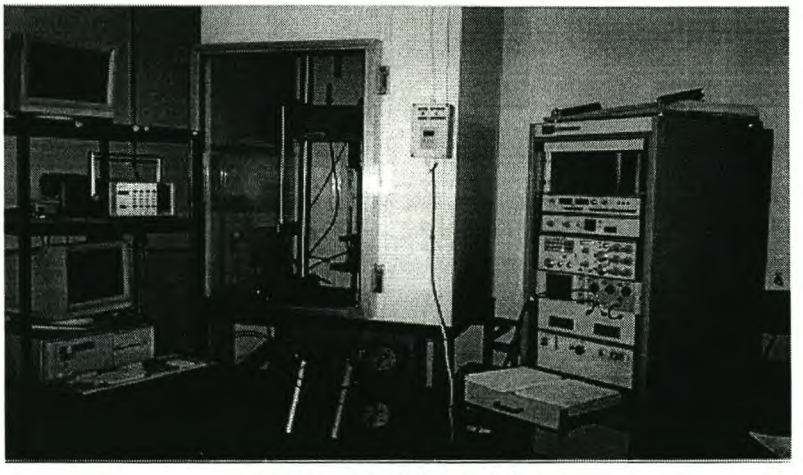

Figure 4.3: The MTS

The hydraulic pump supplies the necessary pressure to control the hydraulic loading mechanism. The pump is in a separate housing unit next to the MTS room.

5.3 VOLUMETRICS

Volumetric tests were conducted to determine the density of the pavement material before and after MMLS3 trafficking. Standard test method C3 (TMH1, 1986) was used for determining the bulk relative density (BRD) of the specimens. Epps (1999) also conducted a substantial number of density tests, which were used in the study. Some specimens were wetted for a period of about 2 hours according to the AASHTO test method T283 (1998) to assess the volumetric effect of water on the specimens (Epps, 1999). The test results are presented in Table 3.5.1 in Appendix III.

5.4 MOISTURE SENSITIVITY TESTS

Some 100 mm-diameter specimens were used for moisture sensitivity testing at 25°C (AASHTO T283, 1998) to determine the retained tensile strength ratio (TSR) after 2 hours wet conditioning (Epps, 1999). Table 3.5.2 in Appendix III shows the average moisture sensitivity test results for the specimens cut from both northbound and southbound cores

5.5 SHEAR TESTING

The shear tests were conducted to determine the shear and elastic modulus (stiffness) of the pavement as well as the phase angle (Epps, 1999). Results for the 1, 2, 5, and 10 Hz frequencies are presented in Table 3.5.3 in Appendix III. The tests were conducted at 25 °C and 40 °C for composite specimens (C) and at 40 °C for lightweight (L) specimens from the northbound pavement structure.

5.6 INDIRECT TENSILE STRENGTH (ITS)

The Indirect Tensile Strength (ITS) (SABITA, 1997, Schreuder, 1992) test was done to determine the tensile strength of the core specimens. The values obtained were related to the pavement strength and used in an assessment of the effect of MMLS3 trafficking through a comparison of the strength of trafficked and untrafficked cores. The ITS values were also used to establish the benchmark levels for each layer for testing the indirect tensile fatigue life at the same relative level of stress (namely 20% of ITS).

ITS testing was done in diametrical (axial) mode at 20°C and at a displacement-loading rate of 50mm/min. This is the displacement-loading rate recommended for the static ITS test in the SABITA manual 13 (1997). Specimens were pre-conditioned to 20°C for a minimum period of 2hrs. The maximum failure load (Figure 5.5) at break (splitting of the specimen) was used to calculate the indirect tensile strength using the Equation below.

$$\sigma_{ITS} = \frac{2*10^3 P}{(\pi.t.D)} \quad \text{.....(Equation 5.1)}$$

Where:

σ_{ITS}	=	indirect tensile strength in kPa
P	=	maximum failure load at break in N
t	=	thickness of specimen in mm
D	=	diameter of specimen in mm

The parameters, *t* (thickness) and *D* (diameter) are defined as illustrated in Figure 5.4.

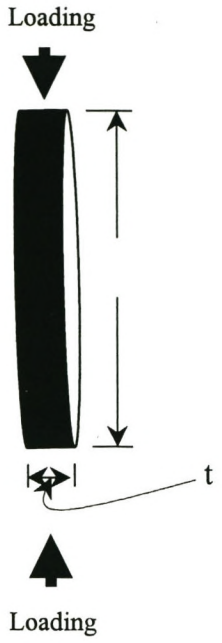

Figure 5.4: ITS Sample specimen

Figure 5.5 below shows a plot of the load-displacement data captured during ITS testing.

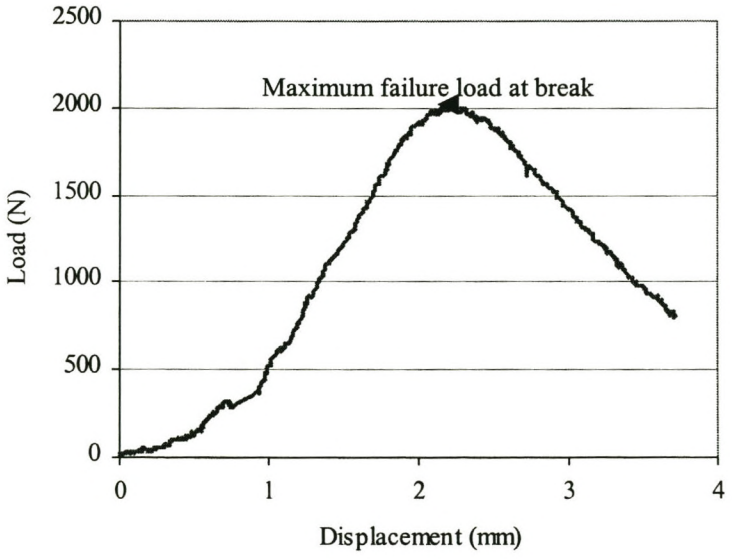

Figure 5.5: ITS Load-Displacement Curve

5.7 INDIRECT TENSILE FATIGUE TESTING

Indirect tensile fatigue tests were conducted on cores extracted from both the untrafficked and trafficked test pads. The difference in fatigue life compared to that of the untrafficked cores was assumed to be indicative of the distress caused by the MMLS3 trafficking under different environmental conditions (dry, hot, and wet). The test results also provided information on the fatigue characteristics of the AC after trafficking at high temperature and with water on the surface during trafficking.

Specimens from both the trafficked and untrafficked sections of the dry, hot, and wet test pads were fatigued at a stress level equivalent to 20% of their respective untrafficked ITS values with a preload (seating load) of 100N. Twenty percent ITS stress level was used because, trial tests with stress levels higher than 20% did not give a good representation of the specimen fatigue life. With a stress level higher than 20%, the trial specimens failed after only applying about 10 000 load cycles. All specimens were fatigued in indirect tensile test (ITT [diametrical or axial]) mode (SABITA, 1997, Schreuder, 1992) at 20°C with a Haversine load of 10Hz (10 pulses per second). This meant a loading of 10 cycles per second with no rest periods till failure. Fatigue is a stress-controlled test.

The minimum 20°C temperature-conditioning period was 2hours. Average time to fatigue failure was 20hrs. The cores from the heated-trafficked test pads took the longest test time, and had the highest residual fatigue life. The test results are presented in Table 3.5.6 (Appendix III).

The test analysis was based on the number of load cycles to full crack propagation across the specimen. The crack failure criterion in the indirect tensile fatigue test was based on the development of tensile stresses in the centre zone of the specimen under repetitive dynamic-compressive loading.

5.8 SEMI-CIRCULAR BENDING (SCB) TESTING

Some semi-circular bending (SCB) tests (Smit et al, 1997) were done to supplement the ITS strength tests. The SCB tests involved determination of the maximum tensile stress (strength) at break (cracking) at the bottom zone of a three-point loaded semi-circular shaped specimen as shown in Figure 5.6. The maximum tensile stress at break was used as an indicator of the material strength and the effect of MMLS3 trafficking under different environmental conditions (when compared to the untrafficked cores) on the material properties.

After indirect tensile fatigue testing, specimens (both trafficked and untrafficked) were sawn into some semi-circular shaped (almost half-cylindrical) specimens. These were tested at a displacement-loading rate of 5mm/min. The test temperature was 20°C.

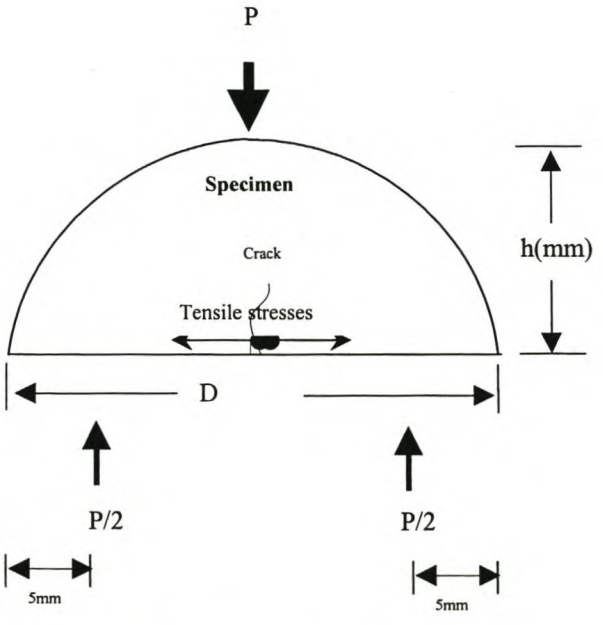

Figure 5.6: SCB Test Configuration

The maximum failure load at break as indicated in Equations 5.2 and 5.3 were used for computing the maximum horizontal tensile stresses at the bottom zone of the specimen.

$$\sigma_{t(SCB)} = \frac{(Y * P)}{(t * h)} \quad \text{.....(Equation 5.2)}$$

$$Y = -0.0008h^2 + 0.0541h + 0.5465 \quad \text{.....(Equation 5.3)}$$

Where:

$\sigma_{t(SCB)}$	=	maximum horizontal tensile stress in MPa
P	=	maximum failure load at break in N
t	=	thickness of specimen in mm
h	=	height of the semi-circular shaped specimen in mm
Y	=	specimen height factor

The maximum tensile stress $\sigma_{t(SCB)}$ is related to the strength of the specimen. It was generally observed that specimens with higher $\sigma_{t(SCB)}$ also had relatively higher ITS and likewise for specimens with low $\sigma_{t(SCB)}$.

A finite element analysis using the computer program ABAQUS (H.K.S, 1996) was used to develop the above Equations. This was to take account of the varying height (h), which in some cases was not equal to half the full core diameter (D/2). The conventional three-dimensional Equation according to Smit et al (1997) is of the following form;

$$\sigma_{t(SCB)} = \frac{(4.906P)}{tD} \quad \text{.....(Equation 5.4)}$$

Where:

$\sigma_{t(SCB)}$	=	maximum horizontal tensile stress in MPa
P	=	maximum failure load at break in N
t	=	thickness of specimen in mm
D	=	diameter of the semi-circular shaped specimen in mm

Results of the SCB tests are presented in Table 3.5.6 (Appendix III).

5.9 SUMMARY

Several laboratory tests including density, moisture sensitivity, shear, strength (ITS and SCB) and indirect tensile fatigue were completed to characterise the pavement materials and to supplement the filed test results. Detailed test results are presented in Appendix III.

For the purpose of comparative studies and assessment of the effects of MMLS3 trafficking on a pavement, cores for laboratory testing should be extracted from both the trafficked and untrafficked sections. It is important that cores from the trafficked sections are extracted from or along the centre of the MMLS3 wheel path where the traffic loading is considered most concentrated. Prior to laboratory testing, it is important that the specimens are well conditioned to the required temperature or moisture level. For each pavement layer and test type, at least two core-specimens were tested, so as to get a good representation of the material behaviour.

As will be discussed later, the laboratory test results being a supplement to the field measurements provided valuable information on the effects of MMLS3 trafficking on the asphalt pavement under different environmental conditions.

Chapter 6

6 FIELD APT TEST RESULTS

The following results are presented and analyzed; temperature profiles, the surface ruts, pavement layer deformations, micro cracking, stripping, and non-destructive in situ asphalt stiffness measurements. In the analysis, where otherwise used, AC refer to asphalt (asphalt concrete), and LWAC refer to lightweight aggregate asphalt concrete.

6.1 TEMPERATURE PROFILES

The MMLS3 trafficking temperatures are discussed below.

6.1.1 Hot Tests (Pads *n1, n2, s1* and *s2*)

Three thermocouples embedded at depths 25, 75 and 95mm within the test pads were used to monitor the temperature variation within the pavement layers, on an hourly basis as discussed in Chapter 4. The target MMLS3 trafficking temperature at 25mm depth for all the hot tests was 50°C. This was achieved by heating the pavement prior to and during trafficking. Figure 6.1 shows the mean MMLS3 trafficking temperatures for the hot tests. The overall mean MMLS3 trafficking temperatures were 49.9°C at 25mm depth, 42.5°C at 75mm depth, and 40.3°C at 95mm (Table 2.4.1, Appendix II).

The temperatures remained fairly constant with minimal variation during trafficking. The temperature gradient decreased with depth, with the highest variation at 25mm depth (±1.5°C) and the least at 95mm depth (±0.5°C). The mean pavement surface temperature within the temperature chamber during trafficking was 56.9 °C.

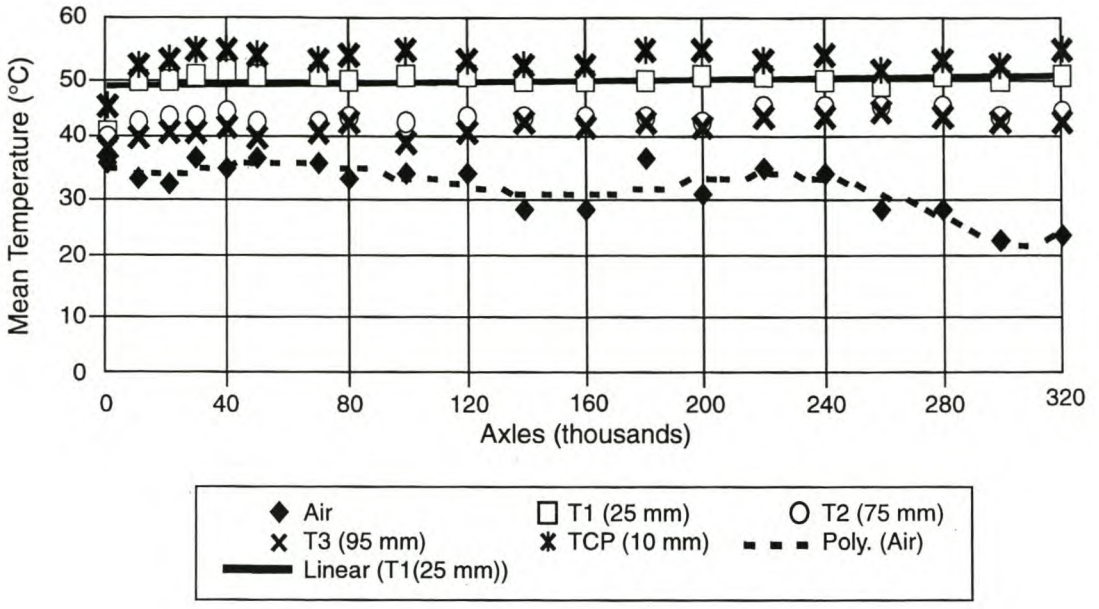

Figure 6.1: Mean MMLS3 Trafficking Temperatures for the Hot Tests

The mean air temperature during MMLS3 trafficking was 35.5°C. The air temperature was generally low at the start of the tests in May/June particularly for the *n*-tests but increased to as high as 47°C in July towards the onset of summer (hot season). The *s*-tests were subsequently run at higher air temperatures than the *n*-tests. Such temperatures affected only the amount of heating required during testing. It took far less time to heat the pavement to the required temperature on a hot day than on a cool day. Maintaining the MMLS3 trafficking temperature was also relatively easy under the hot weather.

The daily air temperature variation was cyclic with highest temperatures at noon (midday) and lowest at midnight. The highest temperature recorded was 47.6°C and the lowest, 18.2°C. Figure 6.2 shows a typical example of the daily air temperature variation during MMLS3 trafficking. A 5th order polynomial trend line is added to emphasize the cyclic daily air temperature variation.

As shown in Figure 6.2, the lowest temperature recorded (on this particular day) was at 3.00am and the highest around 2.00pm. It should be noted that trafficking with the MMLS3 was also done at night on the northbound lane, which was permanently closed to conventional traffic at the test section.

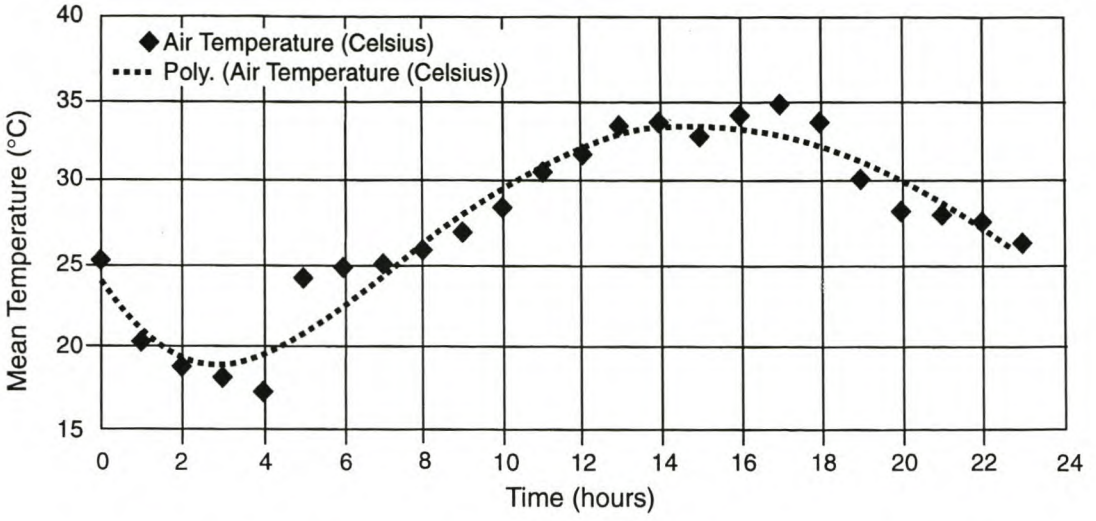

Figure 6.2: Typical Example of the Daily Air Temperature Variation during MMLS3 Trafficking

6.1.2 Wet Tests (Pads *n3* and *s3*)

Figure 6.3 shows the mean temperature profiles for wet tests. The thermocouple set up was similar to that of the hot tests and the target MMLS3 trafficking temperature at 25mm depth was 30°C. This was maintained constant through use of hot water (about 1mm thick at 45°C) and occasional heating, aided by the natural hot weather as the summer season approached.

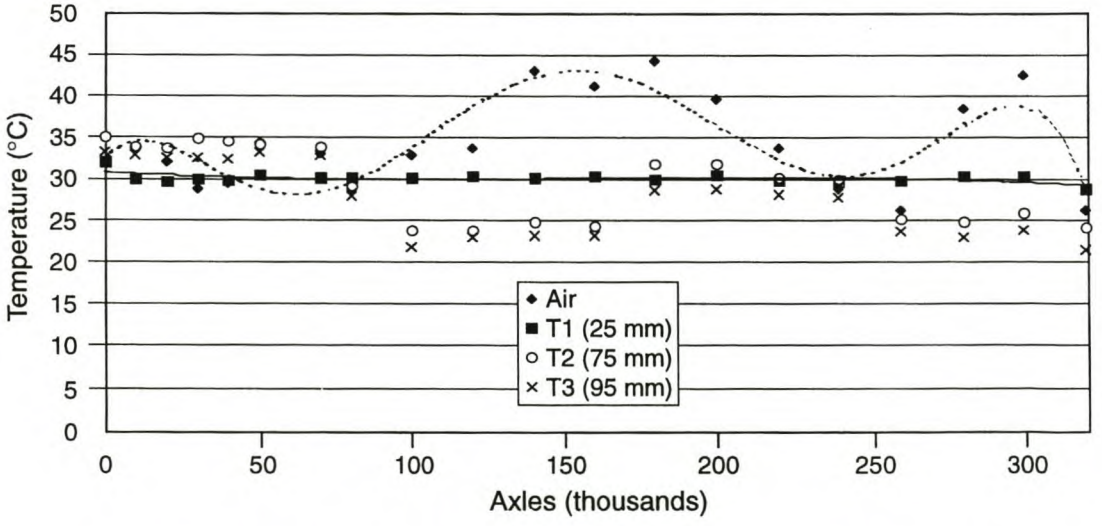

Figure 6.3: Mean MMLS3 Trafficking Temperatures for the Wet Tests

The daily air temperature variation followed a cyclic trend just like for the hot tests, with the highest recorded being 46.1°C and the lowest 17.2°C.

6.1.3 Temperature Distribution versus Pavement Depth

Figure 6.4 shows the average temperature profile within the pavement layers up to a depth of about 180 mm (at the base of the AC material) for the hot tests *n1*, *n2*, *s1* and *s3*. Beyond the 180 mm depth is the seal coat, flex base, subgrade, and bedrock. The properties of these layers are for the most part insensitive to temperature. Temperatures below 95mm were approximated using a constant decreasing gradient of approximately 0.12^0C per millimeter (Straub et al, 1968).

The temperature profile within the pavement structures was such that there was a gradual decrease in both temperature gradient and variation with depth. The temperature on the surface was the highest and decreased with pavement depth. The temperature on the surface of the pavement was in most instances higher than the air temperature.

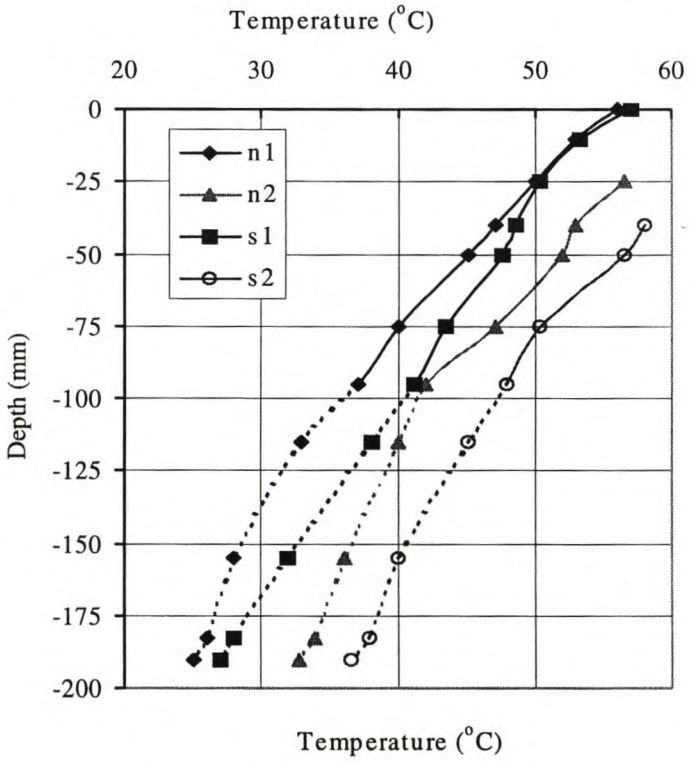

Figure 6.4: Pavement temperature versus Depth

Figure 6.4 shows that the milled test pads, *n2* and *s2* had higher temperatures within the pavement layers than *n1* and *s1*, respectively. This contributed to the higher rutting of the milled hot pads, as will be discussed subsequently.

6.2 SURFACE RUTTING

The maximum pavement surface ruts were computed using an excel spreadsheet. The calculations involved normalization of all the deformations with respect to the untrafficked sections/surface and the zero axle load measurement as shown in Figure 6.5. The basic principle was to super impose the target profile readings on the 0k readings, and then the maximum rut at the 240mm trafficked section was calculated as shown in Figure 6.5. Figure 6.5 shows an example of a maximum rut of 2.75mm after 320k axle load repetitions.

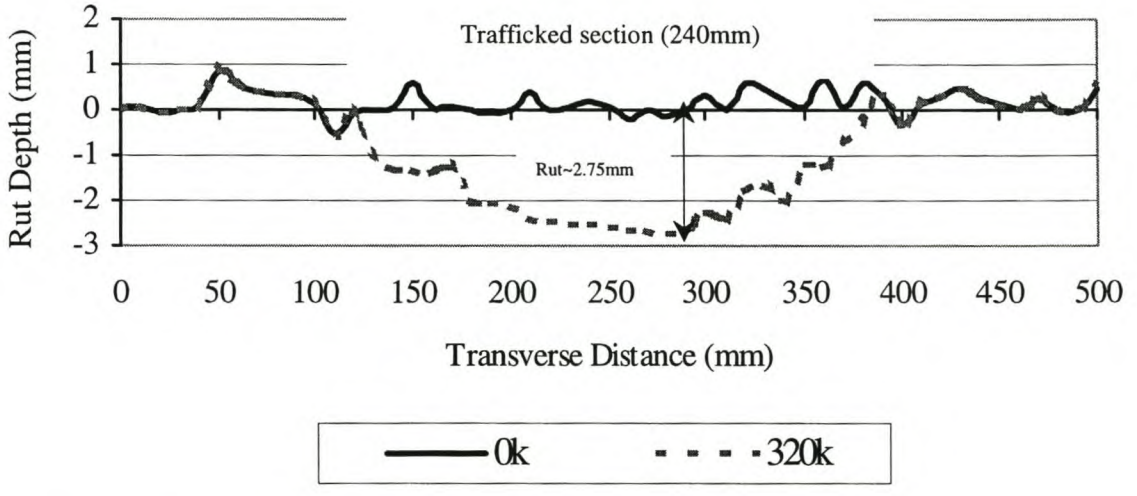

Figure 6.5: Example of Surface Rut determination from the Profilometer Data

The ruts presented in this study are the mean maximum of the 0.4m, 0.6m and 0.8m transverse gridlines, where most of the MMLS3 traffic loading was considered to be concentrated. On the milled pads, the transverse gridlines 0.2m, 0.4m, 0.6m, 0.8m and 1.0m were used to determine the mean maximum rut so as to counter the uneven surface.

Due to time and logistical constraints, some of the tests were not completed to equivalent number of axle loads. Results of some of these tests were therefore interpolated/extrapolated as will be seen in the Figures and subsequent discussions. In the Figures, all the dotted lines indicate extrapolation.

6.2.1 The Northbound Lane (Pads *n1, n2* and *n3*)

After 160k, the ruts on pads *n1*, *n2*, and *n3* were 1.4, 2.7, and 1.4 mm, respectively. At 320k, the rut depth on *n1* was 2.2 mm and 2.4 mm on *n3*, whilst the extrapolated rut depth for pad *n2* was 4 mm. For test pad *n1*, trafficking was done directly on the limestone AC surface, and the *Dustrol* material in the case of test pads *n2* and *n3*, after milling off the top limestone AC layer. The results are shown in Figure 6.6. The *n2* rutting profile was extrapolated to 320k as only 160k axles were applied on this test pad. At the trafficking temperature of 50 ^{0}C (at 25mm depth), it was evident that the in situ processed *Dustrol* and LWAC layers of test pad *n2* were less resistant to permanent deformation and more sensitive to temperature compared to the limestone AC overlay.

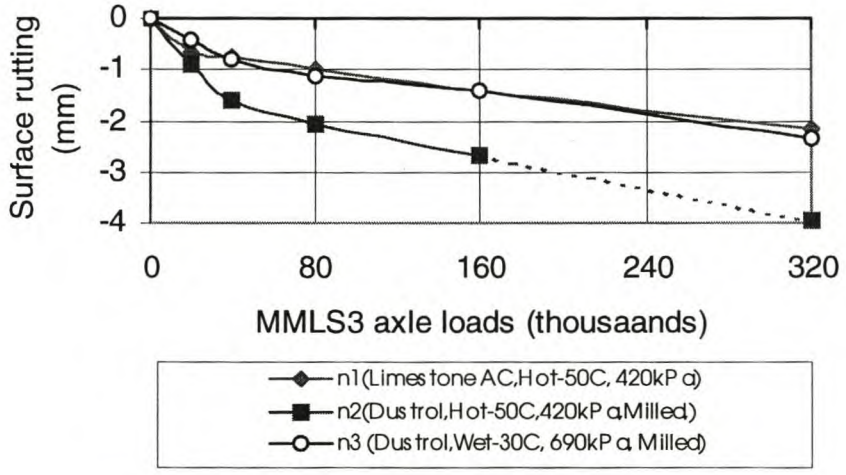

Figure 6.6: The northbound surface rutting
[MMLS3 axle load = 2.1kN]

Dynamic effects due to the rough surface could have caused some of the increased rutting on milled pads *n2* and *n3* compared to pad *n1*. However, this is not considered likely since the MMLS3 wheel load was found to vary by no more than five percent, with a difference in vertical height movement of about 20 mm. Nevertheless, in future, test preparation of milled surfaces should receive greater care to counter any possible effects of the uneven surface. The change in tyre pressure to 690kPa (from 420kPa on pad *n1*) could have contributed to the relatively greater rutting on pad *n3* compared to *n1*. At the same temperature, this would have increased the rutting by probably about 60%. However, the lower temperature of pad *n3* (30 ^{o}C at 25mm depth) would have mitigated this effect. Therefore, no correction was made. Both the tyre pressure (420kPa versus 690kPa) and test temperature (50 ^{o}C versu 30 ^{o}C) differ by about 60%.

6.2.2 The Southbound Lane (Pads *s1, s2* and *s3*)

The results are shown in Figure 6.7. Trafficking was done on the surface of the upper *Remixer* for *s1*, and the lower *Remixer* for *s2* and *s3*, respectively (after milling off the top upper *Remixer*). The new *Remixer* overlay (*s1*) appeared to have been more resistant to permanent deformation and less sensitive to temperature than the second layer of *Remixer* (*s2*). The higher rutting on pad *s3* compared to pad *s1* at 160k suggests that the *Remixer* and the in situ LWAC could be susceptible to water damage. Just like for the northbound (pad *n3*), the higher tyre pressure on pad *s3* (690kPa versus 420kPa) would have affected the rutting, but no correction was made.

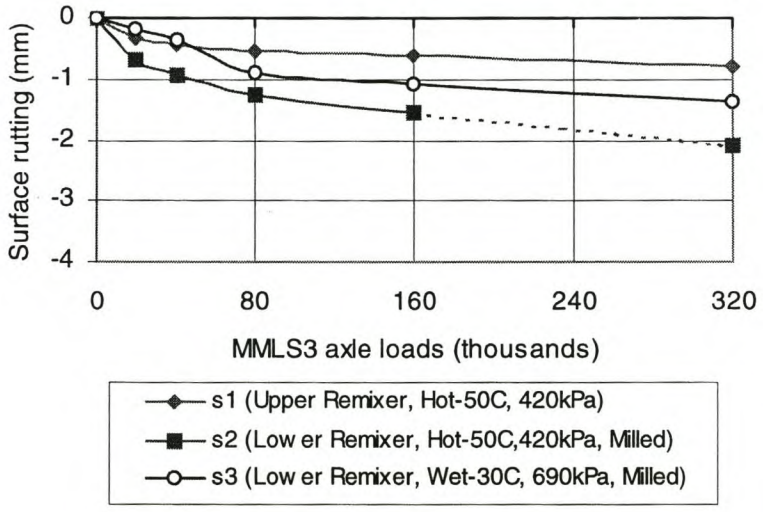

Figure 6.7: The southbound surface rutting

[MMLS3 axle load = 2.1kN]

6.2.3 Test Pads *n1* (north) and *s1* (south)

Similar testing conditions were prevalent on the two pads. The maximum rut of *s1* at the termination of testing at 180k was 0.6mm and about 1.5mm for *n1*. The rutting trend was the same in both cases as can be seen in Figure 6.9. However, *n1* (on the limestone AC surface) rutted about 2.8 times more than *s1* (on the *Remixer* surface), and its surface ruts were higher than *s1* at equivalent axle counts. Figure 6.8 shows the *n1* and *s1* rut profiles.

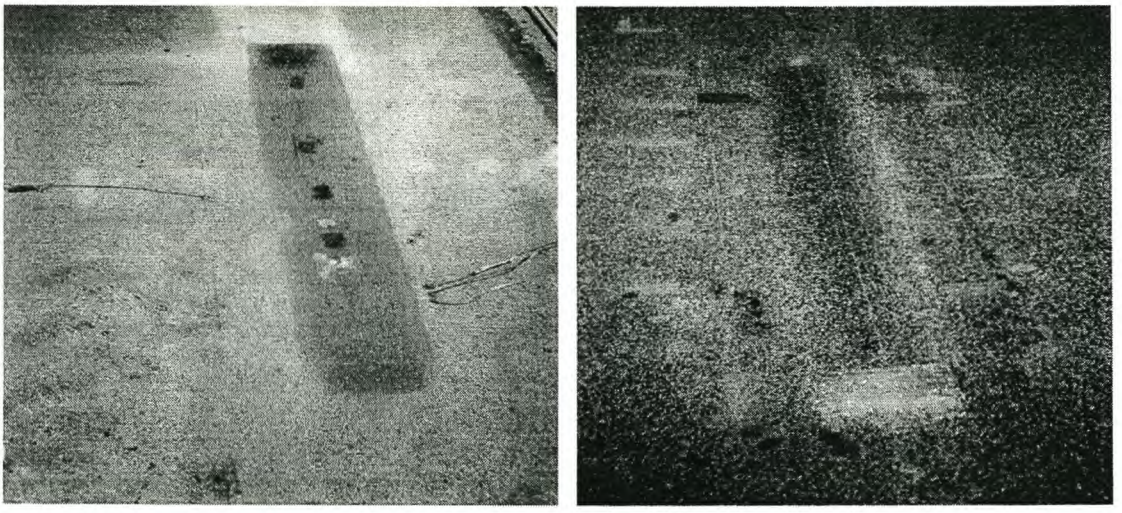

[Northbound lane] [Southbound lane]

Figure 6.8: *n1* (~2.2mm @ 320k) and *s1* (~0.6mm @ 180k) Ruts

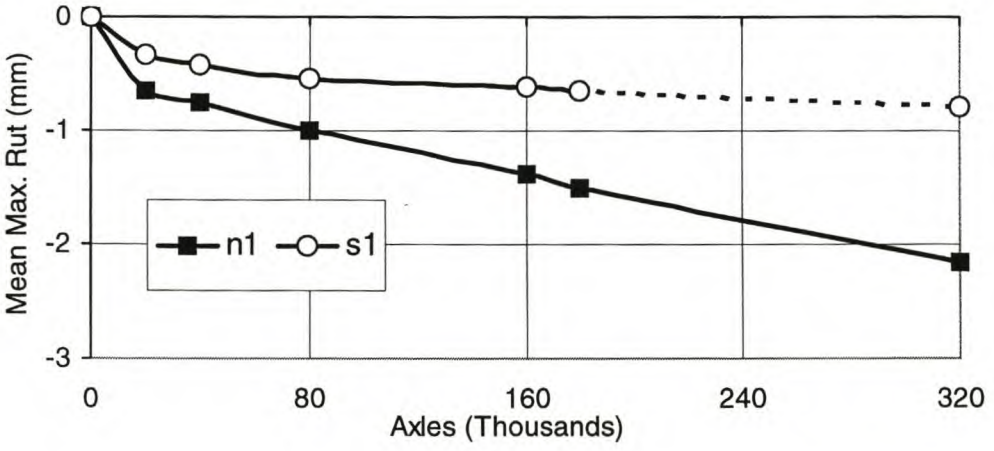

Figure 6.9: *n1* and *s1* Ruts
[Hot- 50°C, MMLS3 axle load = 2.1kN, tyre pressure = 420kPa]

6.2.4 Test Pads *n2* (north) and *s2* (south)

The *n2* maximum rut after 160k was 2.7mm (Figure 6.10). The *n2* ruts were higher than those on pad *s2* at equivalent axle counts. After 80k, the rut depth on pad *n2* was approximately 2.1mm and 1.3mm on *s2*. On average, pad *n2* (*Dustrol* + in situ LWAC) had rutted about 1.7 times more than pad *s2* (lower *Remixer* + in situ LWAC).

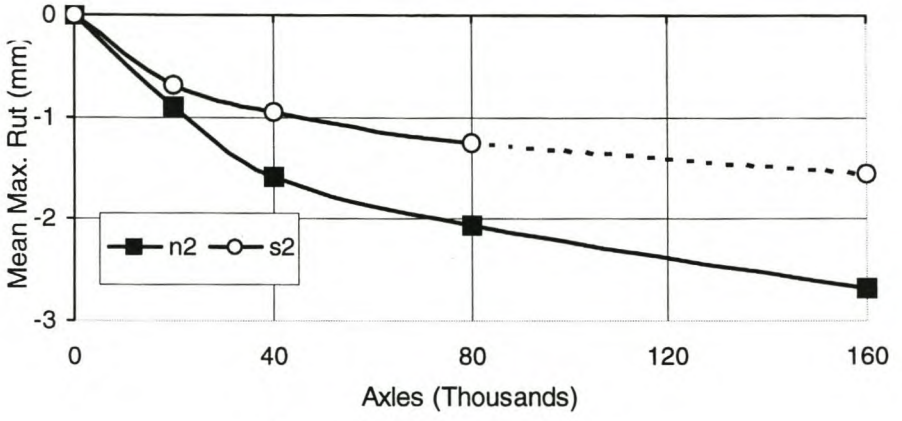

Figure 6.10: *n2* and *s2* Ruts
[Hot- 50°C, MMLS3 axle load = 2.1kN, tyre pressure = 420kPa]

6.2.5 Test Pads *n3* (north) and *s3* (south)

From Figure 6.11, the *n3* maximum rut after 320k was 2.35mm. Pad *n3* rutted more than *s3* at equivalent axles. The increased rutting experienced on the wet tests in comparison to the hot-dry tests was probably due to the increased tyre pressure (690kPa) and distress due to water pressure on the LWAC.

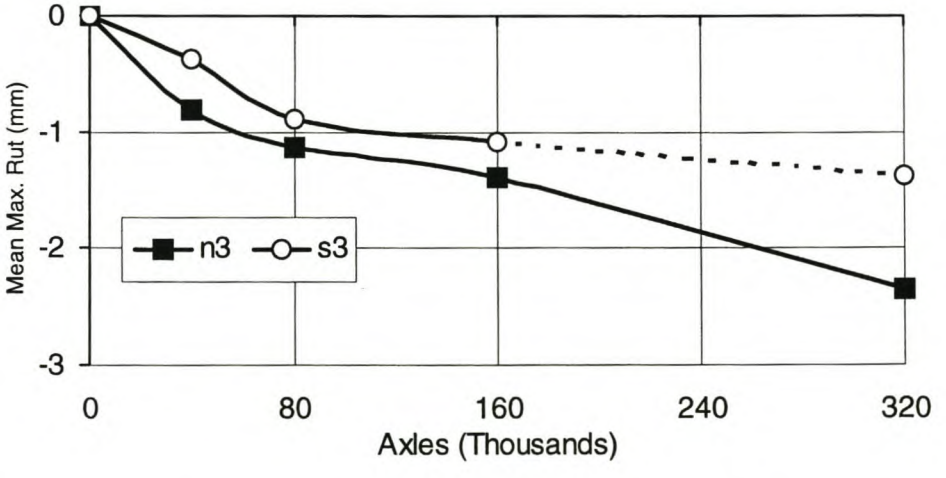

Figure 6.11: *n3* and *s3* Ruts
[MMLS3 axle load = 2.1kN, tyre pressure = 690kPa, Wet, 30°C]

6.2.6 Comparing the Northbound and Southbound Lanes

On average, the northbound lane had rutted about two times more than the southbound pavement structure at equivalent MMLS3 axle loads and under similar conditions. This was probably due to the difference in the top material composition (the limestone AC and *Dustrol* versus the upper and lower *Remixer*, respectively), sensitivity to temperature and moisture damage. The *Remixer* process on the southbound structure performed more rigidly and had a better surface rut performance compared to the *Dustrol* process on the northbound structure. This is an indication that the *Dustrol* process was more sensitive to temperature and moisture damage than the *Remixer*.

Overall, the increased rutting of the milled pads compared to the surface tests was probably due to the increased temperature influence lower down the pavement structures in the case of the hot tests, and water damage on the wet tests. Also the surface layers were previously (prior to MMLS3 testing) more exposed to normal traffic compaction and environmental effects compared to the underlying layers, and were therefore expected to behave more rigidly. The milled pads were thus likely to be more susceptible to deformation and traffic damage after milling off the protective surface layers.

6.2.7 Comparison of the 1998 MMLS3 and 1999 MMLS3 Rutting Results

Figure 6.12 shows a plot of the rut profiles for the 1998 and 1999 MMLS3 tests. The loading for the 1998 MMLS3 tests were 2.1kN axle load and 690kPa tyre pressure, for both the dry (38°C) and wet (24°C) test (Smit et al, 1999). There was no temperature control in the 1998 MMLS3 tests and the tests were done only on the northbound lane directly on the limestone AC surface. In the case of the 1999 MMLS3 tests, the loading were 2.1kN and 420kPa tyre pressure for the hot tests at 50°C, and 2.1kN and 690kPa for the wet tests (30°C).

After 320k axle loads, the 1999 MMLS3 (*n1*) rut was 2.2mm, and the 1998 MMLS3 (*n-dry*) rut was 1.4mm. The hot test rutting was about 60% more than the 1998 dry test. At the termination of the 1998 dry test at 1.0 million axles, the rut was only 1.8mm (about 83% of the hot test rut after 320k).

The average MMLS3 trafficking temperature at 25mm depth was 49.8°C for *n1* (1999) and 37.9°C for *n-dry* (1998), a difference of about 12°C. Since the MMLS3 axle loading was similar (2.1kN) in both cases and that the tyre pressure of *n-dry* was even higher, the increased temperature probably caused the high rutting of test pad *n1* (1999).

In comparison to *n2* (on the *Dustrol* surface) at 160k, the *n-dry* rut was about two times less.

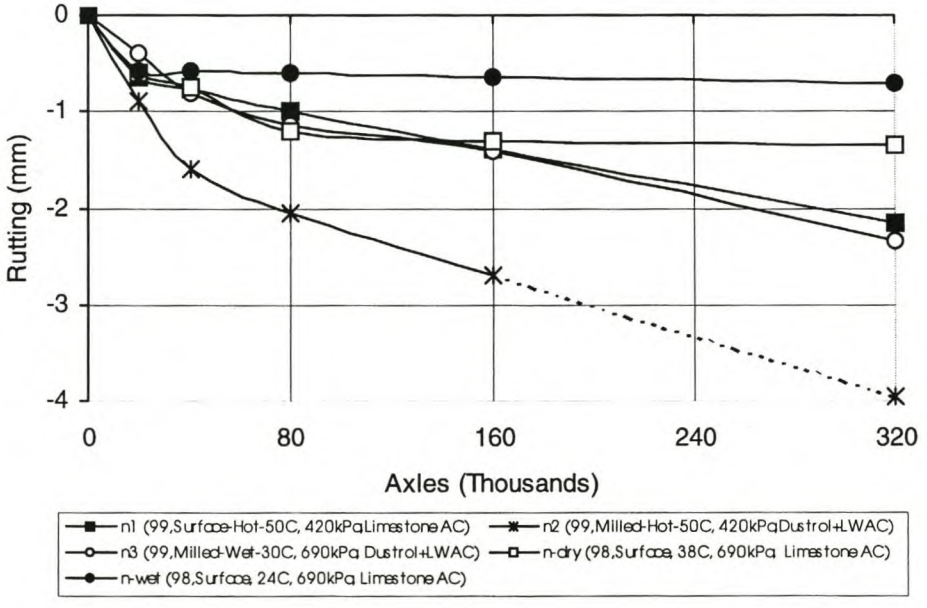

Figure 6.12: MMLS3-1998 and MMLS3-1999 Rutting
[MMLS3 axle load = 2.1kN]

For *n-wet* (1998) with water on the pavement surface and an average trafficking temperature of 24°C at 25mm depth (Figure 6.12), the rut was about one-third (0.33) the amount measured on pad *n1* (1999) at 320k (0.7mm versus 2.2mm). This is indicative of the marked influence of temperature on the rut performance of the upper layers.

In comparison to pad *n3* (1999-milled wet, 30°C at 25mm depth), the rut depth on *n-wet* (1998) was only 1.0mm at the termination of testing after 1.4 million axle loads compared to 2.4mm for pad *n3* just after 320k. After 320k, the *n-wet* rut was only about 0.7 mm. This suggests that the *Dustrol* layer was more sensitive to moisture than the top limestone AC surfacing layer.

6.2.7 Comparing the 1999 MMLS3 and Full-Scale TxMLS Rutting Results

The comparative rut profiles are shown in Figure 6.13 for both the northbound and southbound lanes. For the TxMLS, only the deformations (not total rutting) in the top surface layers up to a depth of about 90mm were considered. The 90mm depth was the position of the first multi-depth deflector (MDD) and was also considered the depth to which the MMLS3 had much loading influence. The MDDs were used to measure the layer deformation under the TxMLS (Hugo et al, 1998 [b] and [c]). Both the TxMLS rutting from the left (L) and right (R) wheel path respectively, for each lane were plotted (Figure 6.13).

The TxMLS loading were about 75.6kN dual-axle wheel load and 690kPa tyre pressure. Therefore, a single TxMLS wheel applied approximately a load of 18.9kN. The average uncontrolled trafficking temperatures ranged between 30.5°C and 32°C for the northbound lane, 25.5°C and 28°C for the southbound lane. All were dry tests and there was no milling.

After 320k axles, the one-third (1/3) scale MMLS3 rutting (*n1* [1999]) was about one third of the full-scale TxMLS (2.2 mm versus 6.5 mm). The *n-dry* (1998) rut was 1.4mm, compared with the TxMLS rut of 6.5 mm at 320k. This measure was only about 21% of the full-scale TxMLS rut. On pad *n2*, the rutting was 2.7 mm after 160k, which is 67% of the 4 mm TxMLS rut at the same axle count. Among other differences, there was no environmental control in the full-scale TxMLS trafficking or in the 1998 MML*S3* dry tests. Furthermore, the TxMLS traffic loading is much higher than the MMLS3, and naturally more rutting was to be expected. By contrast, there was more surface rutting on the southbound sections under the milled pads *s2* and *s3* (in the upper AC layers) than in the tests conducted with the TxMLS.

Pads *n2* and *s2* yielded a better rut comparison owing to the milling effect, which resulted in high stresses being induced deeper down in the pavement layers.

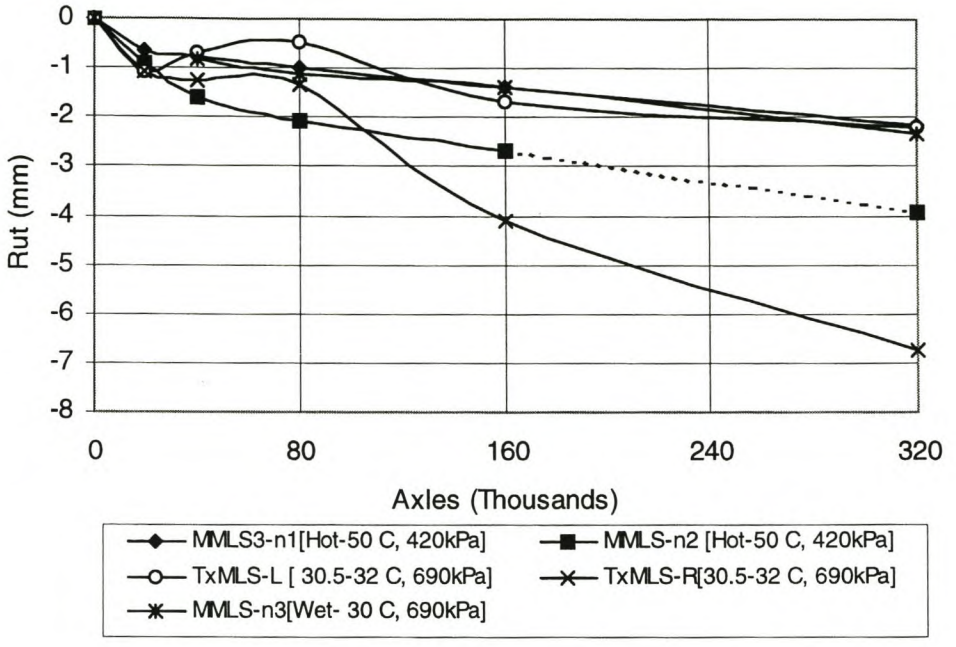

(a): Northbound Lane

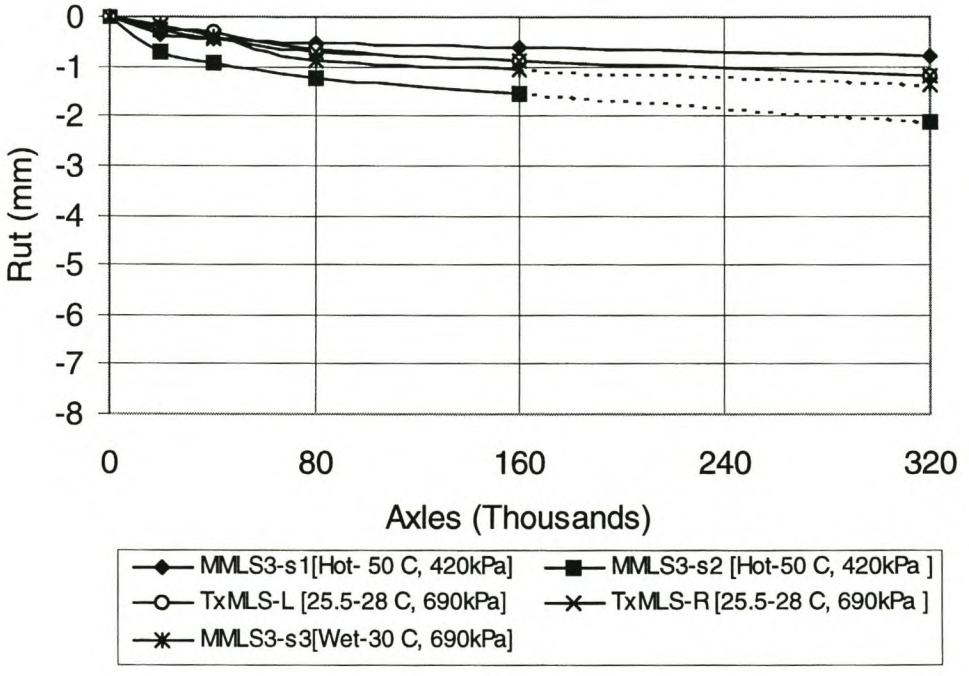

(b): Southbound Lane

[Where L refers to the left wheel path, and R to the right wheel path]

Figure 6.13: MMLS3 and TxMLS Ruts

6.3 PAVEMENT LAYER DEFORMATION

The relative deformation of the pavement layers with MMLS3 trafficking was monitored using the small LDPs. The respective pavement layer deformations are shown in Table 6.1.

Table 6.0.1: Pavement Layer Deformations

(a) Northbound lane							
		Hot - 50°C, 420kPa				**Wet- 30°C, 690kPa**	
Thickness (mm)	**Layer**	***n1* [320k]**		***n2* [160k]**		***n3* [320k]**	
		Def. (mm)	**% of total def.**	**Def. (mm)**	**% of total def.**	**Def. (mm)**	**% of total def.**
25	Limestone AC	1.06	49				
25	*Dustrol*	0.53	24	2.36	88	1.96	83
20	In situ LWAC	0.22	10	0.18	7	0.19	8
Below 70	Old AC layers, seal coat, base, and subgrade	0.36	17	0.15	5	0.20	9
Total		**~2.2**	**100**	**~2.7**	**100**	**~2.4**	**100**
(b) Southbound lane							
		Hot - 50°C, 420kPa				**Wet- 30°C, 690kPa**	
		***s1* [180k] - Hot**		***s2* [80k] - Hot**		***s3* [160k] - Wet**	
25	Upper *Remixer*	0.23	36				
25/10	Lower *Remixer*	0.17	27	0.64	51	0.45	42
20	In situ LWAC	0.11	17	0.43	34	0.41	38
Below 70	Old AC, seal coat, base, and subgrade	0.13	20	0.18	15	0.22	20
Total		**~0.6**	**100**	**~1.3**	**100**	**~1.1**	**100**
Key: Def. = Deformation, % = Percentage contribution to total deformation							

6.3.1 The Northbound Lane

The total *n1* rut after 320k was 2.2 mm, of which 49% occurred in the top 25 mm limestone AC layer. Some 24% occurred in the 25 mm recycled LWAC (*Dustrol*) and 10% in the 20 mm LWAC layer. A 17% deformation occurred in layers below the in situ LWAC.

After 160k, *n2* had rutted about 2.7mm. About 88% occurred in the "*Dustrol*" processed layer (0–25 mm) and was probably due to the direct heating effect and MML*S3* trafficking after the protective limestone AC surfacing layer was milled off. Approximately 7% deformation occurred in the in situ LWAC layer and the rest in underlying layers.

Eighty-three percent of the 2.4 mm total rutting of pad *n3* at 320k axles occurred in the *Dustrol* layer (~25 mm recycled LWAC plus Reclamite). This effect was probably due to degradation and stripping of the LWAC as a result of water application on the surface. The rest (17%) occurred in underlying layers, with about 8% occurring in the 20 mm in situ LWAC layer.

6.3.2 The Southbound Lane

On pad *s1*, about 63% deformation occurred in the top 50 mm of recycled LWAC (*Remixer*), and about 17% occurred in the in situ LWAC layer. Approximately 20% deformation occurred in layers below the in situ LWAC. The *s1* total permanent deformation after 180k axles was 0.64 mm.

Pad *s2* rutted about 1.3 mm after 80k axles. About 51% occurred in the bottom *Remixer* layer, which was directly exposed to MMLS*3* trafficking and heating after the top 40 mm rehabilitation layer was milled off. The bottom layers contributed about 49%, with 34% occurring in the in situ LWAC.

Of the approximate 1.1mm rutting of pad *s3*, about 42% deformation occurred in the top 10 mm second *Remixer* layer, which was undergoing stripping and degradation owing to the effects of water. About 38% deformation occurred in the in situ LWAC and 20% in underlying layers. This effect was probably a result of water damage.

6.4 MICRO-CRACKING AND STRIPPING

Rutting as well as surface micro cracking and stripping was the anticipated mode of distress on the wet tests. Small micro-cracks were found on the *n3* and *s3* test pads after termination of the tests. In addition, there were small loose aggregate particles on the surface of the wet test pads after MMLS3 trafficking indicating occurrence of stripping. Stripping was also evident on the wet pads at the lower interface of the in situ LWAC and the 1971 AC after coring, particularly on pad *n3*. No surface cracking was found on the hot test pads.

The surface cracking and stripping of the wet test pads was most probably due to degradation of the surface of the asphalt concrete due to the effects of water. The micro cracks were more prominent on pad *n3* compared to *s3*.

6.5 PAVEMENT INSITU AC MODULI

The change in stiffness of the asphalt concrete "surface" layers both for the hot and wet tests due to trafficking were monitored using the PSPA and SASW devices at selected points on the test pads as discussed in Chapter 6. The asphalt stiffness is strongly influenced by the pavement temperature at the time of measurement and is also a function of the loading frequency. The results were therefore normalized to standard temperatures of 25°C (PSPA) and 21°C (SASW) respectively (Li et al, 1994 and Aoud et al, 1993). These are the standard temperature values selected by the original proponents of the respective devices, and in this study, no attempt was made to adjust these values. This does not cause any discrepancy in the analysis since no "comparison" is being made between the two systems (PSPA and SASW).

For the loading frequency, all the moduli values were standardized to 30Hz which is considered to be the frequency applicable to the falling weight deflectometer (FWD) test. This value (30Hz) is the natural frequency of the tyre walls due to unevenness (roughness) and corrugations on the surface of the pavement (Molenaar et al, 2000).

6.5.1 The PSPA Method

Figure 6.14 shows a plot of the normalized PSPA moduli ratios relative to the respective untrafficked sections. The AC moduli shown in Table 2.4.4 (Appendix II) were normalized to 25°C and 30Hz using the relationship proposed by Li and Nazarian for adjusting raw AC modulus measured at a temperature T in °C to a reference temperature of 25 °C (Li et al, 1994 and Aoud et al, 1993). The calculations were based on an average pavement AC density of 2000 kg/m^3 and Poisson's ratio of 0.33.

Equation 6.1 was used to calculate the raw moduli from the measured PSPA Rayleigh wave phase velocity, the assumed average pavement AC density and the Poisson's ratio:

$$E_{Raw} = 2*10^{-6}\rho(1+\upsilon)*(1.073R_V)^2 \quad \text{.....(Equation 6.1)}$$

Temperature Correction to 25 °C

The AC moduli-temperature adjustment relationship according to Li et al (1994) is:

$$E_{T_{25C}} = \frac{E_{Raw}}{(1.35-0.014T_m)} \quad \text{.....(Equation 6.2)}$$

Frequency Correction to 30Hz

A multiplication factor of one-third (1/3) as expressed by Equation 6.3 was used to take account of the frequency.

$$E_{f_{30Hz}} = \frac{E_{T_{25C}}}{3} \quad \text{.....(Equation 6.3)}$$

Where:

E_{Raw}	=	raw pavement AC moduli measured at a temperature T_m in MPa
$E_{T\,25C}$	=	adjusted pavement AC moduli to 25 °C in MPa
$E_{f\,30Hz}$	=	normalized pavement in situ AC moduli to 30Hz and 25 °C in MPa
ρ	=	pavement AC density in kg/m^3 (~ 2000 kg/m^3)
ν	=	Poisson's ratio (~ 0.33)
R_V	=	PSPA Rayleigh wave phase velocity in m/s.
T_m	=	pavement temperature at the time of measurement in °C.

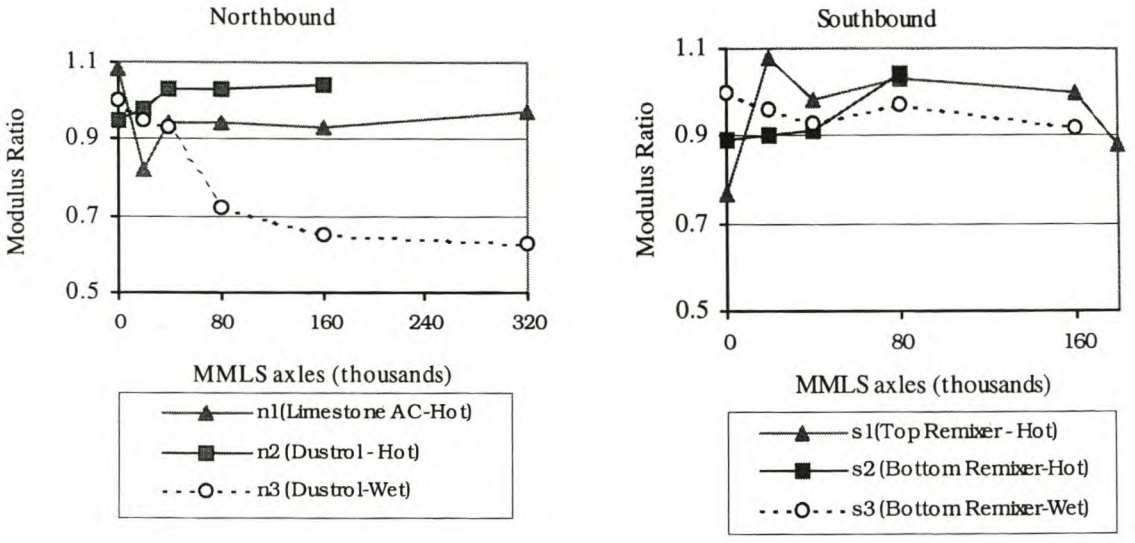

Figure 6.14: Normalised PSPA Modulus Ratios

Figure 6.14 shows that there was a decrease in pavement AC moduli on pads *n1*, *n3*, and *s3* with MMLS3 trafficking. On pads *s1*, *n2*, and *s2* there was an increase. Due to anticipated traffic damage, the moduli would normally be expected to decrease with trafficking. However, material densification due to traffic and ageing of the bitumen may offset the effects of traffic damage for a certain temperature as was evident in pads *s1*, *n2*, and *s2*. Tangella (1990), and Raithby and Ramshaw (1972) had also reported this phenomenon. If the stiffness values after trafficking are related to those measured at 0k from the same trafficked sections/positions, the increase in stiffness are approximately 10% for *n2*, 14% for *S1* and 17% for *s2*, whilst the loss for *n1* is about 10%. It should be noted the modulus ratios plotted in Figure 6.14 are the ratio of the asphalt moduli calculated from the trafficked sections relative to the moduli calculated from untrafficked sections outside the MMLS3 wheel path.

The decrease in AC pavement moduli in the wet tests (*n3* and *s3*) suggests water damage (AC degradation and stripping). At the end of testing, there was a loss in stiffness of about 37% (after 320k) in the northbound structure and about 8% (after 160k) for the southbound due to MMLS3 trafficking in the presence of water. At 160k axles, pad *n3* had a loss of about 35% (versus 8% for pad *s3*), a clear indication of more water damage susceptibility than the southbound structure (*s3*). This was also confirmed by the rutting results.

On comparative terms, the average composite PSPA modulus for the southbound pavement structure (~3 550MPa) was about 17% higher compared to the northbound (~3 035MPa). This compares favourably with Hugo et al's findings that the 281S1 (south) average modulus was approximately 20% higher than the 281N1 (north) (Hugo et al, 1999 [c]). Lee et al (1997) found similar results. This partially explains the higher resistance to deformation and the smaller ruts obtained on the southbound lane during MMLS3 trafficking.

8.5.2 The SASW Method

The SASW measurements were done after termination of the tests and the moduli analysis was based on a comparison with control measurements from the un-trafficked sections. The measurement points are shown in Figure 4.8 (Chapter 4). All the trafficked positions were measured along the test pad centerline and coincided with the PSPA positions.

The raw moduli were calculated from the SASW surface wave velocity using Equation 6.4. This was based on the linear-elastic relationship between the shear and Young's modulus of elasticity and the assumption that the surface wave velocity is approximately 90% of the shear wave velocity (Aoud, 1993, and Ming et al, 2000).

An average AC density of 2000 kg/m^3 and Poisson's ratio of 0.33 were assumed. The raw moduli were normalized to 30Hz frequency and 21°C using the correction Equations developed by Aoud (1993) as given in Equation 6.5 and 6.6.

$$E_{Raw} = 2*10^{-6}\rho V_s^2(1+\upsilon) \quad \text{.....(Equation 6.4)}$$

Frequency Correction to 30Hz

$$E_{f_{30Hz}} = E_{Raw} * \left(\frac{f_m}{f_{30Hz}}\right)^{-A} \quad \text{.....(Equation 6.5)}$$

Temperature Correction to 21°C

$$E_{T_{21\,C}} = \frac{E_{f_{30Hz}}}{(1.51 - 0.00729(1.8T_m + 32))} \quad \text{.....(Equation 6.6)}$$

Where:

E_{Raw}	=	raw pavement AC modulus in MPa.
E_{f30Hz}	=	pavement AC modulus normalised to 30Hz frequency in MPa.
E_{T21C}	=	pavement AC modulus normalised to 21°C in MPa
ρ	=	average pavement AC density in kg/m^3 (~2000 kg/m^3)
V_s	=	shear wave velocity in m/s
ν	=	Poisson's ratio (~0.33)
A	=	temperature dependent factor (obtained from Table 2.4.5 or Figure 2.4.1 in Appendix II)
f_m	=	frequency at the time of SASW measurement
f_{30Hz}	=	30Hz frequency
T_m	=	pavement temperature at the time of SASW measurement in °C

Table 6.2 below shows the calculated and normalized AC moduli measured from the respective test pads after MMLS3 trafficking.

Table 6.0.2: Normalised SASW AC Moduli (MPa) Results

Normalised to 21°C and 30Hz						
Pad	***n1***	***n2***	***n3***	***s1***	***s2***	***s3***
Material	Limestone AC	Dustrol	Dustrol	Top Remixer	Bottom Remixer	Bottom Remixer
Untrafficked (U)	2 870	3 060	3 034	3 123	3 058	2 997
Trafficked (T)	2 866	3 136	2 019	3 596	3 120	2 670
RR (T/U)	0.99	1.02	0.67	1.15	1.02	0.89
Comment			**33% loss**	**15% gain**		**11% loss**
MMLS3 Axle Loads Applied	320 000	160 000	320 000	180 000	80 000	160 000
Trafficking Conditions	Hot, 50 °C		Wet, 30 °C	Hot, 50 °C		Wet, 30 °C
MMLS3 Loading	2.1kN, 420kPa		2.1kN, 690kPa	2.1kN, 420kPa		2.1kN, 690kPa

The SASW normalised moduli ratios in Table 6.4 show that there was a significant drop in stiffness on the wet pad *n3* (~33%) and a drop of about 11% on wet pad *s3*. Also the trafficked moduli for the wet pads were of relatively lower magnitude compared to the corresponding hot pads. This correlates with the PSPA results and the loss in stiffness

appears to be primarily due to water. However, the high tyre pressure (in comparison to hot dry tests) could have contributed, but this was not taken into account.

The results indicated that there was no significant change in modulus on pad *n1*. However, pad *s1* appeared to have gained stiffness on the order of about 15% probably due to MMLS3 compaction. This is indicative of the difference between the performance of the limestone AC and the lightweight aggregate asphalt concrete (LWAC) pavement (see subsequent discussion).

6.5.3 Comparing the PSPA and SASW Results

There is a difference in the moduli values between the PSPA and SASW results, particularly for *s1* (untrafficked) and *s2* (both trafficked and untrafficked) as shown in Table 6.3.

Table 6.0.3: PSPA and SASW Moduli Values

Test pad	Trafficking/Test condition	Modulus value (MPa)	
		PSPA method (normalized to 25°C)	**SASW method** (normalized to 21°C)
s1	Untrafficked	4 280	3 123
s2	Untrafficked	3 500	3 058
s2	After trafficking under hot-dry conditions @ 50 °C @ 25 mm pavement depth	3 650	3 120

It was expected that the SASW moduli would be of relatively higher magnitude compared to the PSPA values, since they were normalized to a relatively lower temperature. However, this was not the case. This difference could be explained by the following reasons:

(1) The raw moduli were normalized to different temperatures (25°C for the PSPA and 21°C for the SASW)

(2) The untrafficked moduli values of the PSPA and SASW were measured from different positions on the test pads (see Figure 4.4 in Chapter 4).
(3) The PSPA and SASW measurements were not done at the same time, but actually on different dates. The PSPA measurements were always done immediately after MMLS3 trafficking where as the SASW were not. This difference in time of measurement could have affected the results, considering that the AC stiffness is very sensitive to temperature.
(4) No accuracy comparison was done between the two devices. The primary intention was just to compare the "performance trend" of the AC material with respect to change in stiffness under different MMLS3 trafficking conditions.

In terms of the AC performance, both devices indicated a similar trend in the stiffness change. Both devices indicated stiffness loss under wet trafficking and a gain under hot dry trafficking, except the limestone AC on the northbound lane, which exhibited a unique behaviour.

6.6 SUMMARY AND FINDINGS

The summary and findings of the analysis of the field test results are discussed below.

6.6.1 Temperature Profiles

The temperature profile within the pavement structures was such that there was a gradual decrease in both temperature gradient and variation with depth, particularly for the hot tests. The temperature on the surface was the highest and decreased with pavement depth.

6.6.2 Comparison of the Surface Ruts

Table 6.4 shows a summary of the testing and loading conditions for the MMLS3 and TxMLS trafficking in Jacksboro.

Table 6.4: Summary of Test and Loading Conditions.

	MMLS3 1999	MMLS3 1998	TxMLS
Test and Loading Conditions	Hot – 50° C [2.1kN, 420kPa] Wet – 30° C [2.1kN, 690kPa]	Dry – 38° C [2.1kN, 690kPa] Wet - 24° C [2.1kN, 690kPa]	Dry, 25.5 - 32° C average [75.6kN dual-axle wheel load, 690kPa]
Pavement structures	Both North and Southbound lanes	Only Northbound lane	Both North and Southbound lanes
Comment	Temperature controlled	No temperature control	No temperature control

For the 1999 MMLS3 tests, the southbound lane had relatively smaller surface ruts compared to the northbound lane at equivalent axle loads and under different but similar environmental conditions. The rutting on the northbound lane was about two times more than the rutting on the southbound lane. The *Remixer* rehabilitation process (southbound lane) was more resistant to permanent deformation compared to the limestone AC and the *Dustrol* rehabilitation process.

In the northbound lane, the *Dustrol* process showed less resistant to deformation than the limestone AC surfacing layer. For the southbound, the upper *Remixer* exhibited much resistance to deformation compared to the lower *Remixer* and the in situ LWAC. In the case of the milled pads *n2* and *s2*, direct environmental exposure and particularly heating were contributing factors to the increased rutting compared to the surface rehabilitation processes. The marginally higher rut depths in the wet pads *n3* and s3 indicate that water damage, degradation, and stripping of the LWAC may be as damaging if not more damaging than heat.

The substantially higher rut depths of the MMLS3 1999 northbound hot-dry sections as compared to the MMLS3 1998 northbound dry sections was attributed to the effects of "*temperature*", as it was the primary variable condition. At equivalent axle loads, the measured rut depth in the 1999 MMLS3 hot test was about 60% more than the 1998 dry test. This is indicative that high pavement temperatures accelerate rutting.

As expected, much deeper ruts were obtained under the TxMLS. However a comparison based on the surface layer deformation (*not the total rut*) up to about 90 mm depth demonstrated that the MMLS3 (milled test pads) and TxMLS permanent deformations were comparable within acceptable limits. In fact, the southbound milled pads had higher surface deformations in the upper 90 mm layers compared to the TxMLS. This is not to ignore the fact that there was environmental control in the MMLS3 tests, and none, in the TxMLS tests. In both cases, the rutting trends were similar. For example, the northbound lane had rutted more than the southbound lane under both APT devices.

6.6.3 Comparison of the Pavement Layer Deformation

Analysis of the LDP results for the northbound sections showed that a higher percentage of total permanent deformation occurred in the recycled LWAC (*Dustrol*) layer in *n2* (88%) and *n3* (83%) compared to the limestone AC surfacing layer (49%). This demonstrates that the second *Dustrol* LWAC layer was relatively less resistant to permanent deformation and very sensitive to temperature and moisture compared to the limestone AC overlay. On the southbound structure, the new *Remixer* rehabilitation process had deformed much less compared to the insitu LWAC but more than the limestone AC surfacing, indicating a higher resistance to permanent deformation in comparison to the *Dustrol*. The *Remixer* had behaved more rigidly compared to the *Dustrol* process.

6.6.4 Non-destructive Field Testing (PSPA and SASW)

Both the PSPA and SASW results indicated a loss in stiffness on the wet pads due to water damage and a gain in stiffness on the hot pads due to MMLS3 compaction. There was an average loss of about 35% and 9.5% in asphalt stiffness on the *Dustrol* and *Remixer*, respectively, under wet MMLS3 trafficking.

Both PSPA and SASW test results indicated a similar behavioural change in AC stiffness with MMLS3 trafficking under different environmental conditions. From this, it is apparent that the PSPA and SASW devices are suitable tools for evaluating change in the stiffness of in situ AC pavement layers.

Chapter 7

7 LABORATORY TEST RESULTS

The laboratory tests results; volumetrics, moisture sensitivity, stiffness, strength and indirect tensile fatigue are presented and analyzed. Detailed test results are presented in Appendix III. The results represent average values of at least two tests per core-specimen.

7.1 VOLUMETRICS

No overall information on the AC mixes was available. The binder type and contents were unknown. Some basic measurements like density, voids in the AC mix and VMA were done and are presented below.

There was a relative increase in the density after both trafficking and wetting. This increase was attributed to the decrease in voids due to densification under MMLS3 trafficking. However, there was a loss in bulk relative density (BRD) on the wet pads (as shown in Table 3.5.6, Appendix III), of about 4% on the northbound (*Dustrol*) and 2% on the southbound structure (lower *Remixer*) due to stripping. Some of the BRD test results are shown in Table 7.1.

Table 7.1: Average Relative Bulk Density (BRD) Test Results

Material	BRD (kg/m^3)				
	Untrafficked	Trafficked			
		n1 **(Hot, 320k)**	***n2*** **(Hot, 160k)**	***n3*** **(Wet, 320k)**	***n-wet*** **(Wet, 1 000k)**
Limestone AC	2 153	2 258	-	-	2 353
Dustrol	1 664	1 770	1 736	1 605	1 653
In situ LWAC	1 659	1 664	1 668	1 645	1 661
		s1 **(Hot, 180k)**	***s2*** **(Hot, 80k)**	***s3*** **(Wet, 160k)**	
Upper *Remixer*	1 961	1 984	-	-	
Lower *Remixer*	1 712	1 724	1 749	1 686	
In situ LWAC	1 616	1 680	1 680	1 656	

Table 7.1 also shows that the limestone AC and upper *Remixer* had relatively higher BRDs compared to the lower layers *(Dustrol,* lower *Remixer,* and the in situ LWAC). These were therefore, expected to behave more rigidly than the lower layers.

Table 7.2 shows the air voids and voids in the mineral aggregate (VMA) from the northbound untrafficked sections that were measured by Epps (1999).

Table 7.2: Volumetric Results from Northbound Pavement Structure (Epps, 1999)

Material	Section	Specimen	NST	Air Voids (%)	VMA (%)	BSG
Limestone AC + Lightweight	Untrafficked	Composite	12	8.6	20.1	2.0
Lightweight only (*Dustrol*)	Untrafficked	Lightweight	9	9.3	22.5	1.7

Key: NST – Number of Specimens Tested

This high void content could be a contributing factor to the consolidation (i.e. an average of 4% increase in BSG) and high rutting of the lightweight (under hot MMLS3 trafficking) in comparison to the top limestone AC surfacing layer on the northbound structure. Also, this could be part of the factors that contributed to the substantial water damage on the lightweight material (*Dustrol* and in situ LWAC), after removing the top layer.

7.2 MOISTURE SENSITIVITY

The moisture sensitivity test results of the untrafficked core-specimens are presented in Table 7.3. The results indicate that the surfacing limestone AC on the northbound was most sensitive to moisture, and likely to be damaged by water.

Table 7.3: Retained Tensile Strength Ratio (TSR) after Wet Conditioning

Material	Lane	TSR after Wetting (of untrafficked core specimens)
Limestone AC	Northbound	0.57
Dustrol		0.85
Upper *Remixer*	Southbound	0.91
Lower *Remixer*		0.81

According to the AASHTO T283 (1998) and the new TxDOT and SHRP specification procedures, materials with TSR value that is below 0.7 or 0.8 are considered sensitive to moisture and may subsequently be damaged by water. TSR is the ratio of the indirect tensile strength (ITS) of the specimen after 2 hours wet conditioning divided by the dry ITS without wetting.

However, actual field performance indicated otherwise. As will be discussed later, the in situ LWAC, *Dustrol*, and the second underlying *Remixer* were found to be more sensitivity to moisture than the limestone AC. Under wet trafficking conditions and at equivalent MMLS3 axle loads (320k), the rut measured when trafficking directly on the *Dustrol* surface (~2.4mm) was about 3.4 times compared to trafficking directly on the limestone AC surface (~0.7mm). After 320k axle loads under wet trafficking, the *Dustrol* had already indicated a reduction in insitu stiffness of about 35% (PSPA and SASW) and negligible in the limestone AC (Smit et al, 1999). The underlying (lower) *Remixer* had indicated a loss of 9.5% (PSPA and SASW) after only 160k axle loads.

From the above results, it can be concluded that a pavement's meeting the T283 specifications does not necessarily mean that the AC will not be damaged by water or will not strip. Likewise, failure to meet the specification (TSR≥0.8) may not necessarily mean that the AC will be damaged by water or will strip.

7.3 THE SHEAR TESTS

Table 7.4 shows the average shear test results for the northbound pavement structure (untrafficked) that were measured by Epps (199). The respective values for the loading frequencies of the TxMLS (3Hz) and the MMLS3 (4Hz) were interpolated. These results compare favourably with those reported by Smit et al (1999).

Table 7.4: Average Shear Test Results

Material	Section	Test Temperature (°C)	Test Frequency (Hz)	Shear Modulus G* (MPa)	Elastic Modulus E (MPa)	Phase Angle (δ)
Composite	*nu*	40	2	269	715.54	42.1
			3	327	870	41.0
			4	376	1 000	40.2
			5	413	1 098.58	39.9
Lightweight	*nu*	40	2	241	641.06	41.6
			3	289	770	40.5
			4	332	885	39.4
			5	367	976.22	39.1
Composite	*nu*	25	2	1 026	2 729.16	24.2
			3	1 090	2 900	24.5
			4	1 156	3 075	25.0
			5	1 202	3 197.32	25.6

Key: *nu* - Untrafficked section on the northbound lane

The elastic modulus (E) was calculated from the measured shear modulus (G*) using Equation 7.1 given below (Shames et al, 1985), and assuming a Poisson's ratio of 0.33.

$$E = 2G^*(1+\nu) \quad \text{.....(Equation 7.1)}$$

Where:

E = Elastic modulus in MPa

G* = Shear modulus in MPa

ν = Poisson's ratio (~0.33)

With a Poisson's ratio of 0.33, Equation 7.1 reduces to $E = 2.66G^*$.

The results indicate that the upper surface layers and the underlying lightweight layer could be expected to have a higher stiffness at the same temperature under the MMLS3 (4 Hz) than under the TxMLS (3 Hz). This effect of loading time shows why there could be substantial resistance to permanent deformation in the pavement surface layers under the MMLS3 in comparison to the TxMLS, if trafficking conditions are the same. With the MMLS3 influencing only the surface layers, this result partially explains the small rut depths measured in the 1998 MMLS3 tests by Smit et al (1999) under uncontrolled temperature conditions.

By comparison, the two types of specimens' only showed appreciable differences in shear stiffness (G*) and elastic modulus at 40°C, with higher values for the composite (C) specimens at both representative frequencies. In addition, at the lower testing temperature (25°C) the composite (C) specimens exhibited more elastic behaviour (lower phase angle [δ]) with higher shear stiffness (G*) and elastic modulus values as expected. Higher resistance to rutting was thus expected at low temperature than at higher pavement temperatures. This was evident when comparing the surface ruts measured at 38°C (Smit et al, 1999) to those at 50°C.

Furthermore, the relatively higher modulus value of the composite specimen compared to the lightweight (at 40°C) indicated that the limestone AC might be more resistant to rutting compared to the LWAC. This concurs with the *n1* and *n2* surface ruts measured at 50° C (Chapter 6).

7.4 ITS AND SCB STRENGTH TEST RESULTS

Table 7.5 shows some average ITS and SCB results for the core-specimens from the untrafficked sections of the north- and southbound lanes, respectively.

Table 7.5: ITS and SCB Test Results of the Untrafficked Core-Specimens

Material	Layer No.	Lane	Strength (kPa)		BRD (kg/m^3)
			ITS	SCB	
Limestone AC	1	North	1 202	2 450	2 153
Dustrol	2	North	894	2 035	1 664
Upper *Remixer*	1	South	1 128	2 330	1 961
Lower *Remixer*	2	South	1 142	2 070	1 712
In situ LWAC	3	North	458	1 930	1 659
		South	802*	1 910	1 616

From Table 7.5, the SCBs results indicate that the upper layers (Limestone AC and upper *Remixer)* in the north and southbound were of higher strength compared to the lower layers. During trafficking, these layers had exhibited much resistance to deformation as was discussed in Chapter 6. The SCBs also indicate that the in situ LWAC is almost of the same strength in both the north and southbound lanes. This was expected since it is virtually the same material. The ITS results indicated some differences in the strength pattern, particularly for the southbound lane and the in situ LWAC. For instance, the ITS value of the in situ LWAC in the southbound is about two times more than the ITS value of the in situ LWAC in the northbound structure, yet it is the same material. The apparent reason for this is not known, but perhaps some discrepancies during ITS testing could be the reason.

Table 7.5 also shows that with the exception of the surface layer, the ITS values for the southbound layers were relatively higher than those from the northbound structure. The *Remixer* has an ITS value approximately 38% higher than the *Dustrol.*

In Tables 7.6 and 7.7 the ITS and SCB strength results are presented as ratios of the trafficked core-specimens (*n1*, *n2*, *n3*, *s1*, *s2*, and *s3*) to respective untrafficked core-specimens *nu* and *su.*

All the core-specimens were laboratory tested under dry conditions without wetting, but after being trafficked in the field under different environmental conditions (dry, hot, and wet).

Table 7.6: ITS Strength Ratios

Material	Section	Layer No:	Trafficking Conditions	ITS Strength Ratio (relative to untrafficked sections [Table 7.5])	Comment
Limestone AC	*n1*	1	Hot	0.62	38% loss
Dustrol	*n1*	2	Hot	1.27	27% gain
Dustrol	*n2*	2	Hot	1.22	22% gain
Dustrol	*n3*	2	Wet	1.11	11% gain
Upper *Remixer*	*s1*	1	Hot	1.17	17% gain
Lower *Remixer*	*s1*	2	Hot	0.95	5% loss
Lower *Remixer*	*s2*	2	Wet	0.77	23% loss
Lower *Remixer*	*s3*	2	Wet	0.91	**9% loss**

Table 7.7: SCB Strength Ratios

Material	Section	Layer No:	Trafficking Conditions	SCB Strength Ratio (relative to untrafficked sections, [Table 7.5])	Percentage Change
Limestone AC	*n1*	1	Hot	1.02	+2%
	n-wet		Wet	1.11	+11%
Dustrol	*n1*	2	Hot	1.03	+3%
	n2			1.01	+1%
	n3		Wet	0.83	**17% loss**
	n-wet			0.85	**15% loss**
In situ LWAC	*n1*	3	Hot	1.01	+1%
	n2			0.95	-5%
	n3		Wet	0.61	**39% loss**
	n-wet			0.66	**34% loss**
Upper *Remixer*	*s1*	1	Hot	1.09	+9%
Lower *Remixer*	*s1*	2	Hot	1.05	+5%
	s2			0.89	-11%
	s3		Wet	0.93	**7% loss**
In situ LWAC	*s1*	3	Hot	1.01	+1%
	s2			1.02	+2%
	s3		Wet	0.86	**14% loss**

The indirect tensile strengths (ITS) in axial mode indicated an increase of approximately 20% (Table 7.6) in strength for the *Dustrol* process on the northbound structure after MMLS3 trafficking relative to the untrafficked asphalt *nu*. The increase in strength was perhaps due to densification under MML*S3* trafficking, as was evident from the decrease in air voids and the increase in relative bulk density (~4%). This finding partially explains the relatively high fatigue life obtained for pad *n2*, as is presented later. However, this does not account for the micro cracking and stripping or the loss in stiffness on the wet pad *n3*. A decrease of about 38% in ITS strength was observed for the top limestone AC. The semicircular bending (SCB) test results (Table 7.7) indicated a decrease in strength of about 17% for the core-specimen from test pad *n3* (wet test).

In the southbound section, there was a decrease in both ITS (~9%) and SCB (~7%) strength on the wet test pad *s3* (Tables 7.6 and 7.7). The strength loss was attributed to the effects of water. A decrease in strength was also evident for all the other sections and layers, except *s1* layer 1 (the upper *Remixer* overlay), which had indicated an increase of about 17% in ITS strength (Table 7.6). Densification resulting from MMLS3 traffic compaction was the probable cause. Because of the presence of water throughout the s3 test, the ITS strength ratio for the s3 lightweight layer was expected to be lower than the ratio for the s2 lightweight layer. But this was not the case.

7.5 INDIRECT TENSILE FATIGUE LIFE (N_F)

The indirect tensile fatigue test results presented in Tables 3.5.6 (Appendix III), 7.8 and 7.9 are for the three topmost layers of the northbound and southbound structures, respectively. The results represent an average of at least two core-specimens tested. The procedure for the indirect tensile fatigue testing and method of analysis is shown in Figure 7.1.

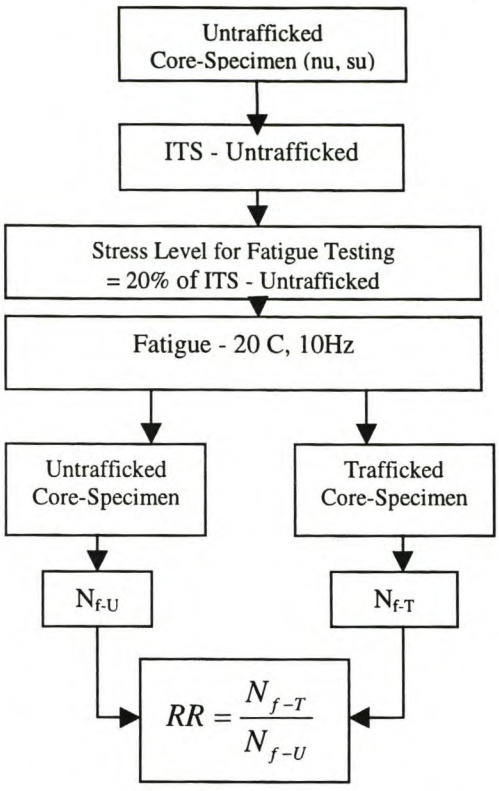

Key: N_{f-U} is the indirect tensile fatigue life of core-specimens from the untrafficked sections, N_{f-T} is the indirect tensile fatigue life of core-specimens from the MMLS3 trafficked sections,

Figure 7.1: Methodology for Indirect Tensile Fatigue Testing and Analysis

Specimens from both the trafficked and untrafficked sections of the dry, hot, and wet test pads were tested at a stress level equivalent to 20% of their respective untrafficked ITS values. Thus for each layer and material type, a similar stress value was used for both the untrafficked and trafficked core-specimens. Analysis was based on comparison of the indirect tensile fatigue life of the trafficked core-specimens relative to the indirect tensile fatigue life of core-specimens from the untrafficked section (RR).

7.5.1 Core-specimens from the Hot-Dry Trafficked Sections

Results for the core-specimens from the hot-dry trafficked sections are presented in Table 7.8, as a ratio of the indirect tensile fatigue life of the trafficked core-specimens relative to the indirect tensile fatigue life of core-specimens from the untrafficked section (RR).

Table 7.8: Indirect Tensile Fatigue Test Results for Core-Specimens from the Hot Trafficked Test Pads [50°C at 25mm pavement depth]

Material Type	Test Section	Layer No.	Stress Level (kPa) (0.2ITS)	N_f		RR $N_{f\text{-}U}/N_{f\text{-}T}$	PC	AL
				U	T			
Limestone AC	*n1*	1	215	884 800	1 519 800	1.7	+70	320
Dustrol	*n1*	2	168	855 000	901 500	1.05	+5	
In situ LWAC	*n1*	3	92	859 880	936 000	1.09	+9	
Dustrol	*n2*	2	168	855 000	1 125 600	1.32	+32	160
In situ LWAC	*n2*	3	92	859 880	742 680	0.86	-14	
Upper *Remixer*	*s1*	1	226	892 743	1 150 000	1.29	+24	180
Lower *Remixer*	*s1*	2	228	398 405	425 600	1.07	+7	
In situ LWAC	*s1*	3	92	733 785	752 400	1.03	+3	
Lower *Remixer*	*s2*	2	228	398 405	472 050	1.18	+18	80
In situ LWAC	*s2*	3	92	733 785	802 000	1.09	+9	

Key: N_f – Number of fatigue load cycles, U – Untrafficked, T – Trafficked, PC = Percentage Change, AL = MMLS3 Axle Loads (k)

The results in Table 7.8 show that the heated asphalt layers (pads *n1*, *n2*, *s1*, and *s2*) gained fatigue life in the order of about 20% for the northbound and 13% for the southbound structures, because of MMLS3 traffic compaction. J. Epps (1969), Tangella (1990), and Raithby and Ramshaw (1972) had also found that traffic compaction and an increase in asphalt stiffness increased fatigue life to the extent that it offset the effects of damage caused by traffic. However, the fatigue life subsequently decreases with extended trafficking owing to damage.

7.5.2 Core-specimens from the Dry Trafficked Sections (Smit et al, 1999)

Relatively shorter fatigue lives were obtained from the *n-dry* section (Smit et al. 1999) on both the untrafficked and trafficked cores. This finding was ascribed to the lower quality material in this section, as was discussed previously. The indirect tensile fatigue life of the *n-dry* core-specimens ranged between 200k to 350k load repetitions (Table 3.5.6, Appendix III). In the case of the *n1* and *n2* core-specimens, the range was from 700k to about 1 500k. However, the relative ratio (RR) of the fatigue life (with respect to the untrafficked section *nu-D*) of the limestone AC (layer 1) and *Dustrol* (layer 2) for the *n-dry* section (Table 3.5.6, Appendix III), exhibited a trend similar to the results for pads *n1* and *n2*, albeit their N_f values were of smaller magnitude. This trend is indicative of the damage from extended trafficking (1.0 million axle loads) and the effect of temperature.

7.5.3 Core-Specimens from the Wet Trafficked Sections with Water on the Pavement Surface

The RR results for core-specimens from the wet trafficked test pads with water on the pavement surface are presented in Tables 7.9. Detailed results are given in Appendix III (Table 3.5.6).

Table 7.9: Indirect Tensile Fatigue Test Results of Core-Specimens from the Wet Trafficked Test Pads with Water on the Pavement Surface

Material Type	Test Section	Layer No.	Stress Level (kPa) (0.2ITS)	N_f		RR	Percentage Change	MMLS3 Axle Loads Applied
				U	T			
Dustrol	*n3*	2	168	855 000	488 600	0.57	-43	320 000
In situ LWAC		3	92	859 880	340 000	0.4	-60	
Limestone AC	*n-wet*	1	215	884 800	785 533	0.89	-11	1 400 000
Dustrol		2	168	855 000	186 437	0.22	-78	
In situ LWAC		3	92	859 880	171 420	0.2	-80	
Lower *Remixer*	*s3*	2	228	398 405	358 200	0.9	-10	160 000
In situ LWAC		3	92	733 785	512 600	0.7	-30	

Key: N_f – Number of fatigue load cycles, U – Untrafficked, T – Trafficked.

The wet pads showed a reduction in indirect tensile fatigue life relative to the untrafficked asphalt as well as in comparison with the heated pads *n1*, *n2*, *s1*, and *s2*. Figure 7.2 shows these results graphically. The *Dustrol* on pad *n3* had a reduction of about 43% (after 320k), while the reduction for the lower *Remixer* on pad *s3* was about 10% (after 160k). These reductions were due to the effects of water. The LWAC on the southbound section had a loss of about 30% after 160k, and the northbound had a loss of 60% for the LWAC after 320k. Figure 7.2 shows that these changes fall on the same line and thus exhibit a degree and extent of water damage similar to the amount they would have exhibited had they been subjected to the same number of MMLS3 traffic axles. This finding was not surprising since it is virtually the same material. The SCBs test results also indicated this.

The damage under extended trafficking for both the *Dustrol* and LWAC was far greater, as evident from the 21% residual fatigue life of *n-wet* after 1.4 million load applications (Table 7.6 and Figure 7.2). However, the slope of the 1998 *Dustrol* and LWAC graphs (Figure 7.2) is not as steep as that of the corresponding 1999 graphs. This difference is an indication that the progression of water damage was not as rapid and as intensive as that in the 1999 wet tests owing to the limestone AC cover in the 1998 test. It should be remembered that the top 25 mm of limestone AC was milled off in the 1999 wet tests. If MMLS3 trafficking had continued in the 1999 wet tests, the predicted extrapolation indicate that the lower *Remixer*, the *Dustrol,* and the in situ LWAC would have been reduced to about 21% residual fatigue life after about 1,226k, 585k, and 455k, respectively.

The damaging effect of wet axles is apparent, and it is clear that the number of axle loads that can be carried is significantly reduced under wet conditions, even under the light wheel loads of the MMLS3. In fact, because the south- and northbound LWACs (L3) were found to be equally susceptible to water damage, both pavement structures would probably perform the same under wet trafficking, in the case water could gain direct access to the LWAC layer through cracks or a porous surface.

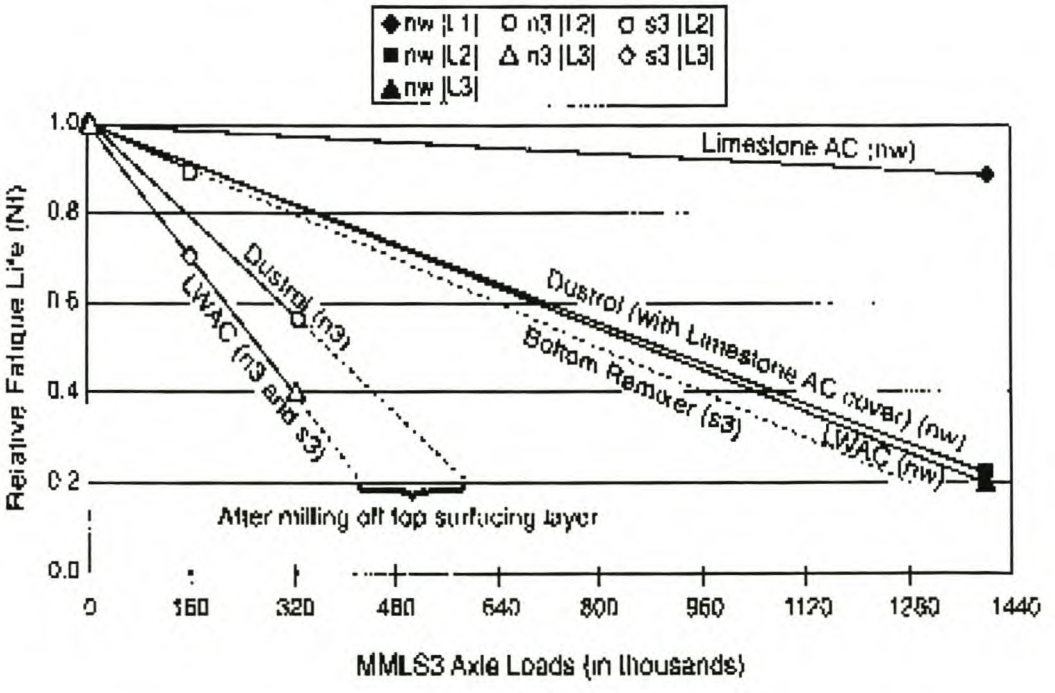

Figure 7.1: Relative Fatigue Life after Wet MMLS3 Trafficking

Both Table 7.6 and Figure 7.2 indicate that the upper limestone AC on the northbound structure appeared to be less affected by water; it had a residual indirect tensile fatigue life of about 89% of the original asphalt after 1.4million MMLS3 axle loads. By contrast, the *Dustrol* and in situ LWAC had a residual fatigue life of approximately 57% and 40% respectively, just after 320k axle loads. This finding is contrary to the prediction in terms of the AASHTO T283 test results. The AASHTO T283 test results (Table 7.3) had indicated that the limestone AC was the most moisture sensitive material and likely to be damaged by water.

In comparison to core-specimens from the heated pads *n1*, *n2*, *s1*, and *s2*, which had indirect tensile fatigue life in the order of about 400k to 1 500k load cycles, core-specimens from the wet pads ranged between 170k to 800k. Core-specimens from the untrafficked sections had between 390k to 900k fatigue load cycles prior to failure.

7.7 SUMMARY AND FINDINGS

Core-specimens from the hot dry trafficked test pads exhibited a relative increase in BRD, strength and N_f due to MMLS3 compaction.

Loss in strength, BRD, and N_f were indicators of moisture damage on wet test pads. As regards to the material performance, it was found that the *Dustrol* material on the northbound pavement structure was more susceptible to water damage than the *Remixer* material. The *Remixer* material exhibited more strength and stiffness than the *Dustrol* material.

In terms of water damage, the worst affected was the in situ LWAC, whilst the least was the limestone AC. The AASHTO T283 (1998) moisture sensitivity test results had predicted otherwise. This difference needs further investigation.

A gain in indirect tensile fatigue life (about 17%) due to heating and MMLS3 traffic compaction was evident from the test results on cores from the hot-dry pads. However, there was an average loss of about 35% in indirect tensile fatigue life on the cores from the wet pads due to water damage. Also, there was an average decrease of about 12% in SCB strength on the cores from the wet test pads (*n3* and s3).

With regard to the strength tests, the SCB test method gave a more consistent picture of the material performance under the MMLS3 trafficking compared to the ITS.

Chapter 8

8 RELATING RUTTING PERFORMANCE OF THE MMLS3 WITH THE TxMLS

The rutting performance of the MMLS3 was compared to that of the TxMLS by taking account of temperature differences as well as the tyre pressures and the stress distribution (Walubita et al, 2000 [a]). The actual field trafficking conditions and loading parameters were used. Both the north- and southbound Jacksboro-Texas pavement structures (Figure 3.1, Chapter 3) were considered. For both the stress and deformation comparisons, only the top AC layers were considered.

The comparison was based on the theoretical and actual field rut ratios. The methodology for the analysis is shown in Figure 8.1.

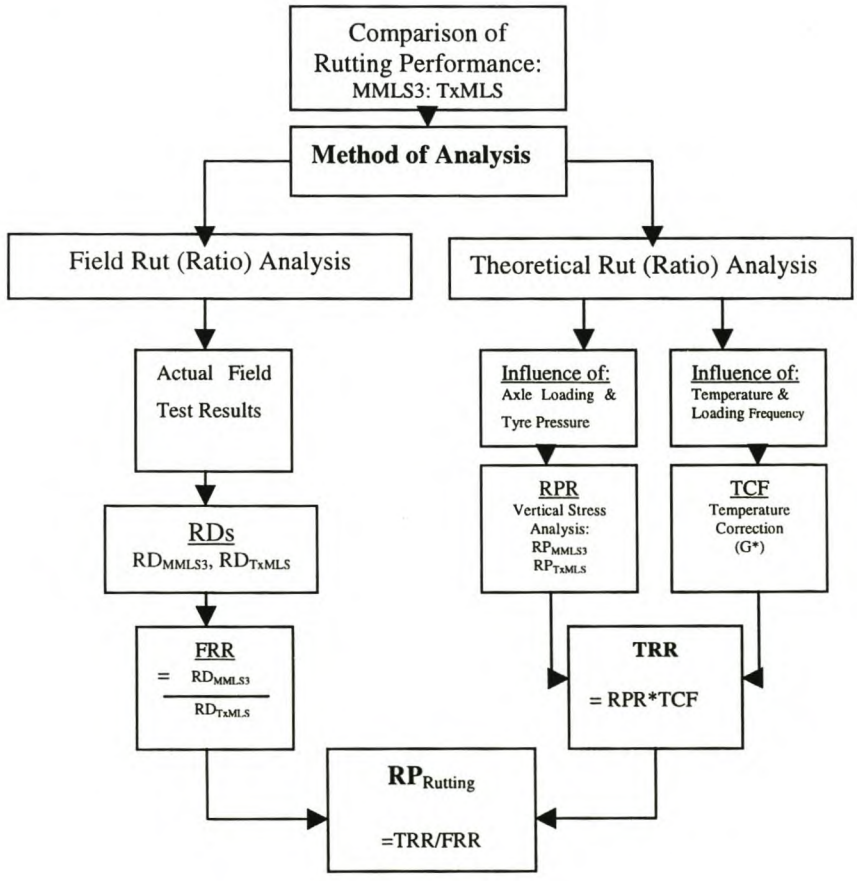

Figure 8.1: Method of Analysis

8.1 METHOD OF ANALYSIS

The theoretical rut ratios (TRR) were calculated from the vertical stress profiles after correcting for the differential factors (vertical stress, temperature, loading frequency, etc), and the actual field rut ratios (FRR) were calculated from the actual measured ruts between the MMLS3 and TxMLS. FRR is simply the ratio of the actual rut depth (RD) under the MMLS3 to that measured under full-scale trafficking, in this case using the TxMLS:

$$FRR = \frac{RD_{MMLS3}}{RD_{TxMLS}} \quad \text{(Equation 8.1)}$$

Where:

FRR	=	ratio of actual rut depth under MMLS3 to TxMLS
RD_{MMLS3}	=	actual measured rut depth under MMLS3
RD_{TxMLS}	=	actual measured rut depth under TxMLS.

These RDs represent measurements on the same pavement structure.

The methodology for the theoretical rut ratio (TRR) analysis involved consideration of the temperature and tyre pressure to determine the vertical stress for the specific loading configurations of both the MMLS3 and TxMLS. Vertical stress analyses are used to determine the TRR. This value represents the ratio of the theoretically estimated RDs under the MMLS3 and under full-scale trafficking (TxMLS):

$$TRR = \frac{Theoretical.RD_{MMLS3}}{Theoretical.RD_{TxMLS}} \quad \text{(Equation 8.2)}$$

Where;

TRR	=	theoretical rut ratio under MMLS3 to TxMLS
$Theoretical.RD_{MMLS3}$	=	theoretical rut depth under MMLS3 determined from vertical stress analysis
$Theoretical.RD_{TxMLS}$	=	theoretical rut depth under TxMLS determined from vertical stress analysis

The areas encompassed by the maximum vertical compressive stress distribution with depth for each loading condition (MMLS3, full-scale) are defined as corresponding rutting potentials (RPs) of a specific pavement section or layer (Epps et al, 2000). The rutting potential ratio (RPR) is then calculated as the ratio of these RP values as follows:

$$RPR = \frac{RP_{MMLS3}}{RP_{TxMLS}} \quad \text{.....(Equation 8.3)}$$

Where;

RPR	=	rutting potential ratio
RP_{MMLS}	=	rutting potential of the MMLS3 which is equivalent to the area encompassed within the vertical stress bowl (MPa*mm).
RP_{TxMLS}	=	rutting potential of the TxMLS which is equivalent to the area encompassed within the vertical stress bowl (MPa*mm).

If the characteristic temperature during MMLS3 testing is not representative of the environmental conditions during full-scale trafficking, a correction factor is applied to account for differences in both temperature and loading frequency. This temperature correction factor (TCF) is based on mixture shear stiffnesses (G*) measured at multiple temperatures and frequencies and, the assumption that rutting is inversely proportional to G* (Walubita et al, 2000 [a], Epps et al, 2000). In terms of rutting, the TRR is then equal to the product of the RPR and the TCF. If the characteristic temperatures for MMLS3 testing and full-scale loading are approximately equivalent (i.e.TCF = 1), then TRR is equal to the RPR.

The framework for validating the performance prediction methodology based on vertical stress analysis and MMLS3 testing as described above, requires that the TRR be equivalent to the FRR. If the ratio of TRR and FRR described subsequently is defined as the rutting performance ratio ($PR_{rutting}$), its value must be assumed equal to one (Epps et al, 2000). I.e.

$$RP_{Rutting} = \frac{TRR}{FRR} \approx 1.0 \quad \text{.....(Equation 8.4)}$$

Where;

$PR_{rutting}$ = Rutting Performance Ratio

8.2 LOADING PARAMETERS

Since the TxMLS tests were done under dry conditions, only the hot dry MMLS3 tests were considered. Therefore, the only variable environmental condition between the two sets of tests (MMLS3 and TxMLS) was temperature.

The loading configuration is that shown in Figure 8.2, and represents the actual loading parameters that were used in the field.

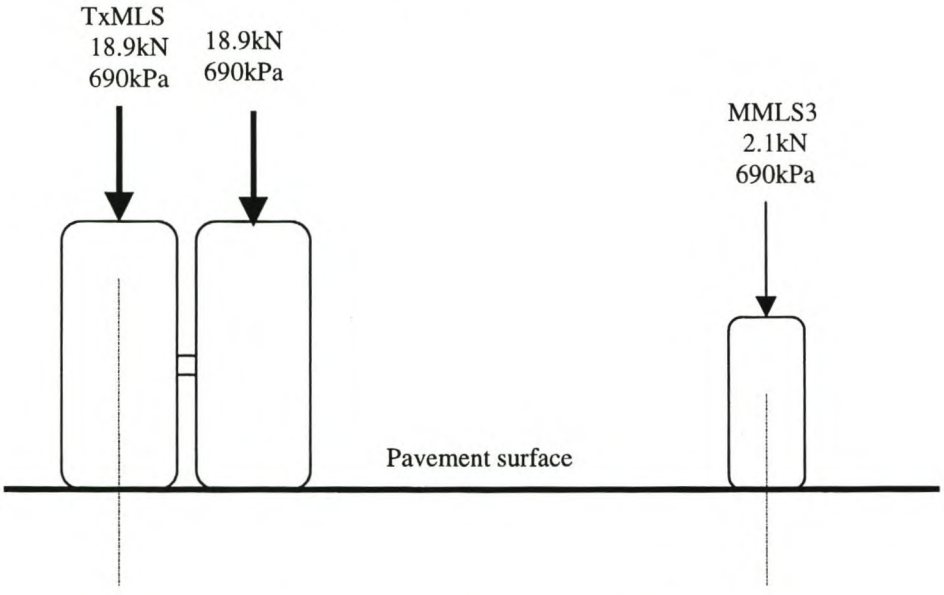

Figure 8.2: MMLS3 and TxMLS Loading Configuration

Analysis was done under the centre of the wheel where the maximum vertical compressive stress occurred.

8.3 PAVEMENT STRUCTURE AND MATERIAL CHARACTERIZATION

The pavement structure and material characteristics that were used in the BISAR 3.0 stress analysis are shown in Figure 3.1 and, Tables 8.1 and 8.2. The respective AC moduli were reduced to the corresponding measured mid-depth layer temperatures from 25°C using the FWD temperature-correction Equations 8.5 and 8.6 developed by Hugo et al (1999 [c]).

$$Y_N = 1.7088 - 0.0254T \quad \text{.....(Equation 8.5)}$$

$$Y_S = 1.4652 - 0.0192T \quad \text{.....(Equation 8.6)}$$

Where:

Y = temperature correction factor for normalization to 25°C.

T = mid-layer depth temperature in °C

In Equations 8.5 and 8.6, the subscripts N and S represent north and southbound lanes, respectively. Equation 8.5 was used to normalize the AC moduli on the northbound structure and Equation 8.6 on the southbound. The two-temperature correction Equations were developed from the FWD tests conducted by Hugo et al (1999 [c]) on the Jacksboro-Texas pavement structure. The initial stiffness values at 25°C were based on measured values determined from SASW in the field and frequency sweep tests, cross-hole tests, and fatigue tests in the laboratory (Hugo et al, 1999, and Smit et al, 1999).

Table 8.1: Pavement Structure and Stiffness Values (MMLS3)

Pad	Layer	Thickness (mm)	Approximate Stiffness Values (MPa)						
			25°C	at 50°C		at 50°C		at 30°C	
				n1	*s1*	*n2*	*s2*	*n3*	*s3*
North	Limestone AC	25	3500	1350					
	Dustrol	25	2200	1070		850		2000	
	Insitu LWAC	20	2400	1400		1170		2270	
South	Upper *Remixer*	25	3500		1700				
	Lower *Remixer*	25/10	3500		1700		1400		3180
	Insitu LW AC (1986)	25	2400		1390		1030		2080
Lower Layers	Limestone AC (1976)	30	3500	2600	2230	1980	1900	3325	3100
	Composite Aggregate AC	40	2000	1740	1470	1380	1280	2000	1740
	Old AC	40	1500	1490	1270	1230	1070	1600	1400
	Seal Coat	15	800	800	800	700	620	880	780
	Base (1957)	380	400	Stiffness values are temperature insensitive					
	Subgrade	1325/2000	200						
	Bedrock		20000						
	Poisson's ratio (ν):								0.35

Table 8.2: Material Properties (TxMLS)

Layer	Material	Approximate Thickness (mm)		Approximate Stiffness Values (MPa)	
		Measured	Tolerable Range	Pad N1 [30.5°C]	Pad S1 [25.5°C]
1	Limestone AC – N1 Upper *Remixer* – S1	25	20-25	2800	2840
2	Dustrol – N1 Lower *Remixer* – S1	25	20-25	2000	2840
3	Insitu LWAC	20	20-25	1900	2000
4	Limestone AC (1976)	30	30-35	2850	2850
5	Composite Aggregate AC (1971)	40	35-40	1600	1630
6	Old AC	40	25-40	1200	1220
7	Seal Coat (1957)	15	15-20	700	650
8	Base (1957)	380	~380	400	400
9	Subgrade	1325/2000	~1325/2000	200	200
10	Bedrock	∞	∞	20000	20000
Poisson's ratio (v):					0.35

8.4 VERTICAL STRESS PROFILES

The vertical stress profiles up to a depth of about 175mm are shown in Figure 8.3. The stress distribution was deliberately truncated at this depth level, as interest was only in the top AC layers (up to about 90mm depth). The TxMLS stress influence extends much deeper into the base and subgrade. From the vertical stress profiles, the respective RPs were calculated as follows:

For the MMLS3 in the northbound lane, the RP was calculated to a depth of about 95mm, combining the top 25mm depth of test pad *n1* and the top 70mm of test pad *n2* as shown in Figure 8.1. These were the depths to which deformations pins (LDPs) were inserted and subsequently, the basis for both the RP and RD calculations in this analysis. The calculated RP of the shaded area in Figure 8.1 is 29.48 MPa*mm. In the case of the TxMLS, the MDDs were provided at a depth of 90mm, and this was the basis for the RP and RD calculations. The computed RP up to this depth for the TxMLS is 50.14MPa*mm. The same principle was used for the southbound lane, but in this case the top 50mm *s1* and top 50mm *s2* were used, as LDPs were provided at these depth levels. The calculated RPs were 42.36 and 63.28 MPa*mm for the MMLS3 and TxMLS, respectively, on the southbound lane.

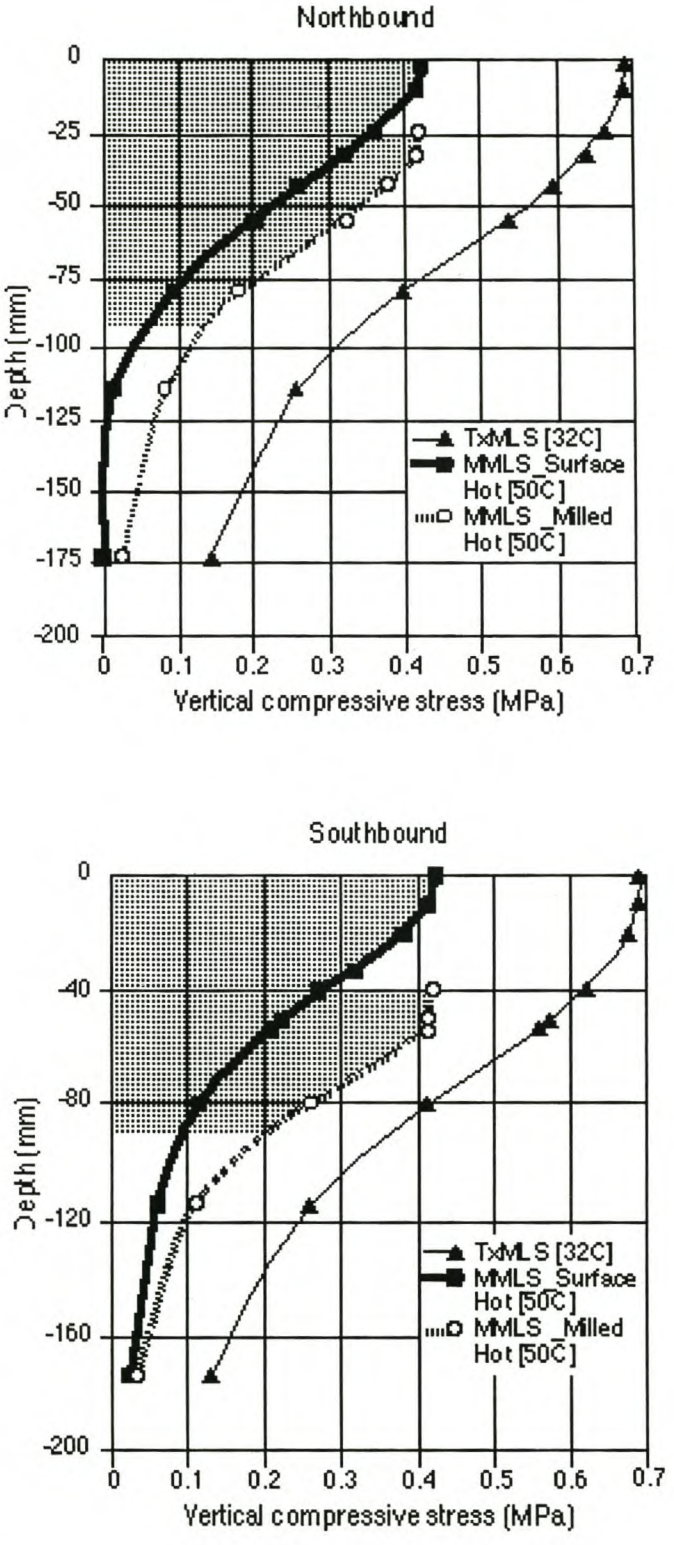

Figure 8.3: MMLS3 and TxMLS Vertical Stress Profiles

NB: The temperatures for the TxMLS should read 30.5 and 25.5 C for the north-and southbound respectively – and not 32 C as indicated. The average trafficking temperature during the 320 k and 160 k phase for the TxMLS, for the north and southbound lanes were 30.5^0 and 25.5° C.

8. 5 TEMPERATURE CORRECTION FACTOR (TCF)

After computing the RP of the MMLS3 and TxMLS, and subsequently the RPR, the second step was to account for temperature and loading frequency difference between the various tests by using G* to determine a TCF. It was assumed that rutting is inversely proportional to the G* values at the respective temperatures. This was taken into account by determining a TCF based on the ratios of the respective G* values in Figure 8.4.

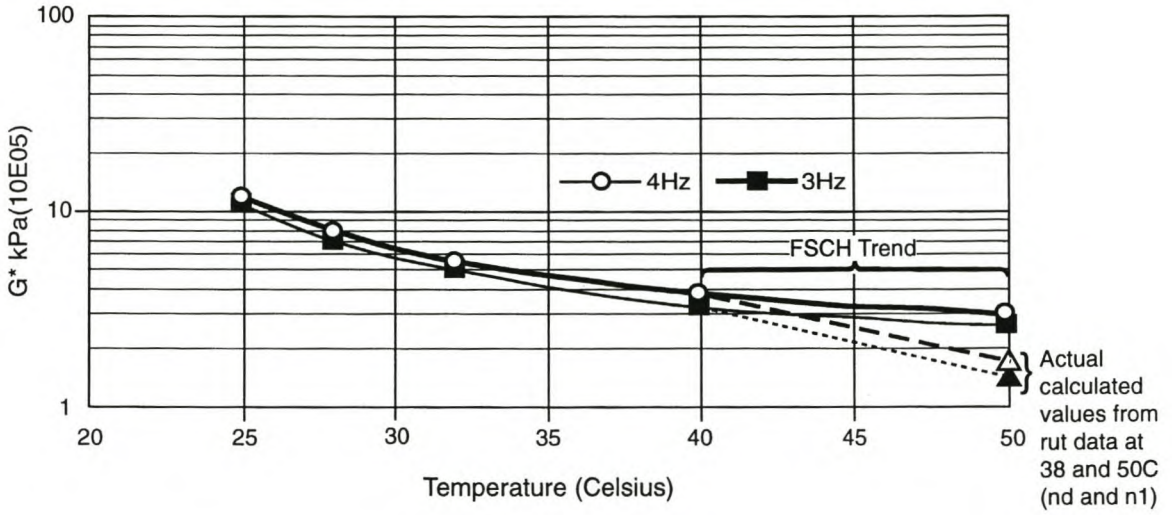

(a) Thre northbound lane

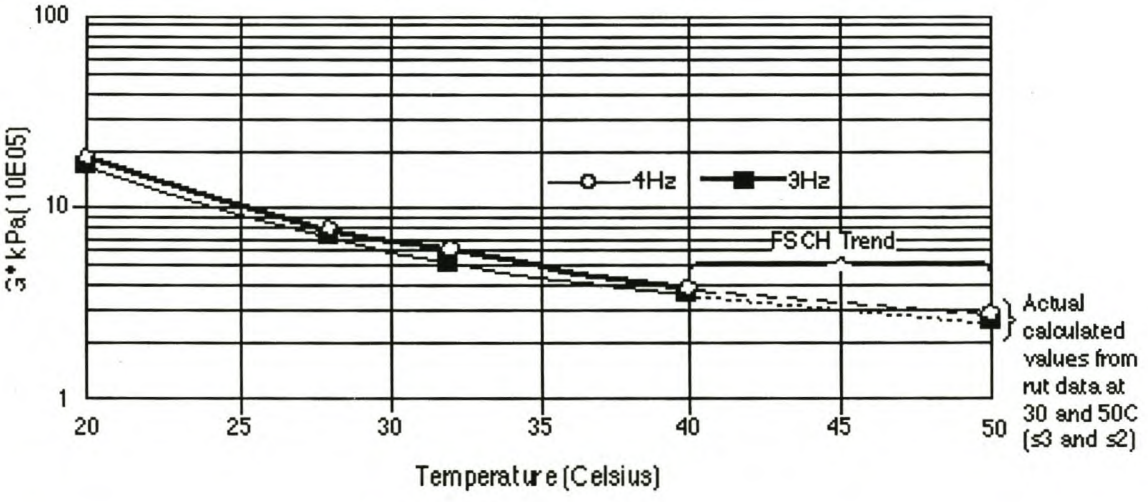

(b) The southbound lane

Key: FSCH - Frequency Sweep test at Constant Head (Epps, 1999, and Smit et al, 1999)

Figure 8.4: Shear Stiffness (G*) of the Mix versus Temperature

Since the G* values had only been determined up to 40°C, values at 50°C had to be determined by extrapolation. However, because of the sensitive nature of extrapolation, these values were checked by using the results of the MMLS3 tests. It was hypothesised that a pseudo G* could be calculated from the rutting data measured in two independent MMLS3 tests.

8.5.1 Determination of the pseudo G* values for the Northbound test section

For this analysis, the results for *n-dry* (Smit et al, 1999) and *n1* were used (Walubita et al, 2000 [a]).

1. Rutting Potential Ratio (690kPa/420kPa): *n-dry/n1* = 32.215/20.6 = 1.56

2. Rut of *n1* at higher tyre pressure, i.e 690kPa, 320k: 1.56*2.165 = 3.38mm
   n-dry rut @ 320k was: =~1.30mm

3. Therefore actual rut ratio @ 320k is *n1/n-dry*: 3.38/1.3 = 2.6

4. Using G* @ 38 °C (Figure 8.4 [a]) as basis, we find a "pseudo" G* at 50 °C for MMLS3 (4Hz) by using the actual rut ratio

   I.e. @ 38 °C, G* = 4.06×10^5 kPa
   @ 50 °C, G* = 4.06×10^5 kPa/2.6 = $\underline{1.56 \times 10^5 \text{ kPa}}$

   This yields 3Hz (TxMLS) pseudo G* of about $\underline{1.4 \times 10^5 \text{ kPa}}$ @ 50 °C

5. Temperature Correction Factor (TCF)

   G* @ 30.5 °C (Figure 8.4 [a])/G* @ 50 °C
   =5.5×10^5 kPa/1.56×10^5 kPa = **<u>3.53</u>**

8.5.2 Determination of the pseudo G* values for the Southbound test section

For this analysis, the results for *s2* and *s3* were used (Walubita et al, 2000 [a]).

1. Rutting Potential Ratio (690kPa/420kPa): *s2/s3* = 1.64

2. Rut of *s2* at higher tyre pressure, i.e. 690kPa, 160k: 1.64*1.5 = 2.46mm
   s3 rut @ 160k was: = ~1mm

3. Therefore actual rut ratio @ 160k is *s2/s3*: 2.46/1.0 = 2.46

4. Using G* @ 30 °C (Figure 8.4 [b]) as basis, we find a "pseudo" G* at 50 °C for MMLS3 (4Hz) by using the actual rut ratio

   I.e. @ 30 °C, G* = 6.8×10^5 kPa
   @ 50 °C, G* = 6.8×10^5 kPa/2.46 = $\underline{2.76 \times 10^5 \text{ kPa}}$

   This yields 3Hz (TxMLS) pseudo G* about of $\underline{2.5 \times 10^5 \text{ kPa}}$ @ 50 °C

5. Temperature Correction Factor (TCF)

   G* @ 25.5 °C (Figure 8.4 [b])/G* @ 50 °C
   = 9.0×10^5 kPa/2.76×10^5 kPa = **3.26**

From the results of the northbound, the calculated pseudo G* did not match the extrapolated trend whereas the south fitted closely (Figure 8.4).

The theoretical rut ratio (TRR) was obtained by multiplying the RPR with the TCF. For the field rut ratios (FRR), the actual measured rut values (RDs) at equivalent axles were used.

8.6 COMPARISON OF THE THEORETICAL AND FIELD RUT RATIOS

The analysis for the comparison is shown in Table 8.3 (Walubita et al, 2000 [a]).

Table 8.3: Comparison of MMLS3-TxMLS Rut Ratios (up to about 90mm Depth)

Lane	Calculations		RPR	TCF	TRR (RPR*TCF)	FRR	TRR versus FRR
	Permanent Deformation (mm) (RD)	RP (MPa*mm)					
North	1.MMLS3: *n1* top 25mm + *n2* top 70mm @ 320k = 1.06+ 3.74 ≈ 4.8mm 2. Average TxMLS rut in top 90mm @ 320k ≈ 2.93mm	MMLS3: 29.48 TxMLS: 50.14	0.59	3.53	2.1	~1.7	1.2
South	1.MMLS3: *s1* top 50mm + *s2* top 50mm @ 160k = 0.391 + 1.395≈1.786mm 2. Average TxMLS rut in top 90mm @ 160k ≈ 0.762mm	MMLS3: 42.36 TxMLS: 63.28	0.67	3.26	2.2	2.3	1.0

Key: RD = Rut Depth,RP = Rutting Potential, RPR = Rutting Potential Ratio, TCF = Temperature Correction Factor, TRR = Theoretical Rut Ratio, FRR = Field Rut Ratio

For the northbound, the MMLS3: TxMLS RPR was 0.59, and it was 0.67 for the southbound. The respective TCFs were 3.53 and 3.26 (Table 8.3). The rut ratios (theoretical versus field) for the northbound sections were approximately 2.1 versus 1.7 for the MMLS3: TxMLS. In the southbound structure, the values were 2.2 and 2.3, respectively. The latter value was possibly higher than its northern counterpart due to the fact that layer 2 (L2) in pad s2 was thinner than layer 2 (L2) in pad n2. The $PR_{rutting}$ were 1.2 and 1.0 for the northbound and southbound structures, respectively.

The above methodology was also used to evaluate the actual rut ratios reported by Smit et al (1999) for their tests with the MMLS3. The results are shown in Table 8.4. It will be seen that the relationship between the actual rut ratios and those theoretically calculated is 1.3, which is almost the same as that found for the comparison between the MMLS3 and the TxMLS on the northbound lane.

The respective theoretical versus field rut ratios ($PR_{rutting}$) are shown in column 8 of Tables 8.3 and 8.4. This is remarkable given the different temperature conditions and trafficking. Nonetheless, it is apparent that G* alone does not include all the factors that impact the rut ratios.

Table 8.4: Comparison of MMLS3 Rut Ratios in the Northbound Lane (*n-dry* versus *n-wet)* (Smit et al, 1999)

Pad	Calculations		RPR	TCF	TRR	FRR	TRR versus FRR
	Rutting after 1.0 million axles (mm) (RD)	RP (MPa*mm)					
n-dry	1.8	32.2	1.1	2.39	2.6	2.0	1.3
n-wet	0.9	30.5					

Considering the pilot nature of the project and the low axle counts, these results are very promising. It appears reasonable to use G* ratios as a temperature correction factor when estimating the field rut ratio due to trafficking. This supports the findings reported by Anderson et al (2000).

8.7 SUMMARY AND FINDINGS

A rutting performance analysis based on stress distribution, actual measured rut values and consideration of the different loading and environmental conditions between the MMLS3 and TxMLS was presented. The methodology used, and the results obtained are very promising. The calculated $PR_{Rutting}$ ranged between 1.0 to 1.3. However, further research into the use and validation of this methodology is recommended.

Given the limited nature of this study and considering all of the influencing factors (loading, trafficking conditions, etc) and the assumptions needed to account for the factors, these results are significant and illustrate the performance prediction capability of the MMLS3.

Chapter 9

9 DISCUSSIONS, CONCLUSIONS AND RECOMMENDATIONS

Discussions of the results, findings, conclusions and recommendations are presented.

9.1 DISCUSSIONS

A comparative analysis of the field and laboratory test results is discussed below.

9.1.1 Rutting, Layer Deformation and Material Properties.

When comparing the measured material properties of the untrafficked core-specimens from both the north- and southbound lanes with respect to rutting and deformation, the following were observed;

- The BRD, the shear test results, the ITS and SCB indicated that the limestone AC had a higher strength and stiffness than the *Dustrol* and in situ LWAC, respectively. The in situ LWAC exhibited the least strength and was in fact the worst affected in terms of water damage. The measured rutting and deformation during MMLS3 trafficking confirmed these results. Smaller surface ruts were obtained when trafficking directly on the limestone AC surface compared to the *Dustrol* surface. This was indicative that the limestone AC was more resistant to deformation.

- A similar trend was observed for the southbound lane. The upper *Remixer* exhibited greater strength, stiffness and high resistance to deformation compared to the lower *Remixer* and in situ LWAC, respectively.

- With regard to hot MMLS3 trafficking, the major adverse effect was increased rutting and deformation, but this increased the fatigue life of the pavement materials due to densification and increase in strength.

9.1.2 Moisture Sensitivity, Wet Trafficking and Water Damage

Table 9.1 shows a summary of the average test results in respect of moisture sensitivity, wet trafficking and water damage from the field and laboratory test results. TSR is used as a measure of moisture sensitivity. The stiffness, BRD, ITS, SCB and N_f test results are presented as the relative ratio of the wet trafficked to the untrafficked sections (RR).

Table 9.1: Summary Results

Material	TSR	RR					Rut	Axle Loads Applied (k)
	AASHTO T283	Stiffness (PSPA/ SASW)	BRD	ITS	SCB	N_f		
Limestone AC	0.57	0.63*	1.09	1.16	1.11	0.89	1.0	1 400
Dustrol	0.85	0.65	0.96	1.11	0.83	0.57	2.4	320
In situ LWAC -1	-		0.99	-	0.61	0.40		
Upper *Remixer*	0.91	-	-	-	-	-	-	-
Bottom *Remixer*	0.81	0.905	0.98	0.91	0.93	0.9	1.1	160
In situ LWAC - 2	-		1.02	-	0.86	0.7		

NB: * Smit et al, 1999

According to the AASHTO T283 and, the TxDOT and SHRP minimum TSR value of 0.8, the limestone AC is the most moisture sensitive material and likely to be damaged by water. In the southbound lane, the lower *Remixer* was expected to be moisture sensitive. No moisture sensitivity tests were done for the LWAC.

However, field performance in terms of rutting and stiffness loss, and the SCB and N_f RR values (Table 9.1) indicate that the *Dustrol* was more sensitive to moisture damage compared to the limestone AC. Despite being trafficked to a much higher number of wet axles, the rut depth on the limestone AC surface was much smaller and the RR values higher than those for the *Dustrol* surface that was trafficked only to about 23% the total number of wet axles applied on the limestone AC surface. The rut on the *Dustrol* surface after 320k axles was about 2.4 times more compared to that measured on the limestone AC surface after 1.4 million axles.

Considering the number of wet axles applied on the limestone AC surface; the measured rut depth and the RR values in Table 9.1 indicate that there was no significant water damage in the limestone AC. Yet the AASHTO T283 test method had predicted high moisture sensitivity and probability of water damage compared to the *Dustrol* and *Remixer*.

Both SCB and N_f RR values indicate that the in situ LWAC was the most sensitive material to water damage. The SCB and N_f RR values further indicate that at equivalent MMLS3 axle loads, the insitu LWAC in both the northbound and southbound structures would probably exhibit a similar degree and extent of water damage. Therefore both pavement structures would perform similarly under wet trafficking, in the case water could gain direct access to the in situ LWAC.

With water on the pavement surface, the impact was loss in stiffness, strength and N_f, micro cracking, stripping, AC degradation and increased rutting. All these effects are indicators of moisture damage.

9.1.3 Other Factors Related to the Performance of the Pavement Structures/Materials

Air void content, material volumetrics and age are some of the factors that could have affected the performanc the performance of the pavement structures/materials. These are discussed below.

9.1.3.1 Air Void Content

According to the retained mix strength –air void relationship (Figure 9.1), the 9.3% and 12.5% air void of the *Dustrol* and *Remixer* respectively, fall within the "pessimum void range" (Ronald et al, 1993). In this air-void content range, the highest water damage is experienced and the asphalt strength after wetting is relatively low. This perhaps contributed to the relatively poor performance of the *Dustrol* and *Remixer* under wet trafficking.

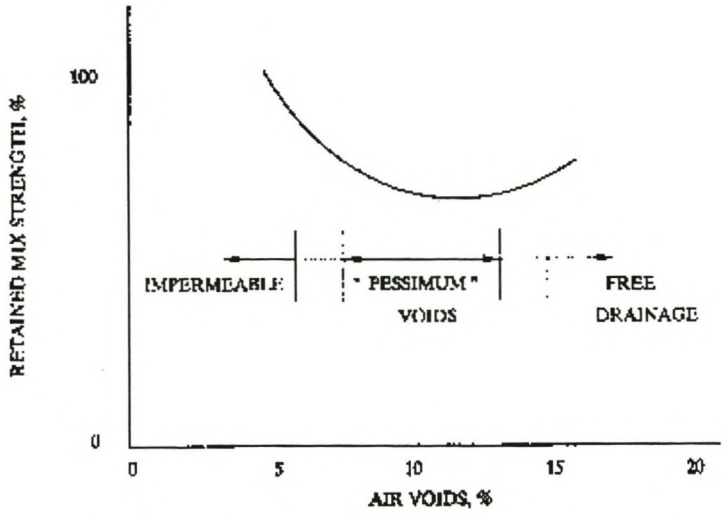

Figure 9.1: Dependence of relative strength of mixtures on access to water in void system (Ronald et al, 1993)

9.1.3.2 Material Volumetrics

Volumetric properties such as binder grade, binder content, the stone aggregate (size and gradation), etc were not taken into account during analysis. These could have had an effect on the performance of the two pavement structures.

9.1.3.3 Age

Age was another factor not considered in the analysis. The *Remixer* (1995) on the southbound lane is one year older that the *Dustrol* (1996) (northbound lane).

9.2 CONCLUSIONS

From the findings of the study, the following conclusions were made.

9.2.1 Temperature and Rutting

High temperatures promote rutting in asphalt pavements. Deeper surface ruts manifested when trafficking the pavement at a higher temperature of 50° C at 25mm depth, compared to 38° C and 24° C, respectively.

9.2.2 Moisture Damage

Under wet trafficking with water on the pavement surface, moisture leads to reduction in asphalt stiffness, stripping, cracking, degradation, and loss in fatigue life. The wide-ranging distress accelerates pavement damage and is undesirable.

9.2.3 Pavement /Material Performance in Terms of Rutting and Deformation

- The *Remixer* material was more rut resistant than the *Dustrol* Material. The surface layers of the northbound pavement structure were also less resistant to permanent deformation than the southbound structure under MMLS3 trafficking. This validates the TxMLS findings.
- Deeper surface rutting manifested in the northbound structure than in the southbound structures under heated testing indicating that it was more sensitive to temperature than the southbound structure.
- The theoretical versus field rut ratios ($PR_{Rutting}$) (MMLS Mk3:TxMLS) ranged from 1.0 to 1.3. Given the limited nature of the study, and considering all the influencing factors, this finding is considered significant and very promising for future applications of the two machines.
- It was found that the use of G* as a temperature correction factor was a reasonable methodology for use in relating rutting at different temperatures. It was used in this manner to compare the rut ratios between the MMLS3 and TxMLS. However, it appears that the use of the G* does not take into account all the factors that affect the rut ratios.

9.2.4 Pavement/Material Performance in Terms of Non-Destructive Insitu Asphalt Stiffness Measurements

In general, there was a gain in insitu asphalt stiffness on the dry-hot pads due to material densification under MMLS3 trafficking. In the wet pads, there was a loss of stiffness due to water damage. Both the PSPA and SASW device had indicated these findings.

9.2.5 Pavement/Material Performance in Terms of Laboratory Indirect Tensile Fatigue Testing

- The *Remixer* had a poorer indirect tensile fatigue performance than the *Dustrol* when comparing cores from the hot dry trafficked sections.
- MMLS3 trafficking with heating, had a compaction effect (densification) on the pavement structure as was evident from the increased BSG of the trafficked cores compared to the untrafficked ones. This densification effect generally increased the relative fatigue life of the asphalt layers.
- The limestone AC and the lower *Remixer* layers were less susceptible to water damage compared to the *Dustrol.*
- In both the north and southbound structures, the underlying insitu LWAC exhibited a similar degree of water damage at equivalent MMLS3 axle loads and they were in fact, the layers worst affected by water (in terms of damage) followed by the *Dustrol.*
- Under wet MMLS3 trafficking and equivalent axle loads, the north and southbound structures would have similar fatigue life expectancies if water has the same accessibility into the respective LWAC layers during trafficking.
- It is apparent that the fatigue life expectancy of AC materials, susceptible to moisture damage, is significantly reduced by wet trafficking, such that even light axle loads with high tyre pressure (690kPa) caused substantial damage.

- The indirect tensile fatigue test results of specimens from the wet trafficked pads served as indicators of moisture sensitivity. These results were compared to those established in terms of AASHTO T283. The comparison seems to show that a pavement's ability to pass the prescribed AASHTO T283 specification does not necessarily mean that the AC material will not be damaged by water or will not strip. Likewise, failure to meet the criteria of the specification (TSR≥0.8, as recommended in the new TxDOT and Strategic Highway Research Program [SHRP] procedures) may not necessarily mean that the AC material will fail as a result of water damage under trafficking.
- Of course, these findings relate to the materials tested, and it remains to be determined to what extent they are valid in general.

9.2.6 General

- The profilometer and LDPs were appropriate tools for monitoring the surface rut development and the relative pavement layer deformation, respectively.

- The PSPA and SASW devices were found to be ideal tools for measuring changes in the elastic modulus of the in situ pavement materials

- The indirect tensile fatigue testing used in this study proved to be valuable as a tool to monitor progressive distress of AC due to traffic and environmental factors such as heat and water.

- Overall, the study demonstrated that the MMLS3, used in conjunction with non-destructive field and laboratory testing, is a significant cost-effective APT device that can be used for evaluating the response and performance of dry, heated, and wet (surface) layers of full-scale, in-service pavements. It can also be used to evaluate the performance of different pavement materials. Furthermore, it proved to be a valuable tool for supplementing full-scale APT devices such as the TxMLS.

9.3 RECOMMENDATIONS

(1) For MMLS3 field testing, pavement structural details and material characteristics should always be considered when selecting MMLS3 test pads so that the test pad performance can be properly evaluated. This is particularly important in comparative studies.

(2) When measuring the in situ pavement asphalt moduli using the PSPA or the SASW device, the following guidelines should be considered:

- The asphalt modulus is strongly dependent on temperature and a record of the pavement temperature at the time of measurement is essential.
- Cracked pavement areas should be avoided, given that they can have a negative effect on the PSPA and SASW readings. For the same reason, measurements should not be taken when the AC pavement temperature is extremely high. In the Jacksboro tests, good seismic readings were obtained within a temperature range of 15°C to 30°C. At temperatures around 50°C, measurements had to be repeated several times, for the devices to capture coherent data.
- Also better test results are obtained if the pavement surface is flat and even.

(3) Where as the rutting, field in situ stiffness measurements, and laboratory strength (SCB) and indirect tensile fatigue tests indicated similar results as regards to moisture sensitivity and water damage of the pavement materials, the AASHTO T283 had indicated different results, particularly for the limestone AC layer. This needs to be further investigated.

(4) Although an acceptable range (1.0 –1.3) of the rutting performance prediction ratio ($PR_{Rutting}$) was obtained between the MMLS3 and TxMLS during the rutting performance comparison analysis, the methodology used, needs further investigations and validation. Better methods to account for the differences in the environmental and loading conditions or to characterize the material behavior at high temperatures should be sought. Also the relationship between the shear stiffness (G*) of an asphalt mix and rutting needs to be further investigated.

REFERENCES

REFERENCES

AASHTO (American Association of State Highway and Transportation Officials), 1993. **AASHTO guide for design of pavement structures.** Washington D.C.

AASHTO (American Association of State Highway and Transportation Officials), 1998. **AASHTO T283, Standard Method of Test for Resistance of Compacted Bituminous Mixture to Moisture Induced Damage, Standard Specifications for Transportation Materials and Methods of Sampling and Testing.** 19th Edition, Part II Tests, 1998.

Allen, J., A. de Fortier Smit, and P. Warren, 1998. **Recommendations for Establishing the Texas Roadway Research Implementation Center.** Research Report 1812-S. Preliminary Review Copy. Center for Transportation Research, University of Texas at Austin.

Ahlborn G, 1969. **Elsym 5, Computer Program for Determining Stresses and Deformations in Five Layer Elastic System.** University of California, Berkeley.

Anderson RM, Huber GA, Walker DE, and Zhang X, 2000. **Mixture Testing, Analysis, and Field Performance of Pilot Superpave Projects: The 1992 SPS-9 Mixtures.** Preprint. Association of Asphalt Paving Technologists, Reno, Nevada.

Aouad, M. F., Stokoe II, K. H., and Briggs, R. C. , 1993. **Stiffness of Asphalt Concrete Surface Layer from Stress Wave Measurements.**Transportation Research Record 1384, Washington, DC, pp. 29-35.

Asphalt Institute, 1993. **Mix Design Methods for Asphalt Concrete and Other Hot-Mix Types.** MS-2, Asphalt Institute, Lexington, Kentucky, 6th Edition.

Blab R, and Monismith CL, 1999. **Introducing Improved Assumptions into Analytical Pavement Models Based on Measured Contact Stresses of Tires**. Paper (Number CS5-3) to be presented at the International Conference on Accelerated Pavement Testing in Reno, Nevada, October 1999.

Burmister DM, 1943. **The Theory of Stresses and Displacements in Layered Systems and Application to the Design of Airport Runways.** Proceedings, Higway Research Board, Volume 23, page 126-144.

Chen Dar-Hao, Fults, K., and Murphy, M, 1997. **The Primary Results for the First TxMLS Test Pad.** Transportation Research Board, Transportation Research Record No. 1570. pp. 30–38.

Chen Dar-Hao, Bilyeu J, Hugo F, Smit ADF, and Lee J, 1998. **Draft for Review. Evaluation of Pavement Response and Performance under MLS Trafficking.** Report prepared for TxDOT.

Chen Dar-Hao, and Hugo Fred, 1999. **Comparison of the Effectiveness of the Two Rehabilitation Strategies.** Draft report prepared for TxDOT.

Chou Chia-Pei J, 1996. **Effects of Overloaded Heavy Vehicles on Pavement and Bridge Design.** Transportation Research Record 1539, page 58.

Correia, AG, 1996. **Flexible Pavements.** Netherlands.

Croney, D and Croney, P., 1998. **The design and performance of road pavements.** 3rd edition. New York, NY 10011.

De Beer M, Kannemeyer L, and Fisher C, 1999. **Towards improved mechanistic design of thin asphalt surfacings based on actual tyre/pavement contact Stress-In-Motion (SIM) data in South Africa.** Paper presented at the 7th Conference on Asphalt Pavements for Southern Africa (CAPSA'99), Plenary session 5: Innovation in asphalt pavement design, Zimbabwe, 30th August - 2nd September 1999.

Department of Transport, 1990. **Cementitious Stabilizers in Road Construction: Draft TRH 13: 1986.** Pretoria.

Department of Transport., 1997. **Structural design of flexible pavements of interurban and rural roads: Draft TRH4: 1996.** Pretoria.

Epps AL, Walubita LF, Hugo F, and Bangera NU, 2000. **Comparing Pavement Response and Rutting Performance for Full-Scale and One-Third Scale Accerelated Pavement Testing.** Paper submitted for presentation and publication at the 80th Annual Meeting of the Transportation Research Board, Washington DC., January 2001.

Epps Amy, 1999. **Material Characterisation** (Unpublished draft report). College Station, Texas.

Epps J.A, 1969. **Influence of Mixture Variables on the Flexural Fatigue and Tensile Properties of Asphalt Concrete.** Doctor of Engineering Thesis, University of California, Berkeley.

Hibit, Karlsson and Sorenson, Inc., 1996. **ABAQUS Users Manual Version 5.5.** Pawtucket, R.I., USA.

Huang Yang ,H., 1993. **Pavement analysis and design.** Englewood Cliffs, New Jersey 07632.

Huhtala M, Pihlajamäki J, and Miettinen V, 1992. **The Effect of Wide-Based Tyres on Pavements.** London.

Hugo Fred, 2000. **APT as a Tool for Evaluation and Rehabilitation.** Power point presentation at the Advanced Course on Flexible Pavement Evaluation and Rehabilitation. Stellenbosch

Hugo Fred, Smit ADF, and Epps Amy, 1999(a). **Model APT in the Field, Paper: CS6-6.** Paper presented at the International Conference on Accelerated Pavement Testing in Reno, Nevada, October 18-20.

Hugo Fred, Fults Ken, Chen Dar-Hao, Smit ADF, and Bilyeu John, 1999 (b). **An Overview of the TxMLS Program and Lessons Learned, Paper GS3-4.** Paper presented at the International Conference on Accelerated Pavement Testing in Reno, Nevada, October 18-20.

Hugo Fred, Chen Dar-Hao, Smit ADF, and Bilyeu John, 1999 (c). **Report on a Comparison of the Effectiveness of Two Pavement Strategies on US 281 near Jacksboro (1814-1).** Draft Report prepared for Texas Department of Transportation by the Center for Transportation for Research (CTR), University of Texas at Austin, Texas.

Kim, S-M., F. Hugo, J. M. Roesset, and T. D. White, 1995. **Dimensional Analysis of the Model Mobile Load Simulator Action on Pavements.** Research Report 2914-1F. Preliminary Review Copy. Center for Transportation Research, University of Texas at Austin.

Lee NKJ, Hugo F, and Stokoe II KH, 1997. **Detection and Monitoring of Cracks in Asphalt Pavement Under Texas Mobile Load Simulator Testing**. Transportation Research Record 1570, pp 10. Washington DC.

Li Y. and Nazarian S.,1994**. Evaluation of Aging of Hot-Mix Asphalt Using Wave propagation Techniques.** STP 1265, ASTM, Philadelphia, PA, pp. 166-179.

Metcalf, J. B., 1996. **Application of Full-Scale Accelerated Pavement Testing, Synthesis of Highway Practice 235.** National Cooperative Highway Research Program.

Ming L, Aouad M.F, and Olson L.D., 2000. **Applications of the SASW Method to Pavements, Structures and Geotechnical Sites**. Paper P200. USA.

Molenaar A.A.A, 2000. **Advanced Course on Flexible Pavement Evaluation and Rehabilitation.** University of Stellenbosch.

Molenaar A.A.A., 1993. **Stresses and Strains in Flexible Pavements.** Lecture notes e5 structural pavement design, Part I, Delft University of Technology.

Molenaar A.A.A., 1998. **Stresses, Strains and Failure**. Delft University of Technology.

Muller Johan FP, 1999. **MMLS3 Traffic Simulator: Operators Manual.** Stellenbosch.

Pottinger Marion G, and Yager Thomas J, 1986. **The Tire pavement Interface** Philadelphia, Pa.

Pretorious FJ, 1990. **Masters Thesis: The Dynamic Effects of Vehicles on Flexible Pavements.** Stellenbosch.

Raithby K.D, and Ramshaw J.T, 1972. **Effect of Secondary Compaction on the Fatigue Performance of Rolled Asphalt.** TRRL-LR 496, Crowthorne, England.

Ronald L, Trerrel, Saleh Al-Swailmi, 1993. **Role of Pessimum Voids Concept in Understanding Moisture Damage to Asphalt Concrete Mixtures.** Transportation Research Record 1386, pages 31-37.

SABITA, 1997. **LAMBS - The Design, Construction, and use of Large Aggregate Mixes for Bases: Manual 13, 1997.** Roggebaai 8012.

Shames Irving H., and Dym Clive L., 1985. **Energy and Finite Element Methods in Structural Mechanics.** USA.

SHELL (Shell International Petroleum Company Limited), 1978. **Shell pavement design manual: asphalt pavements and overlays for road traffic.** London.

Shell Bitumen, 1998. **BISAR 3.0**. Shell International Oil Products BV. London.

Shook J F, Finn F N, Witczak M W, and Monismith C L, 1982. **Thickness Design of Asphalt Pavements - The Asphalt Institute Method.** Proceedings, 5th International Conference on Structural Design of Asphalt Pavements. Volume 1, page 17-44.

Schreuder WJ, 1992. **Effect of Sample Length on Indirect Tensile Test Parameters.** Masters Thesis submitted to the University of Stellenbosch. 1992.

Sousa Jorge B, McGhie Jim, and Shepard Bob, 1990. **Heavily Loaded Trailers: An Aproach to Evaluate Their Interaction with Asphalt Concrete Pavements.** Transportation Research Record 1286. Page 95.

Smit ADF, Van de Ven MFC, and Fletcher E, 1997. **Towards the use of Semi-Circular Bending Test as a Performance Related Specification Test.** Paper presented at the South African Transport Conference (SATC): Transport Infrastructure II, volume 3A. Johannesburg, September 1997.

Smit ADF, Hugo Fred, Epps Amy, and Lee James, 1998. **DRAFT Summary Report of the Jacksboro MMLS Tests.** Draft Report prepared for Center for Transportation for Research (CTR), University of Texas at Austin, Texas.

Smit ADF, Hugo Fred, Epps Amy, and Lee James, 1999. **Report of the First Jacksboro MMLS Tests, Preliminary Review Copy., Research Project 0-1814.** Draft Report prepared for Texas Department of Transportation by the Center for Transportation for Research (CTR), University of Texas at Austin, Texas.

Smith M.J, 1970. **Soil Mechanics. Examination Subjects for Engineers and Builders.** 2nd edition, London WC1N 2HY.

Steven BB, de Pont JJ, Pidwerbesky BD, and Arnold G, 1999. **Accelerated Dynamic Loading of Flexible Pavements at CAPTIF.** Paper (Number GS2-3) presented at the International Conference on Accelerated Pavement Testing in Reno, Nevada, October 18-20.

Straub, A.L, Schenck jnr., H.M., and Przybcien, F.E., 1968**. Bituminous pavement temperature realated to climate.** HRBR N0. 256, pp 53-77

Tangella Rao SCS, Graus J, Deacon JA, and Monismith CL, 1990. **Summary Report on Fatigue Response of Asphalt Mixtures.** Berkeley, California.

Theyse, HL, de Beer M and Rust, FC., 1996. **Overview of the South African mechanistic design analysis method (SAMPDAM)**: 75th Annual Transportation Research Board Meeting - 961294. TRANSPORTEK, CSIR, Pretoria.

TMH1, 1986. **Technical Methods for Highways: Standard Methods of Testing Road Construction Materials.** Second Edition. Pretoria.

TRRL (Transport and Road Research Laboratory), 1977. **Road Note 31, A guide to the structural design of bitumen - surfaced roads in tropical and sub-tropical countries.** London: Her Majesty's Stationery Office.

Uzan Jacob, and Sidess Arieh, 1990. **Extension of the Load Equivalency Factors for Various Pavement Conditions.** Transportation Research Record 1286. Page 133.

Walubita Lubinda F, Hugo Fred, and Epps Amy, 2000 (a)**. Report on the Second Jacksboro MMLS Tests (1814-3). Draft Preliminary Review Copy, Research Project 0-1814.** Draft Report prepared for Texas Department of Transportation by the Center for Transportation for Research (CTR), University of Texas at Austin, Texas.

APPENDICES

APPENDIX I

EXAMPLES OF BISAR 3.0 STRESS COMPUTATIONS

System: 1: MMLS3 -Two-Layered Pavement

		Modulus				Vertical		Horizontal (Shear)					Shear
Layer	Thickness	Elasticity	Poisson's		Load	Load	Stress	Load	Stress	Radius	X-Coordinate	Y-Coordinate	Angle
Number	(m)	(MPa)	Ratio		Number	(kN)	(MPa)	(kN)	(MPa)	(m)	(m)	(m)	(Degrees)
1	0.30	2500.00	0.35		1	2.10	0.69	0.00	0.00	0.03	0.00	0.00	0.00
2		100.00	0.35										

					Stress			Strain			Displacement		
Position	Layer	X-Coordinate	Y-Coordinate	Depth	XX	YY	ZZ	XX	YY	ZZ	UX	UY	UZ
Number	Number	(m)	(m)	(m)	(MPa)	(MPa)	(MPa)	μstrain	μstrain	μstrain	(μm)	(μm)	(μm)
1	1	0.00	0.00	0.00	-0.60	-0.60	-0.69	-60.05	-60.05	-107.30	0.00	0.00	27.56
2	1	0.00	0.00	0.00	-0.57	-0.57	-0.69	-52.24	-52.24	-115.70	0.00	0.00	27.45
3	1	0.00	0.00	0.01	-0.33	-0.33	-0.67	9.07	9.07	-176.80	0.00	0.00	26.11
4	1	0.00	0.00	0.05	-0.02	-0.02	-0.27	33.16	33.16	-102.30	0.00	0.00	19.79
5	1	0.00	0.00	0.10	0.00	0.00	-0.09	11.79	11.79	-34.33	0.00	0.00	16.77
6	1	0.00	0.00	0.20	0.01	0.01	-0.02	4.49	4.49	-9.06	0.00	0.00	15.01
7	1	0.00	0.00	0.30	0.03	0.03	0.00	7.58	7.58	-8.70	0.00	0.00	14.25
8	2	0.00	0.00	0.30	0.00	0.00	0.00	7.58	7.58	-21.60	0.00	0.00	14.25
9	2	0.00	0.00	0.40	0.00	0.00	0.00	5.06	5.06	-14.82	0.00	0.00	12.47
10	2	0.00	0.00	0.50	0.00	0.00	0.00	3.86	3.86	-11.36	0.00	0.00	11.18
11	2	0.00	0.00	1.00	0.00	0.00	0.00	1.76	1.76	-5.02	0.00	0.00	7.46

System: **2: TxMLS - Two-Layer Pavement System**

		Modulus				Vertical		Horizontal (Shear)					Shear
Layer	Thickness	Elasticity	Poisson's		Load	Load	Stress	Load	Stress	Radius	X-Coordinate	Y-Coordinate	Angle
Number	(m)	(MPa)	Ratio		Number	(kN)	(MPa)	(kN)	(MPa)	(m)	(m)	(m)	(Degrees)
1.00	0.30	2500.00	0.35		1.00	18.90	0.69	0.00	0.00	0.09	0.00	0.00	0.00
2.00		100.00	0.35										

					Stress			Strain			Displacement		
Position	Layer	X-Coordinate	Y-Coordinate	Depth	XX	YY	ZZ	XX	YY	ZZ	UX	UY	UZ
Number	Number	(m)	(m)	(m)	(MPa)	(MPa)	(MPa)	μstrain	μstrain	μstrain	(μm)	(μm)	(μm)
1.00	1.00	0.00	0.00	0.00	-0.73	-0.73	-0.69	-92.24	-92.24	-72.63	0.00	0.00	156.90
2.00	1.00	0.00	0.00	0.00	-0.72	-0.72	-0.69	-89.32	-89.32	-75.78	0.00	0.00	156.90
3.00	1.00	0.00	0.00	0.01	-0.62	-0.62	-0.69	-63.47	-63.47	-103.30	0.00	0.00	156.10
4.00	1.00	0.00	0.00	0.05	-0.27	-0.27	-0.61	16.39	16.39	-170.00	0.00	0.00	150.20
5.00	1.00	0.00	0.00	0.10	-0.08	-0.08	-0.40	36.30	36.29	-138.70	0.00	0.00	142.30
6.00	1.00	0.00	0.00	0.20	0.06	0.06	-0.12	32.53	32.54	-64.10	0.00	0.00	132.70
7.00	1.00	0.00	0.00	0.30	0.23	0.23	-0.02	62.71	62.72	-72.12	0.00	0.00	126.80
8.00	2.00	0.00	0.00	0.30	0.00	0.00	-0.02	62.75	62.72	-182.10	0.00	0.00	126.80
9.00	2.00	0.00	0.00	0.40	0.00	0.00	-0.01	43.69	43.69	-129.10	0.00	0.00	111.50
10.00	2.00	0.00	0.00	0.50	0.00	0.00	-0.01	33.87	33.87	-100.30	0.00	0.00	100.10
11.00	2.00	0.00	0.00	1.00	0.00	0.00	0.00	15.78	15.78	-44.90	0.00	0.00	66.99

System: 3: MMLS3 - Four Layer Scaled Model Pavement

		Modulus				Vertical		Horizontal (Shear)					Shear
Layer	Thickness	Elasticity	Poisson's		Load	Load	Stress	Load	Stress	Radius	X-Coordinate	Y-Coordinate	Angle
Number	(m)	(MPa)	Ratio		Number	(kN)	(MPa)	(kN)	(MPa)	(m)	(m)	(m)	(Degrees)
1	0.03	2500.00	0.35		1	2.10	0.69	0.00	0.00	0.03	0.00	0.00	0.00
2	0.05	1000.00	0.35										
3	0.15	400.00	0.35										
4		100.00	0.35										

					Stress			Strain			Displacement		
Position	Layer	X-Coordinate	Y-Coordinate	Depth	XX	YY	ZZ	XX	YY	ZZ	UX	UY	UZ
Number	Number	(m)	(m)	(m)	(MPa)	(MPa)	(MPa)	μstrain	μstrain	μstrain	(μm)	(μm)	(μm)
1	1	0.00	0.00	0.00	-0.96	-0.96	-0.69	-153.70	-153.70	-6.44	0.00	0.00	57.20
2	1	0.00	0.00	0.01	-0.31	-0.31	-0.60	4.36	4.36	-154.70	0.00	0.00	56.06
3	1	0.00	0.00	0.03	0.21	0.21	-0.42	112.80	112.80	-226.70	0.00	0.00	53.67
4	2	0.00	0.00	0.03	-0.05	-0.05	-0.42	112.70	112.80	-384.50	0.00	0.00	53.67
5	2	0.00	0.00	0.05	0.02	0.02	-0.19	82.45	82.44	-209.20	0.00	0.00	46.42
6	2	0.00	0.00	0.08	0.09	0.09	-0.09	90.40	90.36	-153.00	0.00	0.00	42.20
7	3	0.00	0.00	0.15	0.01	0.01	-0.02	32.72	32.72	-72.90	0.00	0.00	32.32
8	3	0.00	0.00	0.23	0.02	0.02	-0.01	34.88	34.87	-50.62	0.00	0.00	28.18
9	4	0.00	0.00	0.23	0.00	0.00	-0.01	34.88	34.87	-89.81	0.00	0.00	28.18
10	2	0.00	0.00	0.08	0.09	0.09	-0.09	90.40	90.36	-153.00	0.00	0.00	42.20

System: 4: TxMLS - Four Layer Full-Scale Pavement

		Modulus				Vertical		Horizontal (Shear)					Shear
Layer	Thickness	Elasticity	Poisson's		Load	Load	Stress	Load	Stress	Radius	X-Coordinate	Y-Coordinate	Angle
Number	(m)	(MPa)	Ratio		Number	(kN)	(MPa)	(kN)	(MPa)	(m)	(m)	(m)	(Degrees)
1	0.08	2500.00	0.35		1	18.90	0.69	0.00	0.00	0.09	0.00	0.00	0.00
2	0.15	1000.00	0.35										
3	0.30	400.00	0.35										
4		100.00	0.35										

					Stress			Strain			Displacement		
Position	Layer	X-Coordinate	Y-Coordinate	Depth	XX	YY	ZZ	XX	YY	ZZ	UX	UY	UZ
Number	Number	(m)	(m)	(m)	(MPa)	(MPa)	(MPa)	µstrain	µstrain	µstrain	(µm)	(µm)	(µm)
1	1	0.00	0.00	0.00	-0.98	-0.98	-0.69	-157.60	-157.60	-2.25	0.00	0.00	184.50
2	1	0.00	0.00	0.04	-0.32	-0.32	-0.60	2.03	2.03	-152.10	0.00	0.00	181.20
3	1	0.00	0.00	0.08	0.20	0.20	-0.42	111.80	111.80	-225.50	0.00	0.00	174.10
4	2	0.00	0.00	0.08	-0.05	-0.05	-0.42	111.80	111.80	-383.00	0.00	0.00	174.10
5	2	0.00	0.00	0.15	0.03	0.03	-0.19	83.12	83.12	-208.60	0.00	0.00	152.40
6	3	0.00	0.00	0.23	0.01	0.01	-0.09	92.97	92.94	-233.70	0.00	0.00	139.70
7	3	0.00	0.00	0.38	0.01	0.01	-0.03	47.45	47.44	-98.80	0.00	0.00	117.00
8	4	0.00	0.00	0.53	0.00	0.00	-0.01	53.63	53.62	-137.70	0.00	0.00	104.80

APPENDIX II

FIELD TEMPERATURE MEASUREMENTS, PSPA ASPHALT MODULI PSPA DEVICE

Table 2.4.1: Mean MMLS3 Trafficking Temperatures

No:	Test Pad	Axles	Mean MMLS3 Trafficking Temperatures (°C)					
			Air	TS (0mm)	T1 (25mm)	T2 (75mm)	T3 (95mm)	TCP (10mm)
1	*n1*	320,000	29.9	56	49.23	40.29	38.6	49.9
2	*n2*	160,000	29.8	57	49.8	42.4	40.1	53.4
3	*n3*	320,000	29.0	33	30.3	30.9	29.5	00.0
4	s1	180,000	38.5	57	50.3	43.5	41.2	53.2
5	s2	80,000	43.7	57.8	50.3	43.6	41.4	53.7
6	*s3*	160,000	40.0	32	30.2	30.6	29.1	00.0
Overall Mean MMLS Trafficking Temperatures		Hot Tests	35.5	56.9	49.9	42.5	40.3	52.5
		Wet Tests	34.5	32.5	30.25	30.8	29.3	00.00

Table 2.4.2: SASW Temperatures

Test Pad	Axle Loads	Average Temperature (°C)		
		Start of SASW Measurements	Stop of SASW Measurements	Average
n1	320 000	26.3	27.0	26.65
n2	160 000	27.5	31.5	29.50
n3	320 000	27.0	31.0	29.00
s1	180 000	28.6	34.8	31.70
s2	80 000	29.2	35.0	32.10
s3	160 000	30.4	36.0	33.20
Overall mean for the hot tests				29.99
Overall mean for the wet test				31.10

Table 2.4.3: PSPA Temperatures during MMLS3 Trafficking

Test Pad	Axle Count	Average Temperatures in °C						
		Air			Pavement Surface			
		Start of PSPA	End of PSPA	Average	Start of PSPA	End of PSPA	Average	Mean Average
n1	0	36.0	38.6	37.3	42.2	41.6	41.90	38.37
	20 000	29.6	33.7	31.65	40.1	43.0	41.55	
	40 000	40.0	39.5	39.75	34.5	37.6	36.05	
	80 000	34.4	36.0	35.20	39.3	40.4	39.85	
	160 000	27.8	28..08	28.30	39.0	40.1	39.55	
	320 000	27.9	31.0	29.45	30.0	32.6	31.30	
n2	0	31	34.5	32.75	30.1	30.3	30.20	36.62
	20 000	28.8	39.8	34.30	34.9	38.7	36.80	
	40 000	40.0	34.6	37.30	50.3	49.4	49.85	
	80 000	24.6	26.6	25.60	27.9	29.1	28.50	
	160 000	35.0	39.6	37.30	36.4	39.1	37.75	
n3	0	34.0	32.8	33.40	41.6	39.9	40.75	29.66
	40 000	28.9	28.1	28.50	31.3	30.5	30.90	
	80 000	26.5	24.0	25.25	30.7	28.1	29.40	
	160 000	27.3	32.1	29.70	15.2	21.9	18.55	
	320 000	25.1	26.4	25.75	28.4	29.0	28.70	
s1	0	39.5	37.4	38.45	40.7	37.9	39.30	41.07
	20 000	32.0	36.4	34.2	38.0	42.6	40.30	
	40 000	37.1	38.0	37.55	39.1	41.8	40.45	
	80 000	27.0	29.1	28.05	29.2	33.0	31.10	
	160 000	38.9	37.4	38.15	49.1	47.9	48.50	
	180 000	44.9	45.1	45.00	46.0	47.5	46.75	
s2	0	36.4	39.1	37.75	38.3	41	39.65	45.83
	20 000	40.2	38.3	39.25	49.5	47.8	48.65	
	80 000	41.6	43	42.30	48.1	50.3	49.20	
s3	0	37.0	39.8	38.4	38.3	40.2	39.25	31.06
	40 000	42.0	40.1	41.05	28.9	26.7	27.80	
	80 000	45.9	40.5	43.20	30.2	28.8	29.50	
	160 000	28.5	31.0	29.75	27.3	28.1	27.70	
Overall mean for the hot tests								40.47
Overall mean for the wet tests								31.21

Table 2.4.4: PSPA Normalised AC Moduli (MPa) versus MMLS3 Trafficking

Normalised AC Moduli (MPa) [to 25°C, 30Hz]						
	n1	s1	n2	s2	n3	s3
E_u (MPa)	2,900	4,280	3,200	3,500	3,005	2,880
Axle Loads	E_{AC} (MPa)	E_{AC} (MPa)	E_{AC} (MPa)	E_{AC} (MPa)	E_{AC} (MPa)	E_{AC} (MPa
0, 000	3,120	3,290	3,030	3,120	3,010	2,890
20, 000	2,380	4,640	3,130	3,160	3160	2,680
40, 000	2,740	4,210	3,210	3,200	2,800	2,640
80, 000	2,720	4,420	3,300	3,650	2,170	2,800
160, 000	2,700	4,280	3,330	-	1,960	2,660
180, 000	-	3,750	-	-	-	-
320, 000	2,800	-	-	-	1,890	-
E_u = Average normalised pavement AC moduli from the untrafficked section						

Table 2.4.5: The A-Value

Temperature		A Value
°C	°F	
00.00	32	0.138
10.56	51	0.152
15.56	60	0.165
21.11	70	0.188
26.67	80	0.240
32.22	90	0.275
37.78	100	0.312
43.33	110	0.365
48.89	120	0.411
54.44	130	0.463
57.78	136	0.485

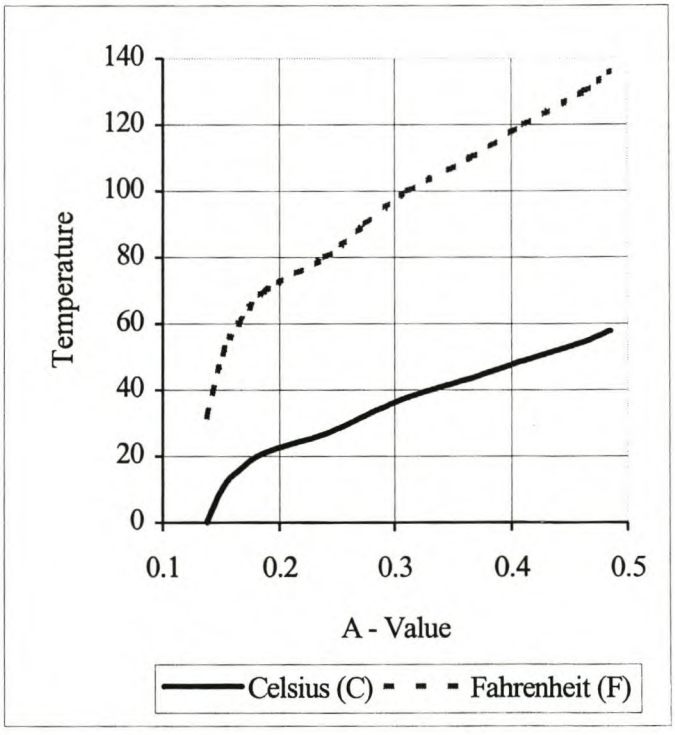

Figure 2.4.1: Temperature versus A - Value

APPENDIX III

LABORATORY TEST RESULTS

Table 3.5.III: Definition of Notations for Core-Specimens, Test Pads and Pavement Layers/Material

Notation	Definition	Material	
		Northbound lane	Southbound lane
L1	Layer 1 (surface layer)	Limestone AC	Upper Remixer
L2	Layer 2	Dustrol	Bottom Remixer
L3	Layer 3	In situ LWAC	In situ LWAC

Notation	Definition
AC	Asphalt Concrete (Asphalt)
LWAC	Lightweight Aggregate Asphalt Concrete
nu	Untrafficked section on the Northbound lane
nu-D	Untrafficked section adjacent to the 1998 dry test section (Smit et al, 1999).
su	Untrafficked section on the Southbound lane
n1,n2,n3	Test pads 1, 2 and 3 on the Northbound lane
s1,s2, s3	Test pads 1, 2 and 3 on the Southbound lane
C	Composite layer comprising layers L1 and L2
L	Lightweight material
*L**	Composite layer comprising layers L2 and L3

Table 3.5.1. Material Volumetrics

Material Type	Section	MMLS Trafficking.	2hrs wet conditioned.	Diameter (mm)	Thickness (mm)	NST	BRD (kg/m3)	Change in BSG (%)
(a) Northbound								
L1	*nu*	no	no	101.60	24.68	4	**2,198.25**	
L1	*nu*	no	yes	101.60	18.95	2	**2,225.50**	+1.4
L2	*nu*	no	no	101.60	25.30	5	**1,660.80**	
L2	*nu*	no	yes	101.60	25.10	2	**1,712.50**	+3.0
L1	*n1*	yes	no	101.60	27.00	2	**2,258.50**	+2.7
L2	*n1*	yes	no	101.60	26.25	2	**1,766.50**	+5.6
L2	*n2*	yes	no	101.60	27.25	2	**1,736.00**	+4.3
L2	*n3*	yes	no	101.60	26.00	2	**1,658.50**	-0.10
(b) Southbound								
L1	*su*	no	no	101.60	28.75	2	**1,968.00**	
L1	*su*	no	yes	101.60	27.00	2	**1,898.00**	-3.6
L2	*su*	no	no	101.60	28.80	2	**1,712.00**	
L2	*su*	no	yes	101.60	25.95	2	**1,723.00**	+0.6
L1	*s1*	yes	no	101.60	27.25	2	**1,903.50**	-3.3
L2	*s1*	yes	no	101.60	26.95	2	**1,680.00**	-1.2
L2	*s2*	yes	no	101.60	16.10	2	**1,749.52**	+2.4
L2	*s3*	yes	no	101.60	23.75	2	**1,717.00**	+0.3
L*	North	no	no	152.40	44.50	2	**1,680.00**	
L*	North	no	yes	152.40	45.65	2	**1,681.00**	+0.1
L*	North *(Wet)*	yes	no	152.40	51.33	2	**1,662.00**	
L*	North *(Wet)*	yes	yes	152.40	56.10	2	**1,731.00**	+4.2
L*	North *(Dry)*	yes	yes	152.40	53.90	2	**1,694.00**	
C	North	no	no	152.40	49.75	2	**2,026.50**	
C	North	no	yes	152.40	49.65	2	**2,034.00**	+0.4

Key: NST - Number of Specimens Tested, BRD = Bulk Relative Density

Table 3.5.2: Moisture Sensitivity Results at 25°C (AASHTO T283)

Material Type	Section	MMLS3 trafficking	2hrs wet conditioning	Diameter (mm)	Thickness (mm)	No. Of Specimens Tested (NST)	ITS (kPa)	TSR
(a) Northbound lane								
L1	*nu*	no	no	100	25	4	1 202	
L1	*nu*	no	yes	100	19	2	679	**0.57**
L2	*nu*	no	no	100	25	5	894	
L2	*nu*	no	yes	100	25	2	760	**0.85**
(b) Southbound lane								
L1	*su*	no	no	100	28.8	2	1 128	
L1	*su*	no	yes	100	27.0	2	1 025	**0.91**
L2	*su*	no	no	100	28.8	2	1 142	
L2	*su*	no	yes	100	26.0	2	923	**0.81**

Key: ITS - Indirect Tensile Strength, TSR - Retained Tensile Strength Ration ($ITS_{After\ wetting}/ITS_{Before\ wetting}$)

Table 3.5.3: Average Shear Test Results

Material Type	Section	Test Temperature (°C)	Test Frequency (Hz)	No. of Specimens Tested	Shear Modulus G* (MPa)	Phase Angle (δ)
C	*nu*	40	1	2	200	42.9
			2	2	269	42.1
			5	2	413	39.9
			10	2	534	43.3
L*	*nu*	40	1	2	320	38.7
			2	2	241	41.6
			5	2	367	39.1
			10	2	467	41.6
C	*nu*	25	1	2	788	26.5
			2	2	1026	24.2
			5	2	1202	25.6
			10	2	1340	29.5

Table 3.5.4: Indirect Tensile Strength (ITS) Results

Material Type	Section	MMLS Trafficking	2Hrs Wet Conditioning	Diameter (mm)	Thickness (mm)	No. Of Specimens Tested	ITS Strength (kPa)
(a) Northbound pavement structure							
L1	*nu*	no	no	100	25	2	1 076
L1	*nu*	no	no	100	25	4	1 202
L1	*nu*	no	yes	100	19	2	679
L2	*nu*	no	no	100	24.5	2	714
L2	*nu*	no	no	100	25	5	894
L2	*nu*	no	yes	100	25	2	760
L1	*nu-D*	yes	no	100	20	2	752
L2	*nu-D*	yes	no	100	18	2	597
L3	*nu-D*	yes	no	100	20	2	584
L1	*n1*	yes	no	100	27.0	2	749
L2	*n1*	yes	no	100	26.3	2	1 131
L2	*n2*	yes	no	100	27.3	2	1 089
L2	*n3*	yes	no	100	26.0	2	991
(b) Southbound pavement structure							
L1	*su*	no	no	100	26.5	2	1 152
L1	*su*	no	no	100	28.8	2	1 128
L1	*su*	no	yes	100	27.0	2	1 025
L2	*su*	no	no	100	25.1	2	1 026
L2	*su*	no	no	100	28.8	2	1 142
L2	*su*	no	yes	100	26.0	2	923
L1	*s1*	yes	no	100	27	2	1 320
L2	*s1*	yes	no	100	27	2	1 083
L2	*s2*	yes	no	100	16	2	875
L2	*s3*	yes	no	100	24	2	1 044

Table 3.5.6 (a): Summary of Lab-Test Results for Northbound inner lane

Core Details			Test	nu		*n1*		*n2*		*n3*		*n-wet*		*nu-D*		*n-dry*	
				Result	**RR**	**Result**	**RR**	**Result**	**RR**	**Result**	**RR**	**Result**	**RR**	**Result**	**RR**	**Result**	**RR**
Layer 1	Limestone AC	~25 mm	ITS [20C, 50mm/min] (kPa)	1076/1202 *	1	749	0.62					1 399	1.16	752	1	972	1.29
			SCB [20C, 5mm/min] (MPa)	2.45	1	2.5	1.02					2.72	1.11	1.26	1	2	1.59
			Relative Bulk Density	2.153	1	2.258	1.05					2.353	1.09	2.16	1	2.205	1.02
			Fatigue Life [20% of 1076kPa, 20C, 10Hz]	884 800	1	1 519 800	1.70					785 533	0.89	271 375	1	311 345	1.15
Layer 2	Dustrol	~25 mm	ITS [20C, 50mm/min] (kPa)	714/894*	1	1131	1.27	1089	1.22	991	1.11	977	1.09	597	1	825	1.38
			SCB [20C, 5mm/min] (MPa)	2.035	1	2.09	1.03	2.05	1.01	1.69	0.83	1.72	0.85	1.14	1	1.29	1.13
			Relative Bulk Density	1.664	1	1.770	1.06	1.736	1.04	1.605	0.96	1.653	0.99	1.718	1	1.685	0.98
			Fatigue Life [20% of 842kPa, 20C, 10Hz]	855 000	1	901 500	1.05	1 125 600	1.32	488 600	0.57	186 437	0.22	268 815	1	277 225	1.03
Layer 3	Insitu LWAC	~20 mm	ITS [20C, 50mm/min] (kPa)	458	1									584	1		
			SCB [20C, 5mm/min] (MPa)	1.95	1	1.96	1.01	1.86	0.95	1.18	0.61	1.28	0.66	0.938	1	1.615	1.72
			Relative Bulk Density	1.659	1	1.664	1.00	1.668	1.01	1.645	0.99	1.661	1.00	1.673	1	1.67	1.00
			Fatigue Life [20% of 458kPa, 20C, 10Hz]	859 880	1	936 000	1.09	742 680	0.86	340 000	0.40	171 420	0.20	235 365	1	336 850	1.43
Number of Specimens Tested				18		12		8		8		12		12		12	
MMLS Axle Loads				none		320 000		160 000		320 000		1 400 000		none		1 000 000	
MMLS Trafficking Temperature (°C)				none		50		50		30		24		none		38	
MMLS Trafficking Condition				none		Hot (heated)		Hot (heated)		Wet (1mm water)		Wet (1 mm water)		none		Dry	

Key: AC = Asphalt Concrete, LWAC = LightWeight Aggregate (Asphalt) Concrete, RR = Relative Ratio to Untrafficked section (*nu*),
ITS = Indirect Tensile Strength, SCB = Tensile stresses in Semi-Circular Bending Test

Table 3.5.6 (b): Summary of Lab-Test Results for Southbound inner lane

Core Details			Test	su		*s1*		*s2*		*s3*	
				Result	**RR**	**Result**	**RR**	**Result**	**RR**	**Result**	**RR**
Layer 1	Top Remixer	~25 mm	ITS [20C, 50mm/min] (kPa)	1153/1128*	1	1320*	1.17				
			SCB [20C, 5mm/min] (MPa)	2.33	1	2.53	1.09				
			Relative Bulk Density	1.961	1	1.984	1.01				
			Fatigue Life [20% of 1128kPa, 20C, 10Hz]	892 743	1	1 150 000	1.29				
Layer 2	Bottom Remixer	~20 mm	ITS [20C, 50mm/min] (kPa)	1026/1142*	1	1083*	0.95	875*	0.77	1044*	0.91
			SCB [20C, 5mm/min] (MPa)	2.07	1	2.08	1.05	1.85	0.89	1.93	0.93
			Relative Bulk Density	1.712	1	1.724	1.01	1.749	1.02	1.686	0.98
			Fatigue Life [20% of 1142kPa, 20C, 10Hz]	398 405	1	425 600	1.07	472 050	1.18	358 200	0.90
Layer3	Insitu LWAC	~20 mm	ITS [20C, 50mm/min] (kPa)	802	1						
			SCB [20C, 5mm/min] (MPa)	1.91	1	1.93	1.01	1.95	1.02	1.65	0.86
			Relative Bulk Density	1.616	1	1.68	1.04	1.680	1.04	1.656	1.02
			Fatigue Life [20% of 458kPa, 20C, 10Hz]	733 785	1	752 400	1.03	802 000	1.09	512 600	0.70
Number of Specimens Tested				18		12		8		8	
MMLS Axle Loads				none		180 000		80 000		160 000	
MMLS Trafficking Temperature (°C)				none		50		50		30	
MMLS Trafficking Condition				none		Hot (heated)		Hot (heated)		Wet (1mm water)	

Key: AC = Asphalt Concrete, LWAC = LightWeight Aggregate (Asphalt) Concrete, RR = Relative Ratio to Untrafficked section (su), ITS = Indirect Tensile Strength, SCB = Tensile stresses in Semi-Circular Bending Test

APPENDIX IV

ANALYTICAL MODELLING OF THE LOAD RESPONSE OF AN ASPHALT-SURFACING PAVEMENT

ANALYTICAL MODELLING OF THE LOAD RESPONSE OF AN ASPHALT-SURFACING PAVEMENT

1 INTRODUCTION

In this Appendix, the pavement response under traffic loading with respect to the asphalt (surfacing) layer was analytically modelled. Focus was on the thin asphalt surfacing layers. The wide use of thin asphalt surfacing layers (≤50mm) in Southern Africa entails that more studies are needed into understanding the traffic load response of these layers. In Zambia for instance, most asphalt pavements consist of thin asphalt surfacing layers, which are considered economical for the third world countries. Also, the use of asphalt layers is a relatively new technology in Zambia.

2 METHODOLOGY – COMPUTER STRESS ANALYSIS

A simplified linear-elastic analysis of the stress-strain behaviour of the pavement structure under traffic loading with emphasis on the asphalt layer is presented. The pavement was modeled as a system of horizontal layers with constant thickness, and infinite in horizontal direction, consisting of isotropic, homogeneous and linear-elastic materials. Layer interface full-friction continuity conditions were assumed and the second composite layer was taken to have infinite thickness. The traffic load was assumed to be statically and uniformly distributed on a circular area over the pavement surface. Layer materials were characterized using the elastic modulus (E) and the Poisson's ratio (ν). The effects of the variation of the following parameters are subsequently presented;

(1) The asphalt surfacing layer thickness
(2) The axle loading
(3) The tyre pressure
(4) The elastic modulus (stiffness)
(5) The Poisson's ratio

The computed stresses and strains were correlated to the pavement service life in terms of fatigue and deformation using the transfer Equations from the Asphalt Institute design method (Asphalt Institute, 1993, and Huang, 1996). The stress-strain distribution in relation to pavement layer depth is also presented.

2.1 Computer Program

Computer programs BISAR 3.0 was used for calculating the stresses, strains and vertical displacements within the pavement layers. BISAR 3.0 is a three-dimensional window based program with a comprehensive input mode, calculation capability and out put format. It encompasses the computerized Shell pavement design method and is based on an elastic multi-layer pavement model with a maximum capacity of 10 layers (Shell Bitumen, 1998).

2.1 Pavement Structure

Since interest for this study was in the top layer (asphalt), a simplified two-layer pavement system as shown in Figure 1.1 was adopted for the analysis. All the underlying layers were considered to be one composite layer with infinite thickness (∞) and composite modulus (E_2). The assumption was that, this would give a realistic analysis of the surfacing layer. Asphalt and unbound granular materials were assumed for the top surfacing layer and the second composite underlying layer, respectively. However, no specific material was implied, provided it met the prescribed material constants.

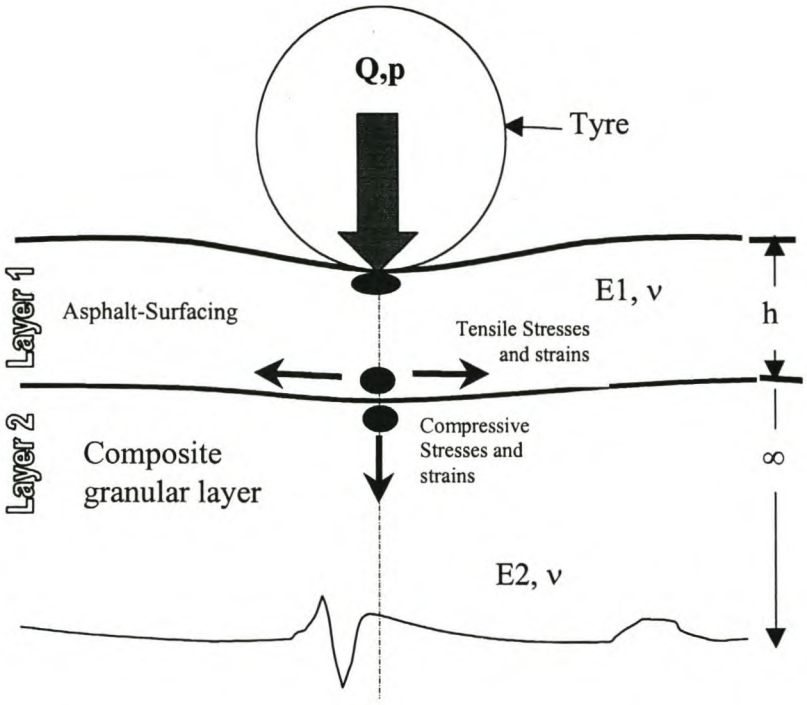

Figure 1.1: Simplified Two-Layer Pavement System

In Figure 1.1 above, Q is the vertical tyre load in kN (this is half the total axle load [Q_T] for a super single), p is the tyre pressure in MPa, h is the asphalt surfacing layer thickness in mm, ν is the Poisson's ratio, and E1, E2 are the elastic moduli in MPa.

For a multi-layer pavement system, the above simplification and characterization of layer-2 may not hold. However, for the purpose of this study, it was considered justifiable since the major interest was in the top asphalt layer. Huang (1996) also recommends that if a pavement is composed for example of three layers, e.g. an asphalt surfacing course, a granular base and a subgrade, the base and the subgrade should be combined into a single composite layer for the purpose of computing stresses and strains in the asphalt layer.

It must however, be pointed out that this is a simplified model assuming static traffic loading conditions, and isotropic, homogenous, and linear-elastic characterization of the materials. In a real practical situation, this assumption may not hold.

2.3 Input Parameters

The various computer-input parameters used for the analysis are presented below. These were arbitrary selected with reference to some of the common values used in pavement design.

2.3.1 Traffic Loading

In the calculations, a super single axle-wheel load was used. Axle loading designated as Q_T was varied from 80kN (standard legal axle load) to 200kN (150% overload). In this case, Q_T refers to total axle load. The tyre pressure (p) ranged from 0.5MPa (500kPa) to 1MPa (1000kPa).

80kN and 0.52MPa (520kPa) were designated as the standard single axle load with dual wheels and tyre pressure respectively, as used in the South African design standards (Theyse et al, 1996). For a super single wheel, 0.7MPa (700kPa) tyre pressure is often used as the standard value. For the calculations and analysis in this study, 0.7MPa was used as the standard design pressure for a super single axle-tyre.

2.3.2 Asphalt (Surfacing) Layer Thickness (h).

Both thin (≤50mm) as well as thicker layers (>100mm) were considered. The asphalt surfacing layer thickness (h) ranged from 20mm to 200mm. Emphasis was on the thin layers (≤50mm), which are prevalent in Southern Africa. Other layer thicknesses were included for comparison purposes.

For the purpose of this study, the following definitions were used to describe layer thickness; $h \leq 50$ mm – thin; $50 < h \leq 100$ mm – intermediate; $h > 100$ mm – thick.

The immediate composite underlying layer was considered to have infinite thickness and was modeled as such.

2.3.3 The Material Elastic Constants (E, v).

The elastic modulus (E_2) of the composite-underlying layer ranged from 50 to 1000 MPa. The modular ratios (MR), ($E_{Asphalt}$ to $E_{Second\ Layer}$) were 1, 3, 5, 7, 8, 10, 15 and 20. The modular ratio was varied in this manner to account for the change in the asphalt stiffness (due to temperature and loading time).

Poisson's ratio of 0.25, 0.35 and 0.5 were used for sensitivity analysis; 0.35 was the most dominantly used.

2.4 Response Points

For the purpose of this study, response points were defined as the points at which computations and analysis were done, within the asphalt surfacing layer depth and the composite-underlying layer. All the calculations were done directly under the centre of the tyre load where principal stresses were considered to be maximum. As discussed in Chapter 2, the horizontal stress and strain magnitude in either the X or Y direction at any point vertically down, under the centre of the wheel load were assumed to be of equal magnitude.

In the asphalt layer, the bottom zone at (h-1) mm was considered the most critical response point with regard to the horizontal tensile stress. In the second composite layer, the critical response point was considered the immediate top (h+1 mm) zone (with regard to vertical stresses). Vertical displacements were analyzed on top of the asphalt and second composite layer, respectively.

3 COMPUTATIONS, RESULTS AND ANALYSIS

The results of the calculations for a super single axle based on linear-elastic theory are presented below. In this analysis, negative (-) and positive (+) refer to compressive and tensile, respectively. The notation 80kN-0.7MPa or 80kN-700kPa for example refers to 80kN axle load and 0.7MPa tyre pressure.

3.1 Stress-Strain Distribution

Arbitrary selected asphalt thickness 20, 50, 75, 150 and 200 mm, respectively, for the same traffic loading (80kN-0.7MPa) and material elastic constants (E_2 = 400MPa, MR = 5, ν = 0.35) were used.

3.1.1 The Asphalt Surfacing Layer

Figure 1.2 shows the stress-strain distribution within the asphalt surfacing layers. In all the surfacing layers, there is a high concentration of vertical compressive (negative) stresses in the immediate top zone (Figure 1.2 [a]). The 20mm surfacing is virtually subjected to compressive stresses within the entire surfacing depth and there are no tensile stresses. The vertical compressive stress at the bottom is almost equal to the tyre-surface contact stress (0.7MPa) and hardly decreases over the surfacing depth. A high vertical load is thus transferred to the immediate underlying layers. The intermediate surfacing layer 75 mm exhibited the highest magnitude of horizontal stress and strain as well as vertical strain compared to the 20, 50, 150, and 200 mm layers.

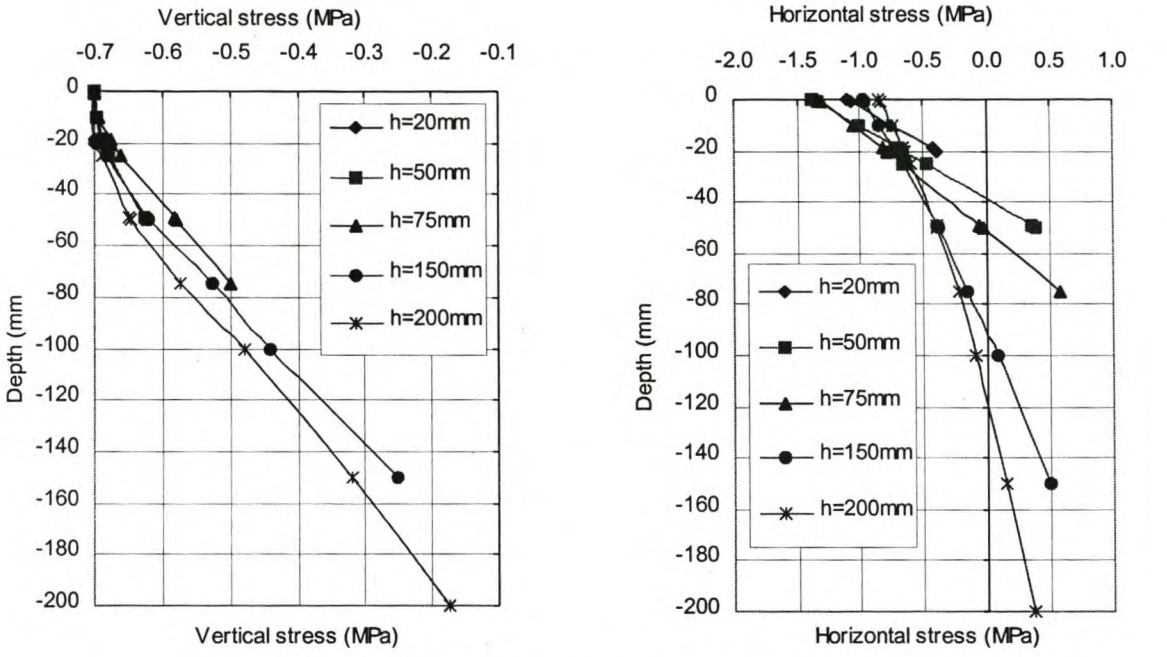

(a): Stresses

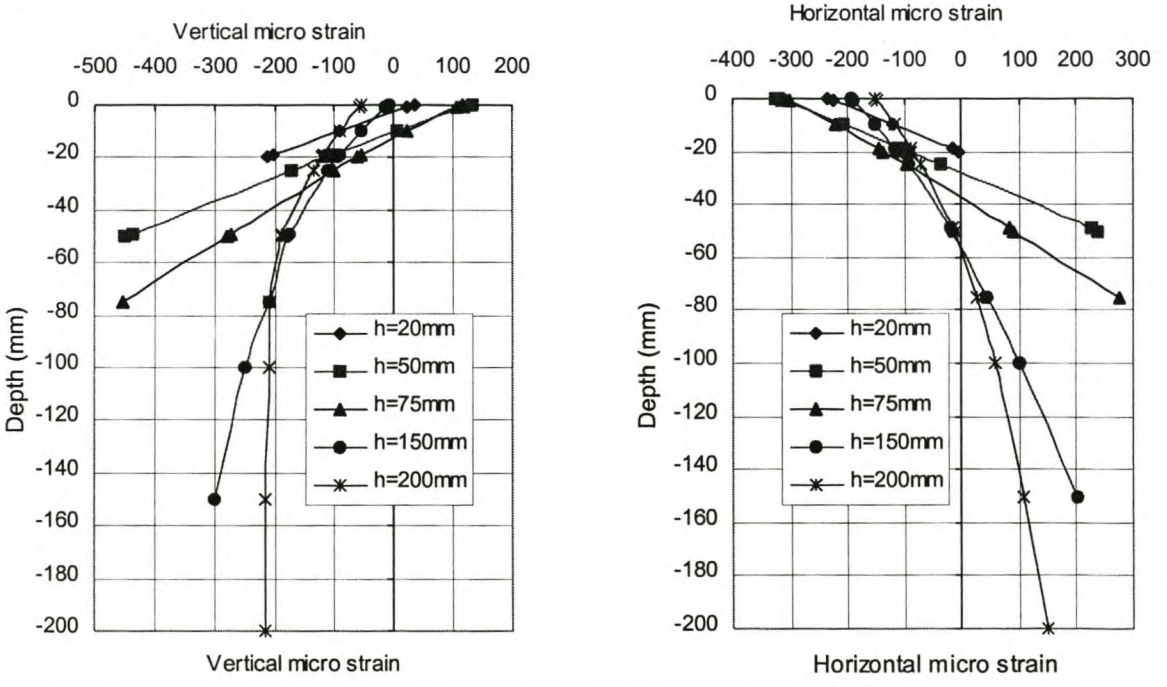

(b): Strains

Figure 1.2: Stress-Strain Distribution in Asphalt-Surfacing Layer

[80kN-0.7MPa, E_1=2000MPa, E_2=400MPa, MR=5, ν=0.35]

In the thicker surfacing base (200mm), the vertical stress significantly decreased with depth, and is infact reduced by about 75% from 0.7MPa at the top to about 0.18MPa at the bottom. Much traffic loading is spread within the layer depth compared to the 20mm surfacing. Like for the intermediate surfacing layers, horizontal stresses change from compression (negative) in the top zone to tension (positive) at the bottom. However, the horizontal stress magnitude is relatively lower than for 50, 75 and 150 mm.

The horizontal strains like the stress are all compressive (negative) within the 20mm surfacing (Figure 1.2 [b]). This is an indication of less sensitivity to fatigue (which is a function of tensile strains). In the other layer thicknesses, the trend is the same as for the horizontal stress, and again the intermediate layers exhibited more sensitivity in terms of strain magnitude.

The vertical (compressive) strains generally increased with depth, and are in fact tensile (positive) in the immediate top zone of the 20, 50 and 75 mm thickness. This is due to the effect of the horizontal stresses and the Poisson's ratio. It must be observed that, in all the layers, horizontal stresses are compressive (negative) in the top zone. Also from the vertical strain profile, the marked influence of the Poisson's ratio on the thin and intermediate surfacing layers is evident.

From the above analysis, it appears that the thin asphalt surfacing layers are essentially load transfer components with little susceptibility to fatigue, but may require high strength support layers to sustain the traffic loads. The thick asphalt layers (surfacing and base) significantly contribute to the structural integrity of the pavement structure and are regarded as structural members.

Based on this analysis and the Figures presented, the vertical strain criterion would be inappropriate as a model for deformation in the top zone asphalt layer. It under-estimates the effect of the vertical stress due to the horizontal stress and the effect of the Poisson's ratio.

3.1.2 The Immediate Composite Underlying Layer

Stresses and strains were computed up to a depth of 500mm for each of the respective surfacing layer thickness in the composite-underlying layer. From Figure 1.3 (a), it is observed that there is a general decrease in the vertical stress with depth, with maximum values in the immediate top zone. The lowest magnitude is indicated for the 200 mm surfacing. This is indicating that a substantial amount of traffic loading is spread within the top 200 mm surfacing layer, compared to other surfacing layers. The highest stress magnitude is indicated for the 20mm surfacing, and infact, the vertical stress in the top zone of the composite layer is equal to the tyre pressure (0.7MPa). This is a clear demonstration that for the thin surfacing, most of the traffic load is transferred to the underlying layers. Since the composite underlying layer was assumed to be granular and equivalent to the subgrade, horizontal tensile stresses were expected to be zero as shown in Figure 1.3 (a). In the 200mm, the horizontal stress is zero, where as in the other surfacing layers, they are compressive in the top zone up to a depth of about 200mm but reduce to zero with depth.

Vertical strains exhibited behaviour similar to the vertical stresses, and indicated that the underlying layers under the 20mm surfacing could be more susceptible to deformation in comparison to the other layers. Although, there are no tensile stresses, the existence of the horizontal tensile strains (Figure 1.3 (b)) is due to contribution from the vertical stress as a result of the effect of the Poisson's ratio.

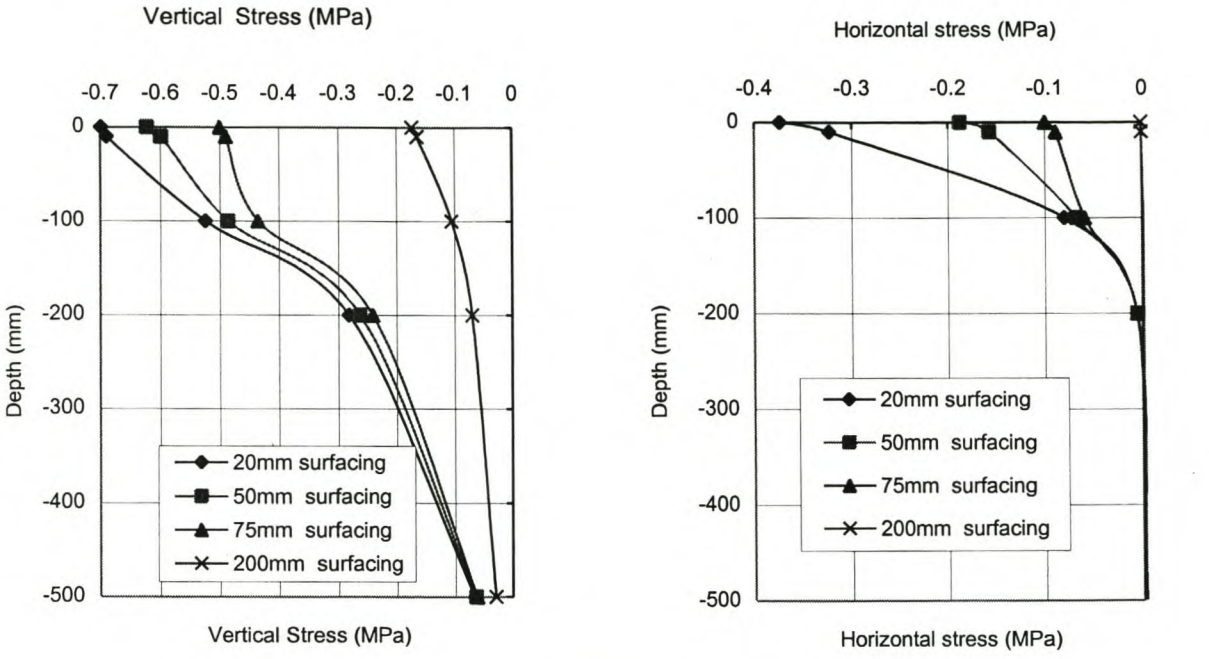

(a) Stress

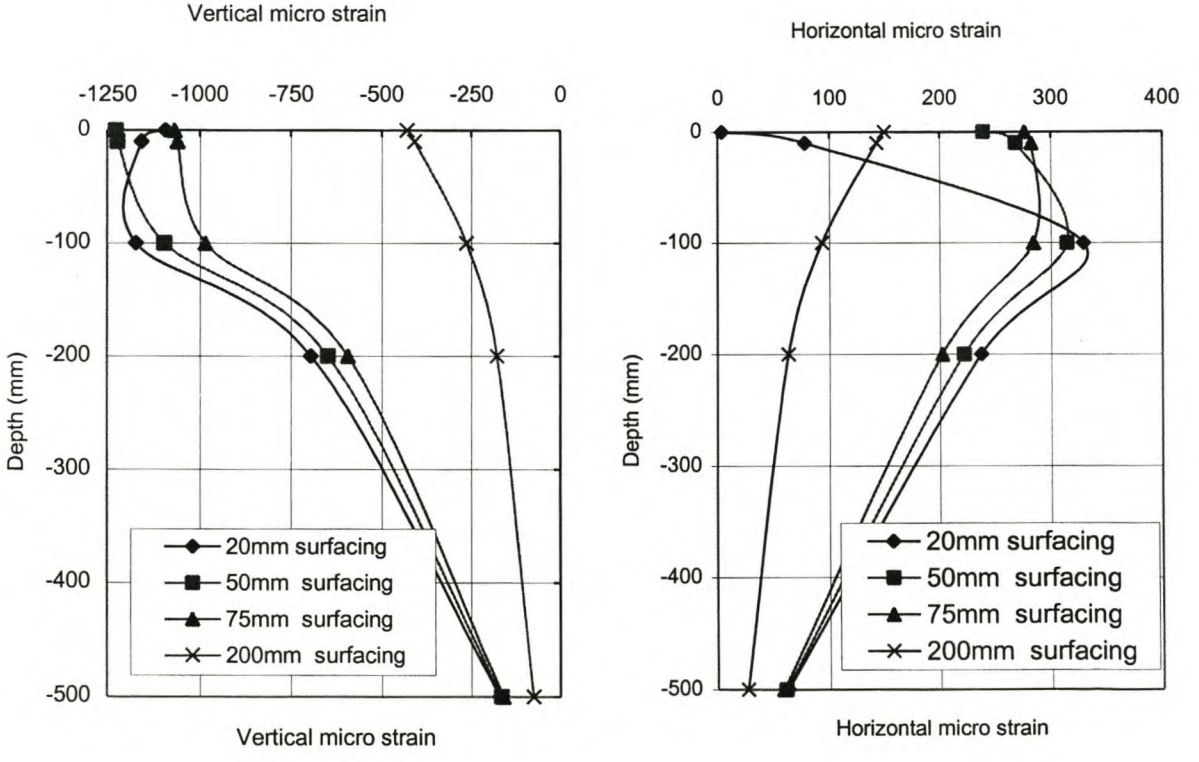

(b) Strain

Figure 2.3: Stress-Strain Distribution in the Second Composite Layer

[80kN-0.7MPa, E_1=2000MPa, E_2=400MPa, MR=5, ν=0.35]

3.2 Variation of the Axle Load at Constant Tyre Pressure (0.7MPa)

The effects of change in axle loading on the stress-strain response and vertical displacements, at constant tyre pressure (0.7MPa) are presented in Figures 1.4 through to 1.6. The pavement material properties used were E_1 of 4000MPa, E_2 of 500MPa and Poisson's ratio of 0.35. The axle loading was varied as indicated in the Figures.

3.2.1 Vertical Stresses

At 0.7MPa constant tyre pressure, the vertical surface contact stress remained constant and was equal to 0.7MPa.

As can be seen from Figure 1.4, the vertical contact stress in the immediate top zone of the second layer at [h+1] mm increased as the axle load was increased. The highest stress magnitude was under the thinner layer (20mm), which is equal to the tyre pressure at all values of the axle loading. Under the other layer thicknesses, the stress increased gradually with the axle loading. The lowest stress magnitude is under the 200mm surfacing, which are about 20% of the tyre pressure at 80kN axle load and 36% at 200kN. This is significantly low compared to the stress magnitude under the 20 or the 40 mm surfacing. From this analysis, it is evident that in the case of pavement structures with thinner asphalt surfacing layers, the traffic load is carried by the underlying layers and these should be adequately designed to support the loads.

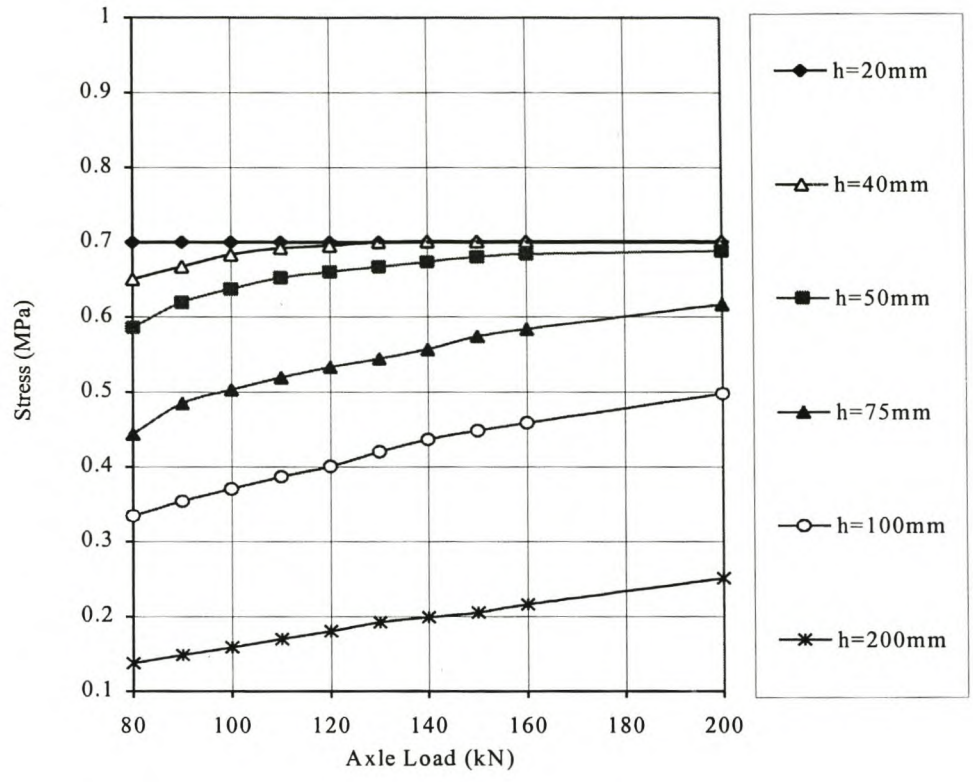

Figure 1.4: Vertical Stress in Top of the Second Layer

[0.7MPa tyre pressure, E_1=4000MPa, E_2=500MPa, MR=8, ν=0.35]

3.2.2 Horizontal Stresses

Figure 1.5 shows a plot of the horizontal stress against axle loading at the bottom zone ([h-1] mm) of the asphalt layers. In the thicker 200mm layer, the stress gradually increased as the axle loading was increased. In the intermediate and thin layers, there was a general decrease in the stress magnitude as the axle loading was increased. This was ascribed to the increase in the contact area relative to the layer thickness as the axle loading was increased (at a constant tyre pressure). The probable effect was that, due to the bigger contact area, the stresses are spread over a wider area, thus reducing localized effects.

In the 20mm surfacing, there are virtually no tensile stresses. All the horizontal stresses are negative (compressive) irrespective of the change in axle loading. The 20mm surfacing is thus least likely to suffer fatigue due to tensile stresses.

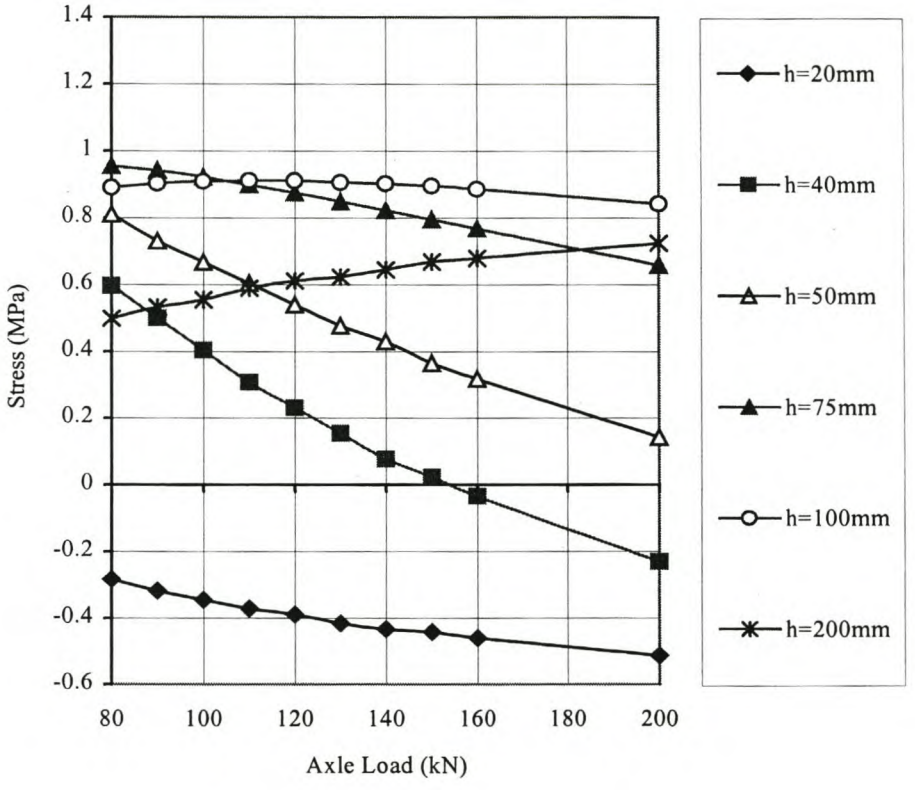

Figure 1.5: Horizontal Stresses at the Bottom Zone of the Asphalt Layer

[0.7MPa tyre pressure, E_1=4000MPa, E_2=500MPa, MR=8, ν=0.35]

The horizontal strains exhibited a response pattern similar to the horizontal stresses. Summarily, and with due regard to horizontal stresses and strains, the thin surfacing layers (≤ 50 mm) exhibited good response at higher axle loading. The stress-strain magnitude decreased as the axle loading was increased. In the same vein, it was observed that the contact area to surfacing layer thickness ratio (*a/h*) plays a significant role in the stress-strain response of these layers.

3.2.3 Vertical Displacements (mm)

Figure 1.6 is an illustration of the vertical displacements that occurred on the pavement surface and on top ([h+1] mm) of the second composite layer as the axle load was varied from 80kN to 200kN. Also the amount of displacement that occured in the respective pavement structures with regard to surfacing layer thickness is demonstrated. Material constants and contact pressure were the same in all the pavement structures.

Figure 1.6 shows that the vertical displacements increased tremendously as the axle loading was increased and the highest in terms of magnitude is for the 20 mm surfacing. The lowest vertical displacement is indicated for 200mm, which is on average about 48% of the 20mm.

Almost all of the vertical displacement occurred in the second layer and hardly in the top layer. Even in the case of the 200 mm asphalt layer, only about 12% of the total vertical displacement occurred in the top layer. Based on this analysis, and assuming similar loading and environmental conditions, the deformation failure criterion for the layers under the 20mm surfacing may be reached much earlier than for the layers under the thicker surfacing-bases like 200mm.

With regard to the vertical stress and displacement in terms of magnitude, the thin layers performed poorly. However, their response in terms horizontal stress magnitude was extremely good.

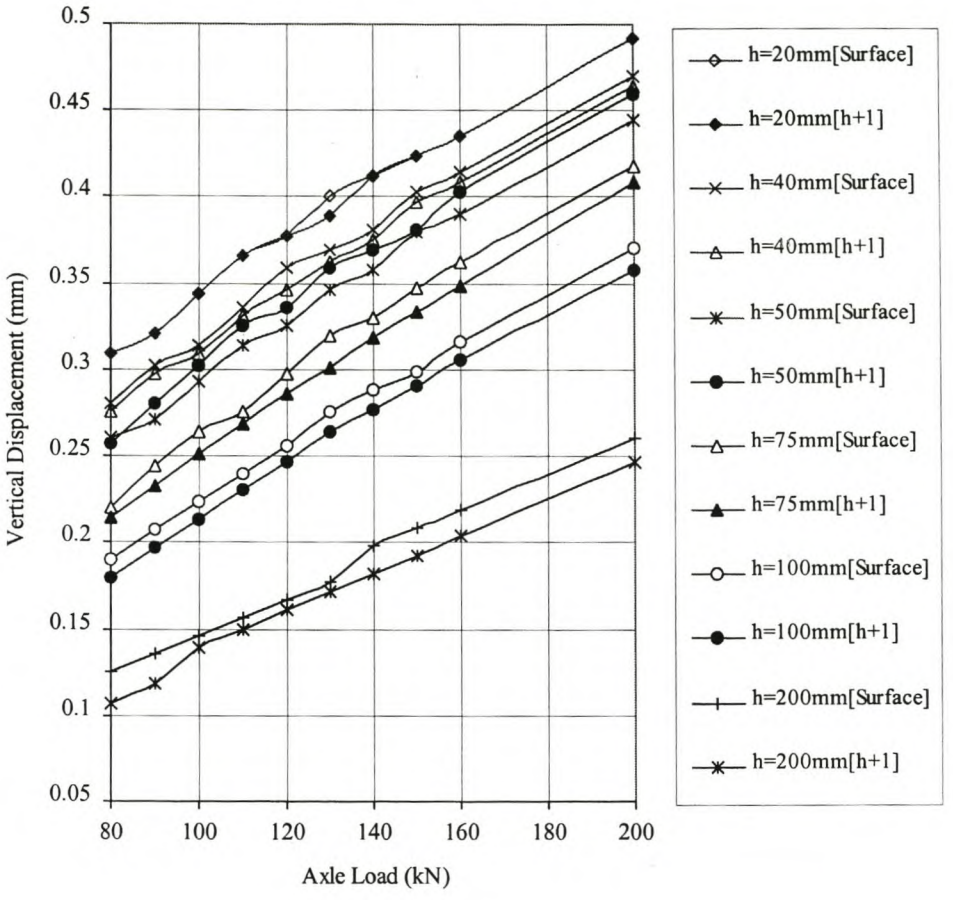

Figure 1.6: Vertical Displacements

[0.7MPa tyre pressure, E_1=4000MPa, E_2=500MPa, MR=8, ν=0.35]

3.3 Variation of Tyre Pressure at Constant Axle Loading (80kN)

Results are presented in Figures 1.7 to 1.10. The axle load (80kN) and material constants were maintained constant whilst only the tyre pressure was varied from 0.52MPa (520kPa) to 1MPa (1000kPa). Just like in the previous case, the following material properties were used; E_1 of 4000MPa, E_2 of 500MPa and Poisson's ratio of 0.35.

3.3.1 Vertical Stresses

For all the values of h, the vertical surface contact stress increased linearly with the tyre pressure as shown in Figure 1.7. According to the current design assumption (as used in this study), the vertical contact stress is equal to the tyre pressure, and hence the proportion of increase was one to one.

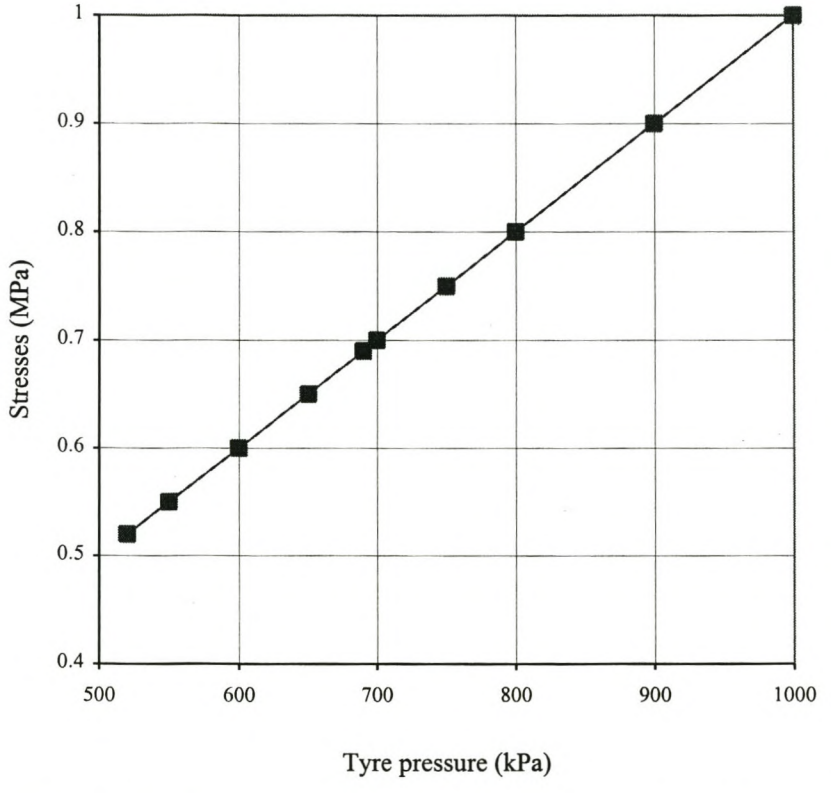

Figure 1.7: Vertical Surface Contact Stresses (for all Values of h)

[80kN axle load, E_1=4000MPa, E_2=500MPa, MR=8, ν=0.35]

On top of the second layer, the vertical stress also increased with an increase in the tyre pressure, with the highest magnitude under the 20mm surfacing. The stresses tended to decrease with thickness and are least under the 200mm surfacing. Under the 20mm surfacing, it is actually equal to the tyre pressure. For example, at 1MPa tyre pressure, it is 1MPa for 20mm versus 0.16MPa for 200mm. This is indicative that for the same traffic loading and assuming all variables to be constant, pavement layers below the thin asphalt surfacing will be more stressed and may reach the failure criterion earlier than the layers under the thick surfacing layers. As can be seen from Figure 1.8, the thicker layers appear to be less sensitive to tyre pressure compared to the pavement structure with thinner surfacing layers.

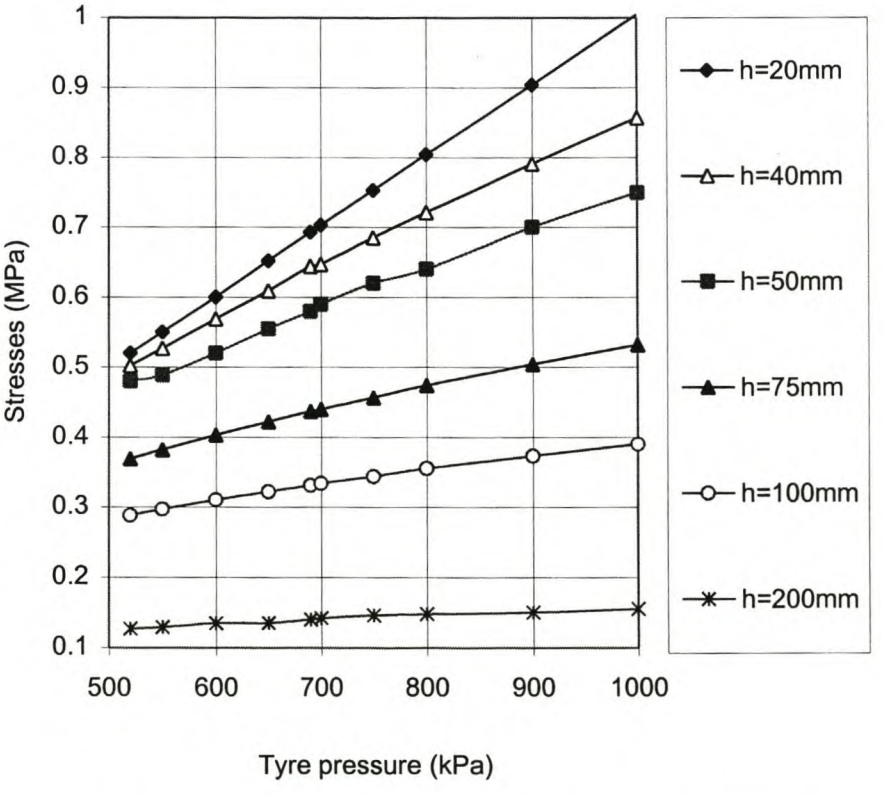

Figure 1.8: Vertical Stresses on Top of Second Layer

[80kN axle load, E_1=4000MPa, E_2=500MPa, MR=8, ν=0.35]

3.3.2 Horizontal Stresses

Horizontal stresses were computed at the bottom zone of each asphalt layer for the respective tyre pressures as shown in Figure 1.9. In all the surfacing layers, the stresses exhibited a general tendency to increase with an increase in the tyre pressure. The lowest magnitude of the tensile stress in indicated for 200mm followed by 40mm. In the 20mm, the horizontal stress is compressive for all the values of the tyre pressure.

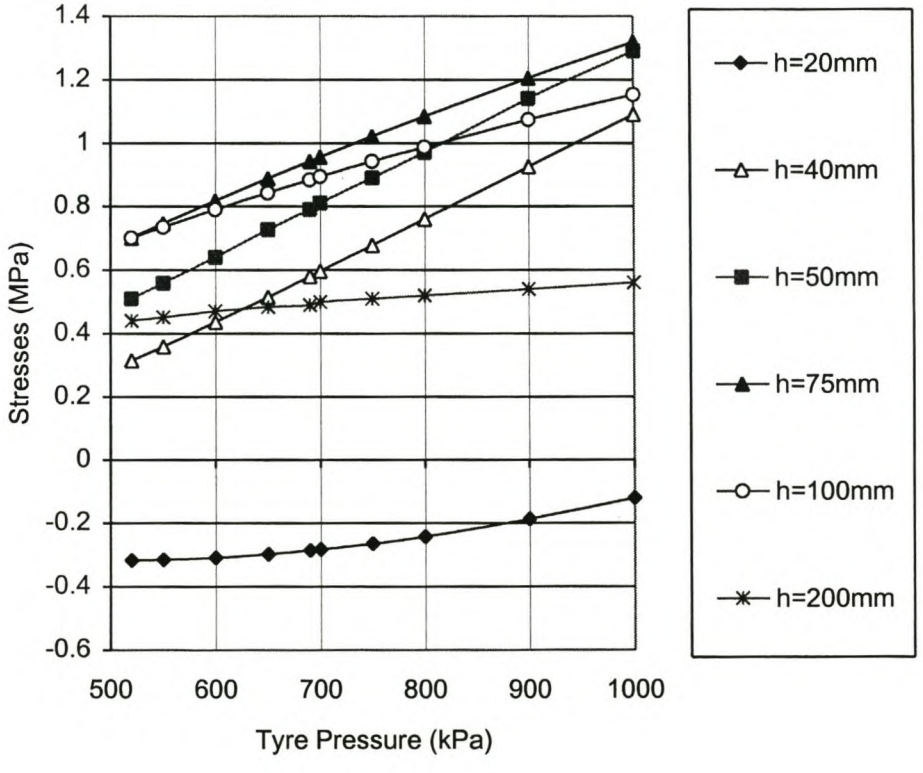

Figure 1.9: Horizontal Stresses at the Bottom Zone of the Asphalt Layer

[80kN axle load, E_1=4000MPa, E_2=500MPa, MR=8, ν=0.35]

3.3.3 *Vertical Displacements*

Figure 1.10 shows the comparative vertical displacements that occurred in the respective pavement structures under varying tyre pressure. As shown in Figure 1.10, there is a general increase in the vertical displacements as the tyre pressure was increased. For the 20mm surfacing, the displacement at 0.52MPa is 0.27mm but increased by about 36% to 0.36mm when the tyre pressure was increased to 1MPa. From this analysis, it was calculated that the total vertical displacement increased by about 0.4% per every 1% increase in the tyre pressure. The maximum displacement occurred in the pavement structure with the 20mm surfacing and least in the 200mm. For 1MPa tyre pressure, the total vertical displacement for 20 mm (0.36mm) was found to be about 2.6 times more than for 200mm (0.14mm).

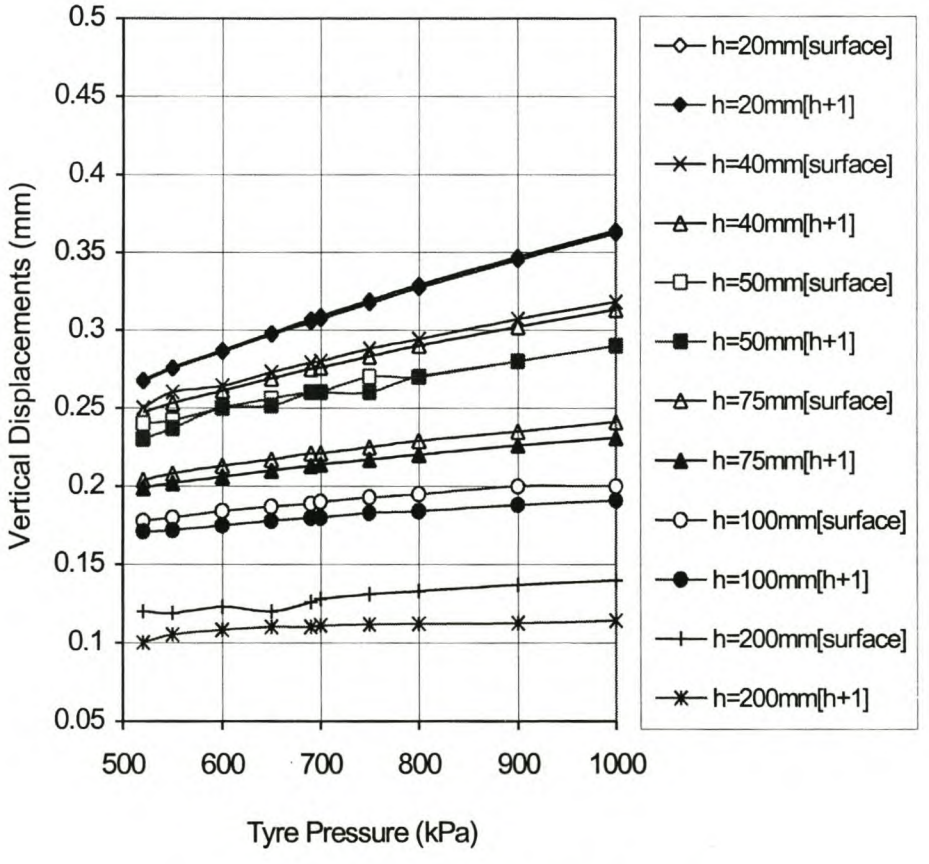

Figure 1.10; Vertical Displacements.

[80kN axle load, E_1=4000MPa, E_2=500MPa, MR=8, ν=0.35]

It was further calculated that about 16% of the displacement occurred in the top asphalt layer for 200mm surfacing, where as the 20mm contributed only about 0.6%, which is negligible. Very little (if not negligible) displacement occurred in the thinner asphalt layers. Most of the deformation occurred in the underlying layer.

The detrimental effects of high tyre pressure in terms of stress-strain response and vertical displacement was demonstrated. In all cases, there was a general increase in the magnitude of stress, strain and displacement as the tyre pressure was increased from 0.52MPa to 1MPa. Where as the 20mm surfacing responded poorly in terms of vertical stress and displacement, its response in terms of horizontal tensile stress and strain was extremely good (particularly at higher axle loading).With regard to axle loading and tyre pressure, it was observed that the vertical stresses and displacement were more sensitive to change in axle loading than tyre pressure. The horizontal stresses exhibited more sensitivity to variation in tyre pressure. In the case of the thin layers (≤50mm), the horizontal stress-strain response improved with an increase in the axle loading, and the tyre-surface area to thickness (*a/h*) ratio appears to be an influencing factor.

3.4 Change in both Axle Loading and Tyre Pressure

An example of the effect of a simultaneous change in both axle loading and tyre pressure on a thin surfacing layer (30mm) is shown in Figure 1.11. Only response in terms of horizontal stress and strain at the bottom of the asphalt layer is given. An E_2 value of 200MPa was used and the modular ratio was varied as indicated in the Figures. As expected, stresses and strains substantially increased as the traffic loading was increased. This is the normal material response to loading, and could indicate more pavement damage as evident from the relative fatigue lives shown in Figure 1.15. The highest stress-strain values (Figure 1.11), and the lowest number of fatigue load cycles (Figure 1.16) are shown for 120kN-1MPa traffic loading compared to 80kN-0.52MPa. It can also be observed that, the stress-strain magnitude increased with an increase in the modular ratio.

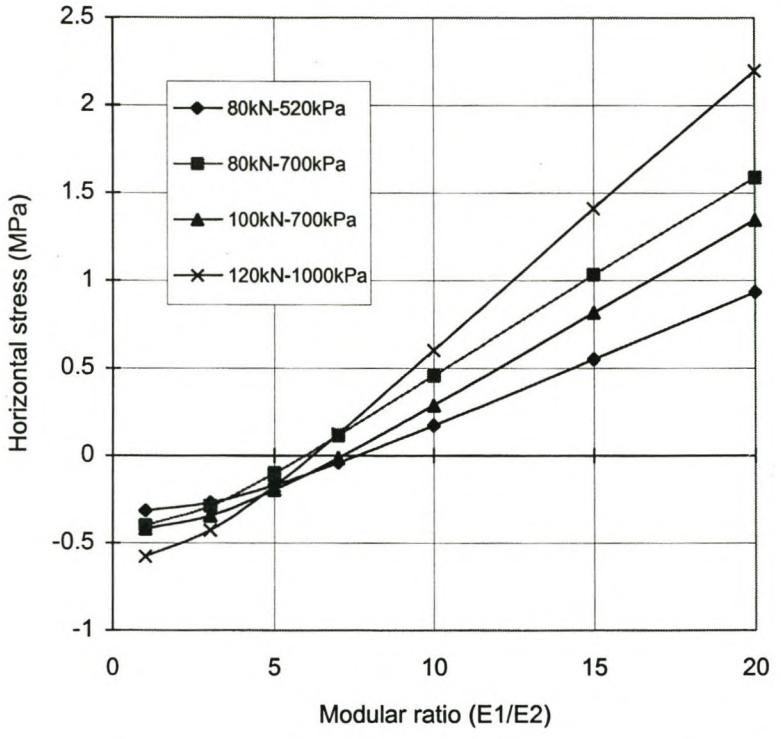

(a) Horizontal Stress at the Bottom of the Asphalt Layer

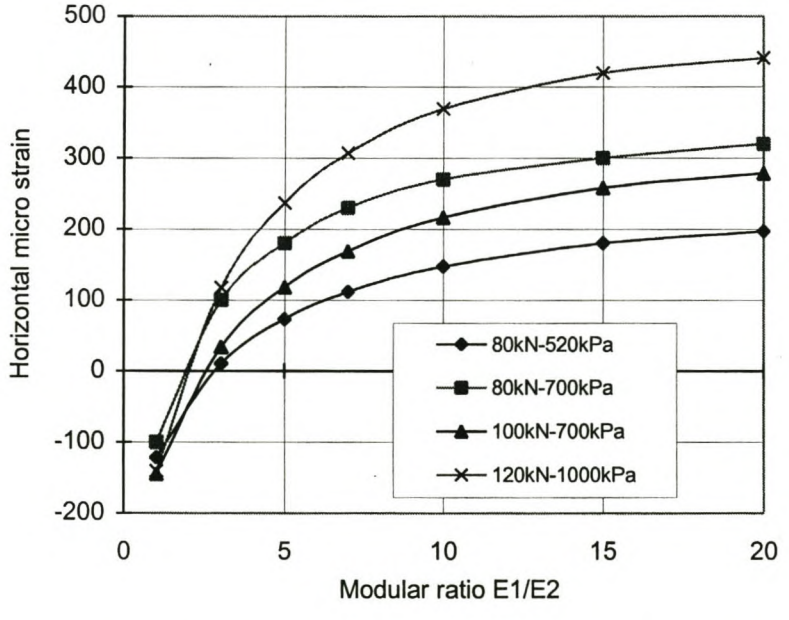

(b) Horizontal Strain at the Bottom of the Asphalt Layer

(c)

Figure 1.11: Variation of Traffic Loading and Modular Ratio

[Asphalt surfacing layer thickness = 30mm, E_2 = 200MPa, ν = 0.35]

3.5 Effect of the Modular Ratio (E_1/E_2)

Figure 1.12 shows an example of the effect of the composite modulus (E_2) of the immediate underlying layers on the stress-strain response of the top asphalt layer for the selected thickness 20 and 150 mm, for the same traffic loading of 80kN-0.7MPa.

As can be seen in Figure 1.12 (a), stresses in the asphalt layer are independent of the stiffness of the underlying layers. Variation of the composite modulus E_2, had no effect on the magnitude of both the horizontal and vertical stresses in the top layer. For all the values of E_2, the stress remained the same, but varied only with the change in the modular ratio. This is indicative that for a two-layer pavement system like in this model, the modular ratio has a significant effect on the stress-strain response of the asphalt layer.

Horizontal tensile strains showed an inverse relationship, and increased as E_2 decreased. In both the surfacing layers, the highest strain values are shown for E_2=50MPa and the lowest for E_2=1MPa. Thus, surfacing layers resting on low strength support layers (base, subbase, and subgrade) may be potentially susceptible to traffic damage.

As observed previously, thin asphalt surface layers have very good tensile stress-strain behaviour at low modular ratio. The thicker asphalt surfacing-bases have a relatively good tensile strain response at higher modular ratio.

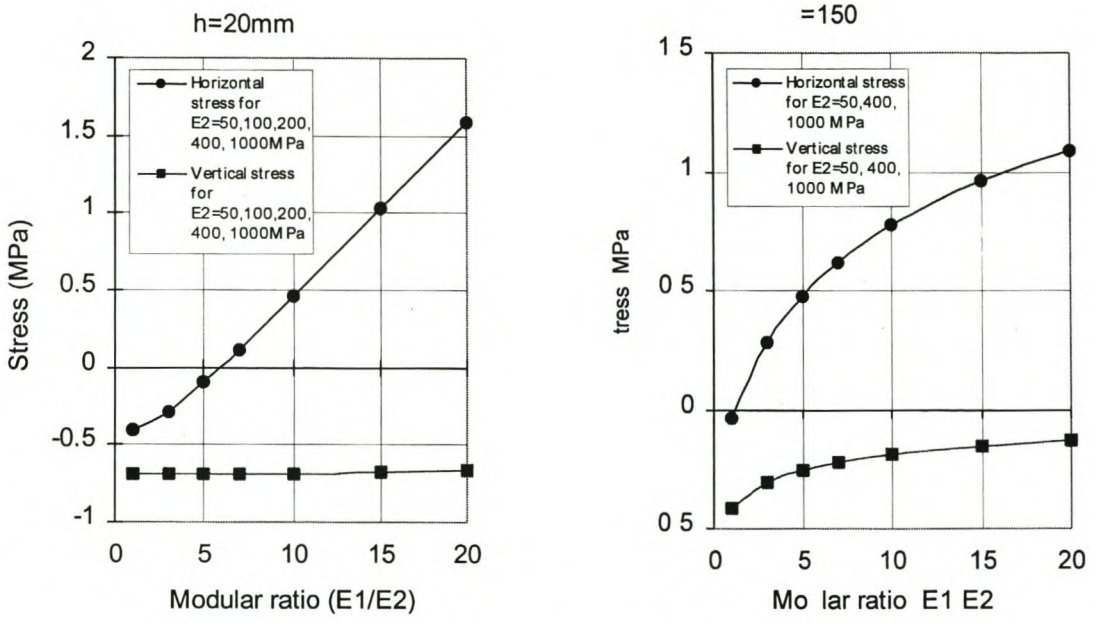

(a) Stresses at the bottom zone of the asphalt layer.

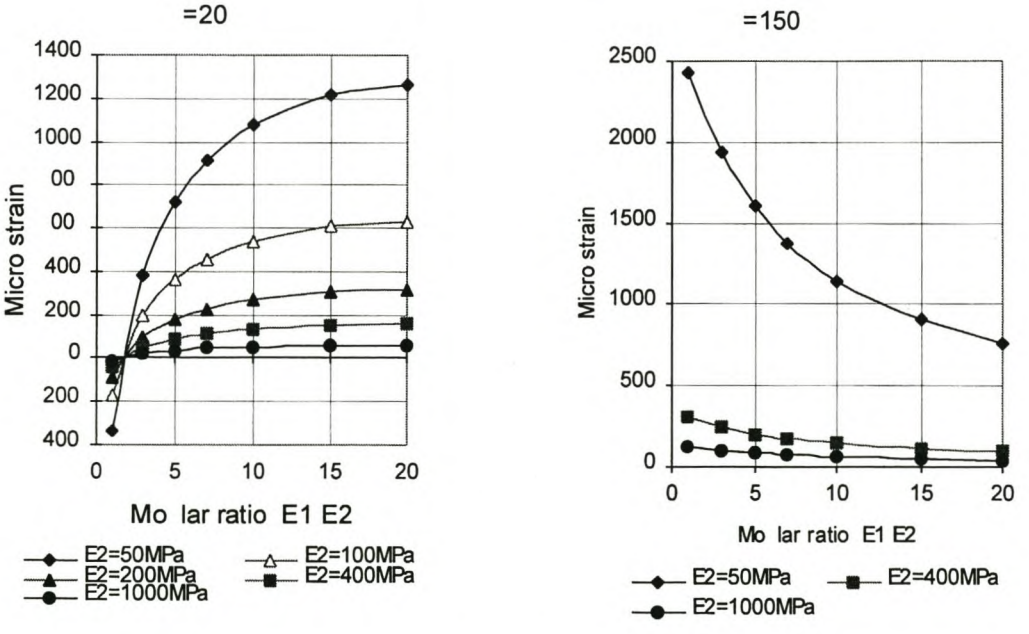

(b) Horizontal strains at the bottom zone of the asphalt layer

Figure 1.12: Effect of the Composite Modulus (E_2)

[80kN axle load, 0.7MPa tyre pressure, ν=0.35]

3.6 The Effect of the Poisson's Ratio (ν)

Results for the selected asphalt layer thicknesses are shown in Figure 1.13. Traffic loading of 80kN-0.7MPa and a composite modulus of E_2 = 400MPa with a modular ratio of 5 were used. The notation 0.25/0.25 on the horizontal axis in Figure 1.13 indicate that the Poisson's ratio for the asphalt layer is 0.25 and it is also 0.25 for the second composite underlying layers. Only horizontal stresses and strains at the bottom zone of the asphalt layers are shown.

As can be seen in Figure 1.13, ν = 0.25 and 0.35 gave the lowest stress-strain values. Most design procedures use 0.35. Optimal stress-strain response of the asphalt layer appears to be at low Poisson's ratio (0.25).

The stress-strain graphs for the thicker asphalt layers (150 and 200 mm) seem to approach a straight line, implying that the horizontal stresses and strains are insignificantly affected by the change in the Poisson's ratio. The large-scale variations of the stress-strain values of the intermediate and thin surfacing layers for the different Poisson's ratios indicate that the response of these layers under loading is significantly affected by the Poisson's ratio. It was also noted that the stress-strain response is dependent on the Poisson's ratio of the second layer. This effect was also observed in Figure 1.2.

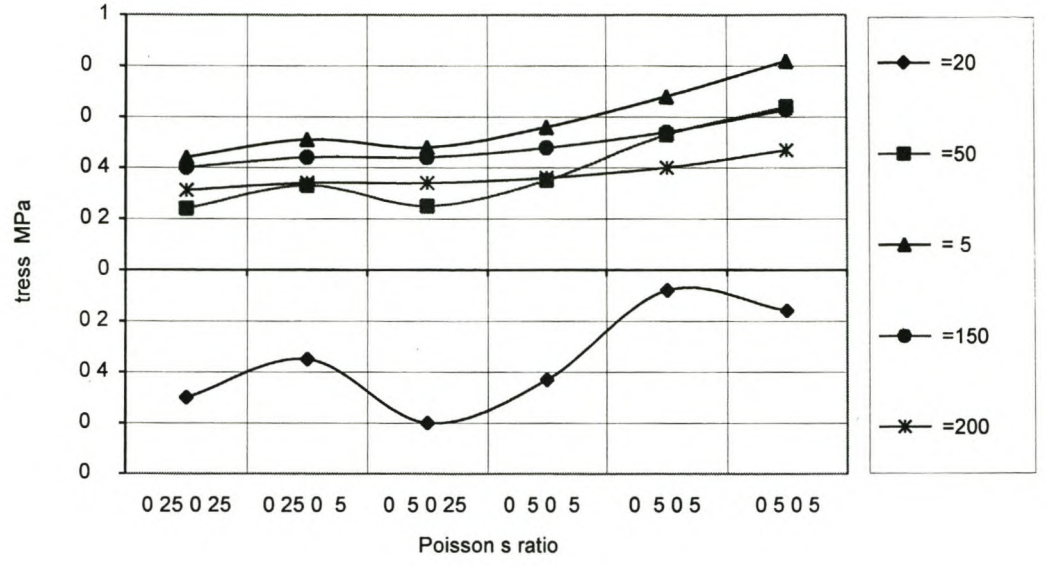

(a) Horizontal stresses at the bottom zone of the asphalt layer

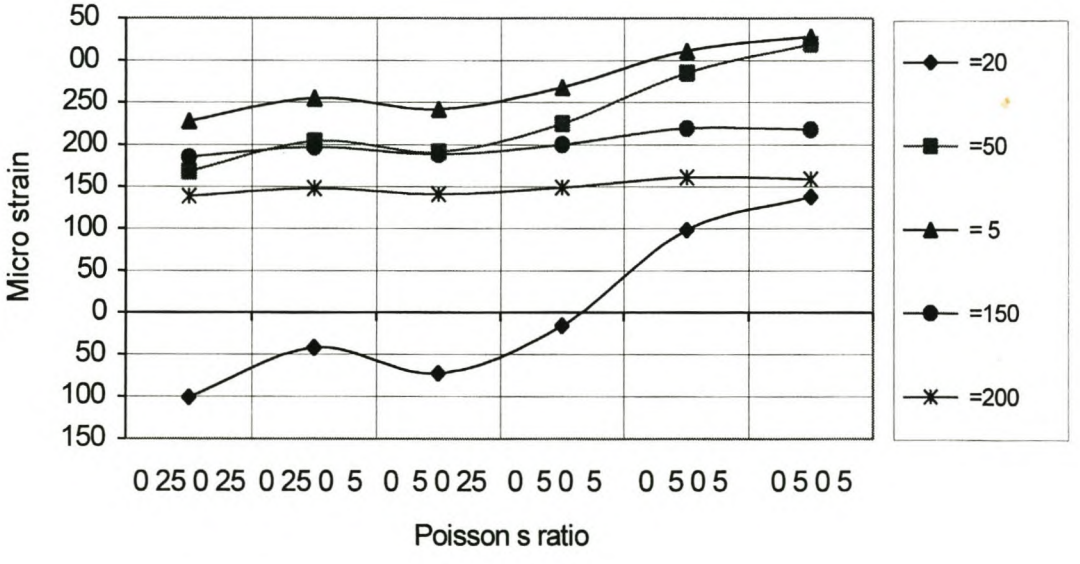

(b) Horizontal strains at the bottom zone of the asphalt layer

Figure 1.13: The Effect of the Poisson's Ratio (ν) – Asphalt Layer
[80kN axle load, 0.7MPa tyre pressure, E_2=400MPa, MR=5]

4 RELATIVE PAVEMENT SERVICE LIFE

The "Fourth Power Law" and, the fatigue and deformation models according to the Asphalt Institute design method (Asphalt Institute, 1993, and Huang, 1996) was used to relate the effect of traffic loading to the pavement service life.

4.1 The Fourth (4^{th}) Power Law

Figure 1.14 shows the relative damage effect of axle loading on the pavement according to the 4^{th} power law. The relative damage ratios plotted in the Figure were calculated using Equation 1.1 shown below.

$$F = \left(\frac{P}{80}\right)^n \quad \text{.....(Equation 1.1)}$$

Where:

F	=	load equivalency factor
P	=	standard axle load in kN
n	=	relative damage exponent, which in this example is 4.

The Figure shows that the relative damage effect increases almost exponentially with axle loading. According to the 4^{th} power law hypothesis, 200kN would cause about 39 times more damage than an equivalent 80kN legal axle load, whilst 100kN (25% overload) would be about 2.4 times more (144% more).

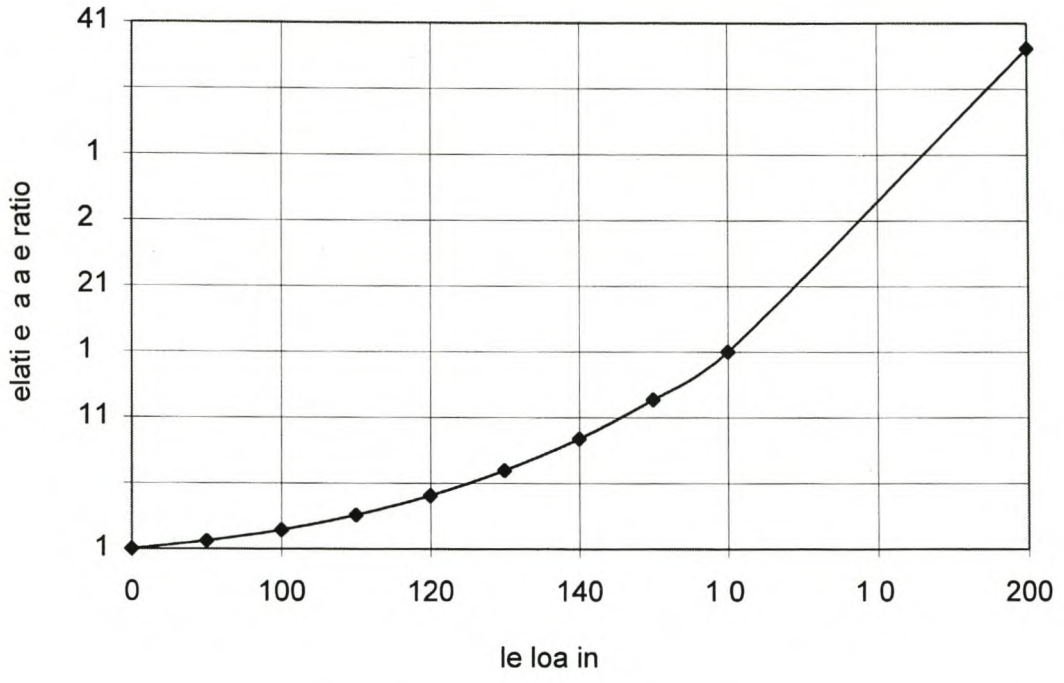

Figure 1.14: Relative Damage according to the 4th Power Law

Figure 1.14 is an indication that the long term damage caused by overloading may not be directly proportional to the overload as may be assumed. The actual damage could be more than the loading proportions. For example, 12.5% overload according to the 4th power law, may cause damage equivalent to about 60% more than a legal 80kN, and not 12.5%.

4.2 Relative Fatigue Life (N_f)

For relative fatigue life analysis, only the top surfacing layer (asphalt) was considered. The Asphalt Institute fatigue Equations with fatigue regression coefficients; f_1= 0.0796, f_2= 3.291, and f_3= 0.854 was used for calculating the relative fatigue life (number of load repetitions) of the asphalt layer (Asphalt Institute, 1993; and Huang YH, 1993) based on the tensile strains at the bottom zone. The elastic modulus E_1 was expressed in MPa and strains in microns (unit-less).

4.2.1 *N_f versus modular ratio, axle loading, and tyre pressure.*

The relative number of fatigue load cycles versus modular ratio for the four different traffic-loading conditions for similar material constants are shown in Figure 1.15. To cause a similar fatigue impact (i.e. fatigue failure), the least number of fatigue load cycles was obtained under the high traffic loading, 120kN-1MPa. This is an indication of more damage compared to the other traffic loading. This implies that under high traffic loading, and assuming all other parameters remain constant, the fatigue failure criteria may be reached much earlier than under low traffic loading.

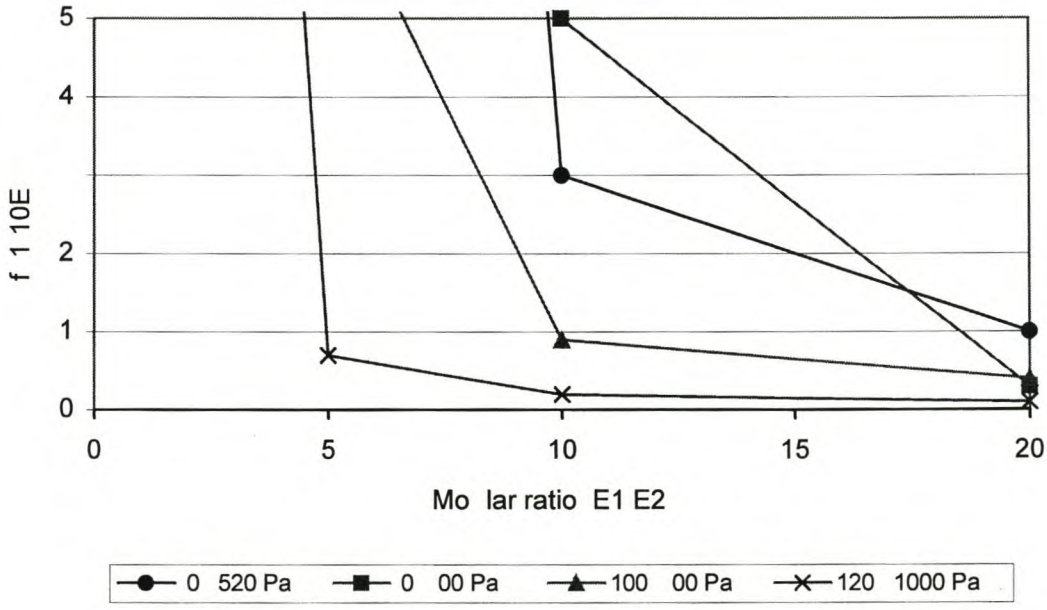

Figure 1.15: N_f Vs Modular Ratio and Traffic loading
[Asphalt surfacing layer thickness = 30mm, E_2 = 200MPa, ν = 0.15]

At modular ratio of 10, the 80kN-0.7MPa traffic loading had a relative fatigue life of about $5x10^6$ load cycles whilst 120kN-1MPa had only $0.2x10^6$. This represents a reduction of about 96% in fatigue life, clearly indicating the potential damage of high traffic loading.

Figure 1.15, further indicates that the thin surfacing layer (30mm) has very high fatigue life at low modular ratios. According to this result, it can be deduced that a thin asphalt surfacing layer will perform better in terms of fatigue, at low than at high stiffness values. However, the validity of this analytical conclusion needs practical proof such as laboratory or field-testing. On the other hand, the good performance of thin bitumen-rubber asphalt layers on granular layers in South Africa is an indication of this behaviour of thin asphalt layers.

The effect of tyre pressure is also evident when comparing the relative fatigue lives of 80kN-0.520MPa and 80kN-0.7MPa traffic loading at a modular ratio of 20. The number of relative fatigue load cycles at 80kN-0.7Pa is 0. $3x10^6$ against $1x10^6$ at 80kN-0.52MPa, which is about 70% lower. Assuming similar environmental conditions and on the same pavement structure, the relative fatigue life of the pavement under 80kN-0.7MPa may be only 30% of the total life under 80kN-0.52kPa traffic loading.

4.2.2 N_f versus axle loading

Figure 1.16 shows an example of the effect of variation of axle loading on the relative fatigue life of the respective asphalt surfacing layers. The tyre pressure was maintained constant at 0.7MPa, and the material constants remained unchanged. It is evident from Figure 1.16 that the thin surfacing layers have higher fatigue life, which appear to increase with axle loading, and it is infact more than 5×10^6 load cycles for 20 mm (due to compressive strains). It must be recalled that at higher axle loading, the thin asphalt layers are predominantly subjected to compressive stresses.

Unlike in the thicker layers greater than 100mm, the thin and intermediate asphalt layers (≤100mm) performed better in terms of fatigue at higher axle loading. This phenomenon was ascribed to the effect of the tyre-pavement contact area (a) and the layer thickness (h). If all variables are assumed to remain constant, one can further deduce that the ratio a/h plays a significant role in the fatigue response of thin asphalt layers under traffic loading. Hence there is need to consider the ratio a/h during both the design stage and performance analysis of such layers.

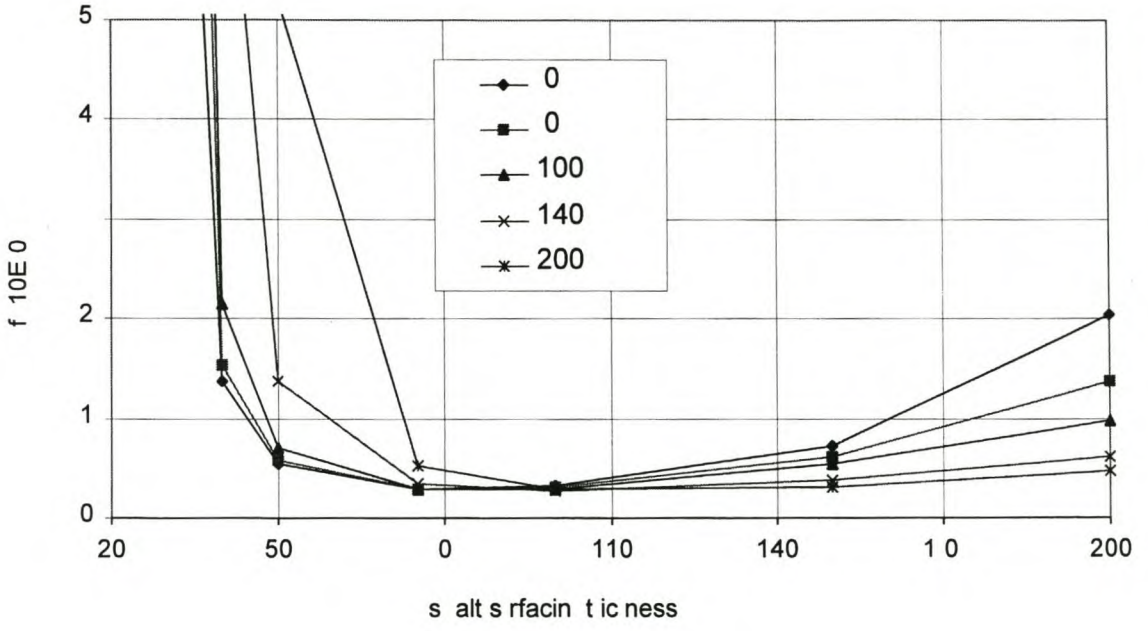

Figure 1.16: Relative Fatigue Life (N_f) Vs Axle Loading at Constant Tyre Pressure

[0.7MPa tyre pressure, E_1 = 4000MPa, E_2 = 500MPa, MR = 8, ν = 0.35]

Up to about 100mm, the highest fatigue life is shown for 200kN, which is about 150% overload above the 80kN standard axle load. According to this theoretical analysis, Figure 1.16 further shows that the relative fatigue life of the 100mm surfacing is unaffected by the variation in axle loading. In the thicker layers, the relative number of fatigue load cycles to failure decreased with increase in axle loading.

4.2.3 N_f versus tyre pressure.

As can be seen from Figure 1.17, the relative fatigue life of all the layers decreased with an increase in the tyre pressure. All the other variables were assumed constant and an axle load of 80kN was used.

For all the values of h, the smallest number of fatigue load cycles is indicated for 1MPa and the highest for 0.52MPa. This is indicative that the high tyre pressure (1MPa) is more damaging than 0.52MPa.

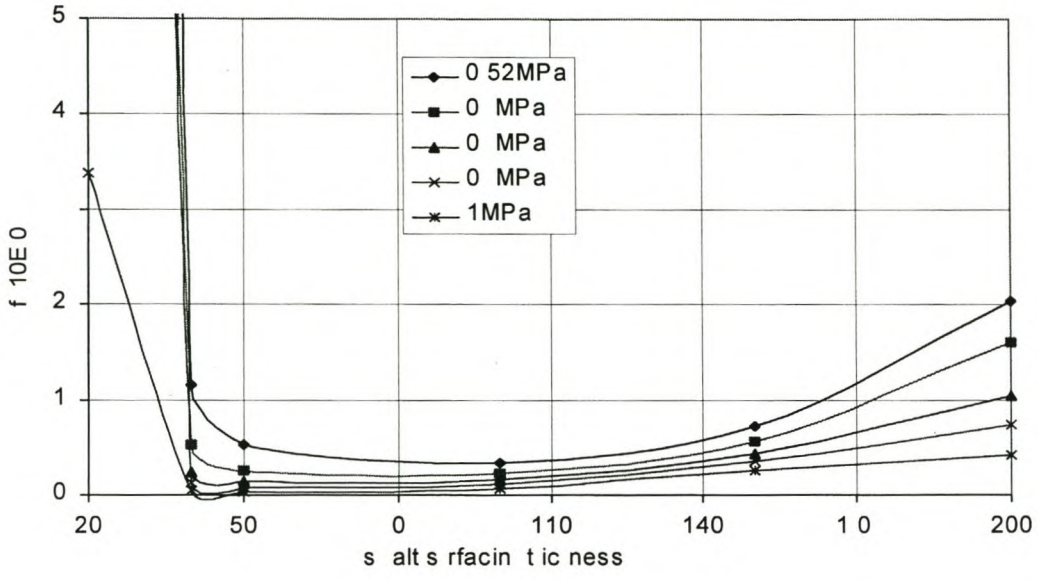

Figure 1.17: Relative Fatigue Life (N_f) Vs Tyre Pressure at Constant Axle Loading

[80kN axle load, E_1 = 4000MPa, E_2 = 500MPa, MR = 8, ν = 0.35]

The intermediate surfacing layers have the lowest relative fatigue life. The 20mm surfacing exhibited the best performance in terms of the number of fatigue load cycles followed by the 200mm surfacing base.

4.3 Deformation in the Second Composite Underlying Layer

Deformation function Equations according to the Asphalt Institute design method (Asphalt Institute, 1993; and Huang YH, 1993) was used to determine the relative number of load repetitions to limit deformation in the second composite underlying layer based on the vertical strains in the top zone.

4.3.1 *N_d versus Axle Loading*

The results for the 0.7MPa tyre pressure are presented in Figure 1.18. For all the surfacing layers greater than 50mm, the lowest number of deformation load cycles are shown for 200kN and appear to increase with an increase in the asphalt surfacing layer thickness. The implication is that, if a similar terminal rutting value of say 20mm is used, this value would be reached much earlier under 200kN axle load than 80kN. Thus the pavement is expected to have a shorter service life at higher axle loading.

From Figure 1.18, it can also be observed that for values till approximately 100mm thickness of the first top layer, resistance is very low. For asphalt layers greater than 100mm, the lower axle loads gives far better results compared to higher axle loads.

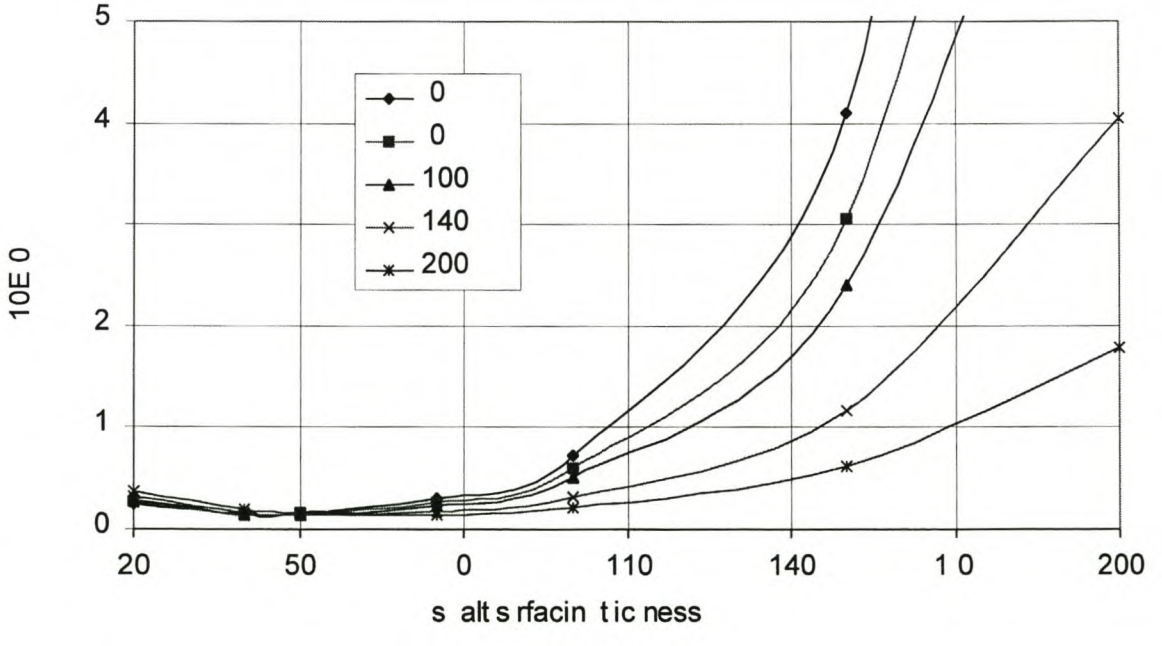

Figure 1.18: Relative Deformation Load Cycles in Second Layer

[0.7MPa tyre pressure, E_1 = 4000MPa, E_2 = 500MPa, MR = 8, ν = 0.35]

4.3.2 *N_d versus Tyre Pressure*

Figure 1.19 shows the relative number of deformation load cycles at a constant axle load of 80kN. Under all the surfacing layer thickness, the lowest number of deformation load cycles to cause a similar terminal permanent deformation (say 20 mm) is shown for 1MPa. This is indicative that abnormally high tyre pressures are detrimental to pavements in terms of both fatigue (as shown previously) and deformation. Since the axle load is constant, this effect is related to the tyre-pavement contact area, which decreases with increase in tyre pressure, and thus localizing the loading effect.

Also from Figure 1.19, layers under the thicker asphalt layers over 100mm have relatively higher number of deformation load cycles, and is infact greater than 5 x 10^6. Therefore, pavement structures with thicker asphalt bases may be less susceptible to deformation in the lower layers compared to those with thinner surfacing layers.

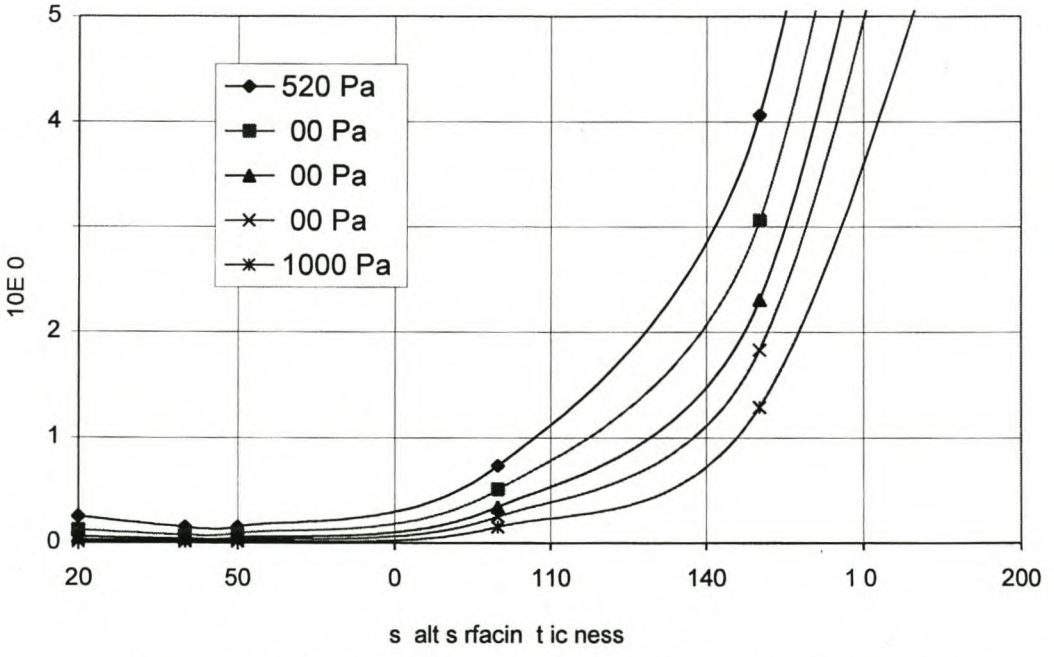

Figure 1.19: Relative Deformation Load Cycles in Second Layer
[80kN axle load, E_2 = 4000MPa, E_2 = 500MPa, MR = 8, ν = 0.35]

Overall, it was observed that, for load transfer to and deformation in the lower layers, the thin and intermediate surfacing layers (h ≤100mm) performed poorly.

5 SUMMARY AND FINDINGS

The methodology for characterizing and modeling a simple pavement structure (based on linear elastic theory and static loading conditions) for computer analysis was presented. A super single tyre load was used for simplicity purpose and ease of calculations, and analysis was done directly under the center of the tyre load. High values of stress occurred under the center of the wheel load.

From the stress-strain distribution analysis, it was observed that for the thin asphalt layers (≤50mm), the vertical stress hardly decreases over the surfacing depth and almost the same applied vertical stress (equal to the tyre pressure) is transferred to the immediate underlying layers. For the thicker (>100mm) structural surfacing/base layers, a considerable decrease in the vertical stress with depth was observed. With regard to permanent deformation, the failure design criteria for pavement structures with thin asphalt surfacing layers should be based on the underlying layers. For the purpose of modelling deformation in the asphalt layer, it was observed that the vertical strain criterion would be inappropriate as it does not give a true reflection of the vertical stress due to the influence of the horizontal stresses and the effect of the Poisson's ratio.

On the contrary, the thin asphalt layers exhibited extremely good stress-strain behaviour relative to fatigue under traffic loading, particularly at low modular ratio and high axle loading. This is due to the fact that, the layer is predominantly under compression. Layers less than 100mm thick performed better in terms of fatigue at higher axle loading.

Among the factors affecting the stress-strain response and subsequent fatigue performance of thin asphalt layers were observed to be; (i) the tyre-pavement surface contact area (a) to layer thickness (h) ratio, and (ii) the modular ratio. Huang (1996) also reports these findings, in his analysis of a two-layered pavement system. It is thus important to consider a/h and modular ratios during design and analysis of thin asphalt layers.